A COMPARTMENTALIZED APPROACH TO SIMULATING REDOX ZONES IN CONTAMINATED AQUIFERS

A DISSERTATION
SUBMITTED TO THE DEPARTMENT OF
GEOLOGICAL AND ENVIRONMENTAL SCIENCES
AND THE COMMITTEE ON GRADUATE STUDIES
OF STANFORD UNIVERSITY
IN PARTIAL FULFILLMENT OF THE REQUIREMENTS
FOR THE DEGREE OF
DOCTOR OF PHILOSOPHY

Robert H. Abrams

March 1999

© Copyright by Robert H. Abrams 1999
All Rights Reserved

I certify that I have read this dissertation and that in my opinion it is fully adequate, in scope and quality, as a dissertation for the degree of Doctor of Philosophy.

Keith Loague (Principal Adviser)

I certify that I have read this dissertation and that in my opinion it is fully adequate, in scope and quality, as a dissertation for the degree of Doctor of Philosophy.

Steven M. Gorelick

I certify that I have read this dissertation and that in my opinion it is fully adequate, in scope and quality, as a dissertation for the degree of Doctor of Philosophy.

David L. Freyberg

Approved for the University Committee on Graduate Studies:

ABSTRACT

The effort reported in this dissertation was motivated by field-scale observations of redox zones. Redox zones typically develop due to microbial oxidation of organic carbon coupled to a sequence of oxidants. For this study, new simulation protocols were developed because currently available methods either (i) use rate-limited reactions and empirical methods to select which oxidant should be used or (ii) use thermodynamic constraints to select which oxidant to use but impose equilibrium among all redox reactions.

A "compartmentalized" approach to solving the geochemical problem, that has a direct analogy to redox zones, was developed and tested for a geochemical batch system. Each compartment uses a set of reactions that is representative of a particular redox zone while ignoring insignificant redox reactions. A statistical model evaluation indicated that the compartmentalized approach performs accurately.

The compartmentalized approach was then coupled to a solute transport simulator using the sequential iteration approach. The decoupled reaction networks that arise from the compartmentalized approach allow for a significant reduction in the number of solute transport equations that are needed to simulate the development of redox zones. The compartmentalized solute transport model was successfully tested in one and two dimensions under simplified conditions.

Two field-scale simulations (one- and two-dimensional) that were based upon the U.S. Geological Survey's Cape Cod research site were then conducted. For the two-dimensional simulation, a groundwater flow model was used to generate a velocity field to demonstrate the usefulness of the new transport model for simulating field-scale reactive transport phenomena. The sequence of redox zones observed in the field and the nature of the boundaries between the zones were captured well with the compartmentalized solute transport model.

The compartmentalized approach uses thermodynamics to select which oxidant to couple to the oxidation of organic carbon, and treats the kinetic aspects of the problem without imposing equilibrium on all redox reactions. Local geochemical conditions are used by the model to determine if redox reactions behave in a rate-limited or thermodynamically-limited manner. The kinetic framework can use any rate expression, allowing the reactions that drive redox zone development to be simulated as rate-limited, biological processes.

ACKNOWLEDGMENTS

I am extremely fortunate to have encountered a superb group of scientists during my graduate education at Stanford. Each of these mentors played a pivotal role in my development as a scientist.

I first encountered Professor George Parks toward the end of my first quarter at Stanford. George and I met because I became interested in studying the interactions of aqueous geochemistry and groundwater solute transport. This interest seemed odd to certain other professors in the Geology Department, because I had been admitted to Stanford to study hard rock petrology, structural geology, and regional tectonics. Nonetheless, George and I shared a curiosity about what had become my new interest. George carefully guided me through a minefield of rules and red tape and nurtured and expanded my interests in coupled geochemical/solute transport modeling. It was through his patience and tutelage that my research career began. George is the quintessential educator. I will never forget what he did for me and I hope someday to be able to similarly help someone else.

My first couple of summers at Stanford were actually spent at the U.S. Geological Survey in Menlo Park. There, I worked with Dr. John Bredehoeft on a basin-scale fluid flow problem in the Illinois Basin. John allowed me to explore the problem as I saw fit. This experience taught me to trust my intuition and abilities.

It was toward the end of my time working with John that I met Dr. Douglas Kent, who also conducts research at the Menlo Park campus of the U.S.G.S. I marched into Doug's office one day and told him that I was interested in simulating the transport of dissolved metals in groundwater. I told him that I had heard he did a lot of field experiments of metals transport, and that I wanted to model his experiments. Miraculously, he said okay. From there, our professional and personal relationship grew to the point where he suggested that I do the study that evolved into this dissertation.

George and Doug provided the geochemical "backbone" to this dissertation. Not only did they keep me honest, but they both provided many helpful suggestions and educated me graciously in all things chemical and thermodynamic. This dissertation is a much better piece of work because of both of their efforts.

I owe Steve Gorelick a big thanks for always insisting that I be thorough, concise, and clear. I learned a great deal from him about the physics of groundwater flow and solute transport. Steve also helped teach me effective ways of communicating research results, both in written documents and in oral presentations. I owe him an even bigger thanks for urging my adviser, Professor Keith Loague, to accept me as his graduate student when Keith first started at Stanford.

Working with Keith has been, in a large sense, the luckiest break I've ever had. Keith and I immediately worked well together. I've done my best to

emulate his careful and insightful approach to science. Above all, under Keith's guidance, I became a scientist. He never got in my way, even when I became interested in pursuing what often turned out to be tangents. He further fostered the confidence that was growing in me while always "running interference" for me, thus avoiding a suite of potential problems. Keith has given me many opportunities to grow as a scientist, both within the framework of my dissertation and while working with him on several other subsurface contamination problems. Keith's enthusiasm for science is infectious. He inspired me many times to keep pushing forward, to keep looking for creative solutions, while always providing valuable insight.

It was during one of the times when Keith needed to push me forward that he introduced me to Professor Garrison Sposito. I was having an incredibly difficult time getting my Ph.D. research off the ground due to some pesky numerical problems. Keith took me to U.C. Berkeley to see Gary, urging me to explain to Gary the nature of the problems I was facing. Gary made the insightful comment, in his casual, off-the-cuff manner, that became the very genesis of the compartmentalized approach. He suggested that I view redox zones as geochemical "islands", that behave in a quasi-independent manner. The compartmentalized approach was born and I was off and running. Hats off to you, Gary.

Many other people were also a great help to me. Professor David Freyberg is one of those people. I took two great classes from him at Stanford,

and many times talked with him at length about his and my research interests. During one of these conversations, in which we were discussing reactive transport modeling, he mentioned an interest in developing a rational method to reduce the number of chemical reactions that are needed in coupled geochemical/solute transport simulations. I tried to incorporate this idea into my Ph.D. research, and it became part of the compartmentalized approach. In addition, David's thorough reading of this manuscript greatly improved the presentation of concepts and ideas.

Believe it or not, I actually did some field work during the time I was working on this dissertation. Denis LeBlanc, Kathryn Hess, Jennifer Savoie, Kimberly Campo, and Timothy McCobb of the U.S. Geological Survey, Massachusetts, Doug Kent of the U.S.G.S. Menlo Park, and D'Artagnan Lloyd of Stanford were all of great assistance to me during my field trips to the Cape. Denis and Kathy have made me part of the sewage plume family, and I am grateful.

I have been very lucky to have many supportive and loving family members and friends. My parents Lynda and Maurice, Sister Bonnie, Aunt Gerri and Uncle Bill, Grandfather Bill and Grandmothers Mae and Selma, and my parents-in-law Millie and Paul have always stood behind me and supported my efforts. Many of them (you know who you are!) helped me greatly at times when I was filled with doubt.

The friendships that I have made with fellow Hydro students, past and present, have meant a great deal to me both personally and professionally. Great colleagues truly do make a graduate program worth much more than the paper it is written on.

The person who is most deserving of my gratitude is my wife, Leslie Hewitt. She has seen me at my worst, and has never left my side. She inspires me to rise above and look outside of myself. She continues to add dimensions to my life that I never thought were possible. She has supported me, and continues to do so, in ways that belie written description. Leslie, I truly love you more than words can tell.

Leslie and I have a new addition to our lives. She arrived right before I defended this dissertation. Her name is Megan Hewitt Abrams. When she was born, she put it all in perspective for me. This dissertation is dedicated to Megan.

I am very grateful for the U.S. Environmental Protection Agency STAR Graduate Fellowship (U 914715-01-2) that allowed me to focus on my research. The work reported in this dissertation was also supported by grants to Keith Loague from the National Science Foundation (EAR-9506467-001), the Western Region Hazardous Substance Research Center (SU95-5), and the California Center for Water and Wildland Resources (SA6070). The computing facilities used in this study were provided by an equipment grant to Keith Loague and Steve Gorelick from the National Science Foundation.

TABLE OF CONTENTS

Abstract iv

Acknowledgments vi

Table of Contents xi

List of Tables xv

List of Figures xvi

Chapter 1: Introduction 1

Objectives of the Dissertation 2

Occurrence of Redox Zones 5

Simulation of Redox Zones 8

Characteristics of the Desirable Model 8

Current Modeling Approaches 8

Microbiologically-based models 8

Geochemically-based models 9

The best of both worlds 12

Cape Cod Field Site 15

Groundwater Chemistry at the Cape Cod Site 20

Sewage Contamination and Geochemical Zones at the Cape Cod Site 20

Treatment of Various Model Components 24

Reaction Rates 24

Iron Reduction 24

Dissolved Organic Carbon 26

Organization of the Dissertation 27

Chapter 2: Development and Testing of a Reaction Network Model for Redox Zones in Contaminated Aquifers 30

Abstract 30

Introduction 31

Redox Zonation 32
Simulation Approaches 35
Model Development and Applications 36
Chemical Reactions 36
Compartmentalized Approach 41
Description 41
Test problem 44
Application of the compartmentalized approach to the test problem 46
Kinetic Framework 50
Description 50
Incorporation of the compartmentalized approach 57
Discussion 60
Impact of Cut-Off Value 60
Impact of Site-Specific Geochemical Assumptions 61
Comparison with Field Observations 62
Simultaneous Occurrence of Redox Reactions 64
Conclusions 65
Chapter 3: Incorporation of a Compartmentalized Reaction Network Model into a Solute Transport Framework for the Development of Redox Zones at Field Scales 67
Abstract 67
Introduction 69
The Cape Cod Site 71
Simulation Approaches 72
Theory 74
Geochemistry 74
Solute Transport 81
Computational strategy 81
Kinetic species 84

Linkage 86
Flow chart of the model structure 88
Elimination of Transport Equations 92
Testing of the Compartmentalized Solute Transport Model 94
One-Dimensional Simulation 94
Two-Dimensional Simulation 100
Motivation 100
Problem setup 102
Simulation results 107
Application and Results 114
One-Dimensional Simulation 115
Two-Dimensional Simulation 121
Motivation 121
Problem setup 122
Simulation results 127
Discussion 135
Implications of the Thermodynamic Inhibition Mechanism 135
Implications of the Simplified Reaction Network 137
Alternative Organic Carbon Sources 139
Carbon Limited System? 140
Conclusions 142
Chapter 4: Future Directions 144
Introduction 144
Additional Reactions 145
Additional Compartments 148
Reacting Complex Organic Compounds 148
Continuing the Development of Redox Zones 151
The Fate of Redox Zones 151
Example 1: A batch geochemical system 152
Example 2: A solute transport system 154

Groundwater Flow and Solute Transport Modeling 155
Chapter 5: Conclusions 159
References 164

LIST OF TABLES

Table 1.1. Summary of redox models in which chemical reactions were coupled with mass transport 16

Table 2.1. Reaction network used to simulate the development of redox zones and evaluate the compartmentalized approach 39

Table 2.2. Equations used for model development 40

Table 2.3. Statistical formulas used to evaluate the compartmentalized approach 51

Table 2.4. Statistical values for two different cut-off criteria 52

Table 3.1. Rate parameters for the one-dimensional simulation used to test the compartmentalized solute transport model 98

Table 3.2. Rate parameters used for the plot-scale, two-dimensional test simulation 105

Table 3.3. Statistical comparison of a compartmentalized batch simulation to the equilibrium test problem described in Chapter 2 117

LIST OF FIGURES

Figure 1.1. Map of the Cape Cod field site showing the extent of sewage contamination 17

Figure 1.2. Cross-section showing oxygen concentrations 22

Figure 1.3. Cross-section showing dissolved iron concentrations 22

Figure 1.4. Concentration versus depth profiles showing the redox zones at the Cape Cod site 23

Figure 2.1. Conceptual illustration of the redox zones in a vertical slice down the long profile of the plume at the Cape Cod site, oriented along a hypothetical flow plane 34

Figure 2.2. Schematic representation of the compartmentalized approach 43

Figure 2.3. Distribution diagram generated without reaction compartmentalization 45

Figure 2.4. Comparison of a 1% cut-off with the results in shown Figure 2.3 49

Figure 2.5. Scatter plots comparing the compartmentalized approach with the approach in which all reactions are used in each redox zone 53

Figure 2.6. Development of redox zones and distribution of redox-sensitive species as a function of time 59

Figure 3.1. Two-part flow chart illustrating how the compartmentalized solute transport model operates 89

Figure 3.2. Concentration profiles for the one-dimensional test simulation..... 95

Figure 3.3. Boundary-value problem for the plot-scale, two-dimensional compartmentalized solute transport simulation 106

Figure 3.4. Plot-scale, two-dimensional simulation results at 2.8 years of simulation time 108

Figure 3.5. Concentration profiles for the one-dimensional, field-scale simulation 118

Figure 3.6. Boundary-value problem for the field-scale, two-dimensional compartmentalized solute transport simulation 124

Figure 3.7. Cross-section showing hydraulic head (m) and flow lines 126

Figure 3.8. Field-scale, two-dimensional simulation results at 1.9 years of simulation time 128

Figure 4.1. Conceptual model of the breakdown of complex organic matter into smaller organic compounds and CO_2 150

CHAPTER 1

INTRODUCTION

Contamination of groundwater resources poses a serious threat to the health of the general public. A major goal of hydrogeologists is to develop an understanding of the physical and chemical processes that control the fate and transport of hazardous substances in the subsurface. As that understanding grows, predictions of contaminant fate and decisions related to remediation can be made on an ever-firmer theoretical basis.

The focus of this dissertation is to contribute to a fundamental understanding of the development of redox zones in contaminated aquifers. The general approach is to use numerical simulation as a tool to test hypotheses. The two particular, overall questions asked are the following: Can models that couple (i) groundwater flow, (ii) solute transport, and (iii) microbially-mediated geochemical reactions simulate the development of redox zones as observed in the field? If widely available, "off-the-shelf" models cannot readily perform the task, what modifications are needed? The requirements to be imposed upon the complete simulation approach are that all three model components (i.e., groundwater flow, solute transport, and geochemical reactions) must be process-

based, described by the appropriate and complete mathematics, and solved rigorously.

Process-based descriptions of groundwater flow, solute transport, and geochemical reactions and techniques for solving the equations that arise from them are well known when these processes are considered separately. However, separate consideration of these processes is insufficient for describing redox zone development because the zones develop as a consequence of the interaction of the processes. Numerical difficulties that are more easily handled when the processes are considered separately present major challenges when they are coupled together. Rate-limited, competing reactions are key in redox zone development yet currently available methods either use empirical approaches to control competing reactions or inappropriately impose thermodynamic equilibrium on competing reactions

Objectives of the Dissertation

This study was motivated by observations that were made at the field scale. Redox zones, which are often delineated by the relative concentrations of dissolved oxygen, have been observed around the globe. The distribution of other redox-sensitive species is also affected by redox zonation. For instance, zones of high concentrations of dissolved iron have been observed in settings where no external source of dissolved iron exists. This is particularly true at the

U.S. Geological Survey's Cape Cod research site, where an anoxic zone that contains high concentrations of dissolved iron has been observed. At the Cape Cod site, the iron zone has sharp boundaries, i.e., the edges of the iron zone have very large concentration gradients.

The driving question posed in this dissertation is: How did the iron zone in the Cape Cod site aquifer form? It is not sufficient to simply apply commonly known ideas to this question in a qualitative manner. For example, in quantifying the processes that led to the formation of the iron zone, it becomes apparent that there is a network of reactions that are interdependent and that this reaction network is greatly influenced by groundwater solute transport.

To simulate quantitatively the development of the iron zone, it is first necessary to simulate the development of the redox zones that precede it. The temporal and spatial scales of this simulation problem can be quite large. It is my opinion that by asking certain germane questions about the solute plume, and, in particular the redox zones, the overall problem can be made much more tractable without losing the essence of the original, motivating question. To this end, select questions related to the evolution of the contaminant plume at the Cape Cod site are asked and answered within this dissertation. The overall objective of this effort is to test hypotheses and develop concepts related to the development of redox zones. Along these lines, the dissertation is divided into three parts; (i) development of a new method to solve the thermodynamic/kinetic reaction network that describes redox zone

development, (ii) incorporation of the new method into a solute transport framework, and (iii) a discussion of potential extensions and future directions related to (i) and (ii).

After an introduction that includes a discussion of the occurrence of redox zones, current approaches to modeling redox zone development, a general description of the Cape Cod field site, the treatment of various components of modeling techniques used in this dissertation, and a detailed description of the organization of this dissertation, the following questions are asked:

- What chemical reactions are responsible for the existence of the redox zones at the Cape Cod site?
- Are all the chemical reactions rate limited?
- What is the impact of considering only the major, or primary, reactions?
- How does one solve the thermodynamic/kinetic reaction network?
- What are some of the issues related to solving the reaction network when it is coupled to a solute transport simulator?
- What causes the anoxic zone to occur downgradient from the source instead of immediately adjacent to the source?
- Does the proposed reaction network explain the changes in *p*H, alkalinity, and concentrations of redox-sensitive constituents that are observed along a flow path?

- Do the simulation results support the idea that the Cape Cod redox system is organic carbon limited?
- What can be gained by going to two dimensions?
- Is the suboxic transition zone that is located above and below the anoxic zone a result of hydrogeology, chemistry, or both?

Occurrence of Redox Zones

Redox zones have been recognized in many aquifers, both pristine and contaminated, throughout the world [*Baedecker and Back*, 1979a, b; *Champ et al.*, 1979; *Edmunds et al.*, 1982, 1984; *Jackson and Patterson*, 1982; *Barcelona et al.*, 1989; *Lyngkilde and Christensen*, 1992; *Baedecker et al.*, 1993; *Bennett et al.*, 1993; *Eganhouse et al.*, 1993; *Cozzarelli et al.*, 1994; *Lovley et al.*, 1994; *Abrams et al.*, 1998]. The zones result from the oxidation of organic carbon coupled to a sequence of inorganic oxidants. The dominant oxidant under any particular geochemical condition is the one that yields the greatest free energy change per mole of organic carbon oxidized [*Champ et al.*, 1979; *Froelich et al.*, 1979]. As each oxidant is depleted, the next most efficient oxidizer is used until there is no more organic carbon or oxidants remaining.

Unconfined aquifers are clearly more vulnerable to anthropogenic contamination than confined aquifers, because of their proximity to contamination sources such as landfills. Solid and liquid industrial and

municipal refuse is frequently disposed in landfills, and leachate plumes that emanate from landfills are typically high in organic carbon. In their study of such a landfill in Delaware, *Baedecker and Back* [1979a, b] noted that high concentrations of dissolved iron and manganese can be attributed partially to metals in the refuse, but more importantly to the reduction of naturally-occurring oxide cements and coatings resulting from the degradation of organic matter. *Baedecker and Back* also distinguished between a regional oxygenated zone, an anaerobic zone, and an intermediate zone; deposition of Fe oxyhydroxides at the interface of the anaerobic and transition zone was noted.

Edmunds et al. [1984] did a comparative study of three aquifers in England. They described redox "barriers" in which there was no dissolved oxygen beyond the barrier. They postulated an iron zone between the redox barrier and the appearance of sulfide.

In a study of agricultural contamination, *Postma et al.* [1991] observed a sharp boundary between oxic groundwater and anoxic groundwater. They also noted that nitrate disappeared at this boundary and dissolved Fe(II) was only present below the boundary. The boundary was relatively stable in time and space; this stability is no doubt a consequence of the interaction of flow rate and reaction rates.

Recent work at the site of a crude oil spill in Bemidji, MN described the relationship between redox zones and the degradation of hydrocarbons [*Baedecker et al.*, 1989, 1993; *Bennett et al.*, 1993; *Cozzarelli et al.*, 1994; *Eganhouse et*

al., 1993]. Three distinct geochemical zones at Bemidji are the result of the presence of an oil body; the (i) anoxic zone, (ii) suboxic transition zone , and (iii) oxic zone. Concentrations of dissolved Fe(II) are high in the anoxic zone (e.g., 17 mg L^{-1}) because reduction of Fe(III) is coupled to the oxidation of organic compounds emanating from the oil body. Sulfate reduction occurs but is minor, because there is little sulfate available. Methanogenesis occurs once Fe(III) and Mn(IV) on aquifer solids have been depleted. The extent of the anoxic/iron zone appears to be limited by precipitation of Fe-rich carbonates [*Baedecker et al.*, 1993]. *Baedecker et al.* concluded that Fe(III) is an important oxidizer of organic compounds (e.g., toluene, among others) under anaerobic conditions. Naphthalene did not degrade under anaerobic conditions in microcosm experiments that they performed, while it did degrade under aerobic conditions.

Bjerg et al. [1995] applied the concept of redox zonation to an aquifer contaminated by a landfill. They developed a "redox criteria scheme" that enabled them to assign a "redox status" to groundwater analyses and thus plot boundaries between the different redox zones on a vertical cross section of the contaminated aquifer. The criteria were based largely upon thermodynamic considerations. More than 90% of the groundwater samples from each zone satisfied the criteria. *Bjerg et al.* did note, however, that there was some overlap between some of the zones.

Simulation of Redox Zones

Characteristics of the Desirable Model

Considering the complex interactions outlined above, the primary goal of this dissertation was to develop a model that treats the fundamental model components in a process-based manner. In nature, reaction rates and reaction feasibility are determined by local geochemical conditions. Accordingly, the model to be developed for this study should:

- Use thermodynamics to control reaction feasibility.
- Use kinetics to control reaction progress.
- Have the flexibility for competing redox reactions to be either kinetically- or thermodynamically-inhibited.
- Not use a redox variable (*e.g.*, *p*E).
- Not be limited to any particular kinetic formulation.
- Have the ability to easily simulate complex fluid flow and solute transport in more than one dimension.
- Treat solute transport as advection and dispersion.

Current Modeling Approaches

Microbiologically-based models

Many models have been developed in an effort to characterize and simulate solute transport coupled with either biodegradation, redox processes, or

general chemical reactions. Most of the models that address redox problems focus on biodegradation; *Essaid et al.* [1995] provide an excellent review. With models of this type, when more than one substrate or more than one biogeochemical process is involved, an empirical inhibition factor [*Kindred and Celia*, 1989; *Essaid et al.*, 1995], a switching function [*Kinzelbach et al.*, 1991; *Schäfer and Therrien*, 1995], or an indicator coefficient [*Smith and Jaffé*, 1998] is needed. These parameters inhibit a reaction that yields a lower free energy change from occurring in the presence of a reaction that yields a higher free energy change. For example, denitrification is inhibited by the presence of appreciable dissolved oxygen.

While empirical approaches to reaction inhibition may seem to satisfy the thermodynamic criteria (i.e., free energy constraints), there is no theoretical basis for calculating them; they are fitting parameters. If one writes out the complete chemical reaction for one or more biodegradation processes, the free energy change associated with each reaction (i.e., the equilibrium constant) will dictate which reactions are feasible under which chemical conditions and no inhibition factors or switching functions are required. In addition, the concentrations of reaction products, as well as reactants, can be easily calculated.

Geochemically-based models

All processes that lead to structural changes in chemicals, whether inorganic, organic-abiotic, or organic-biotic, can be described by chemical

reactions [*Valentine*, 1986a, b]. This is true for biologic reactions that result in organism growth as well as those that do not. For example, balanced chemical reactions involving pairs of electron acceptors and electron donors can be written that represent (i) energy release and (ii) cell synthesis [*McCarty*, 1975]. The energy released from these reactions, and the fraction of the energy that is available for cell synthesis, can be calculated using thermodynamics [*McCarty*, 1971; *McFarland and Sims*, 1991]. Reaction direction and cell and energy yields can also be calculated using thermodynamic principles [*McCarty*, 1971; *McFarland and Sims*, 1991].

Even though the energy released by biogeochemical reactions can be quantified using thermodynamics, the microbiologically-based simulation approaches do not use this information to control reaction feasibility. The microbial population and the chemical reactions that dominate in a given situation are functions of the amount of Gibbs free energy that can be liberated via chemical reactions. The more free energy released by a reaction, the higher the substrate consumption efficiency of the microbial population that is catalyzing the reaction. The geochemically-based modeling approaches take advantage of this information to decide automatically which redox reactions should occur under which geochemical conditions. In this manner, they avoid empirical methods of reaction inhibition.

In addition to providing information about reaction feasibility, important chemical properties, such as the solubility of solid phases and gases, the

speciation of ions, and the equilibrium *p*H are all determined by, and can be calculated via, the principles of thermodynamics. While seemingly obvious, this idea is important and worth reiterating because it provides a means to understand processes and simulate issues related to groundwater contamination and quality. For example, there is an important, incontrovertible link between the inorganic and organic chemistry of both contaminated and pristine groundwater [e.g., *Furrer et al.*, 1990; *McNab and Narasimhan*, 1994, 1995; *Essaid et al.*, 1995]. Microbial oxidation of organic carbon can result in changes in *p*H and alkalinity, which in turn affects the stability of solid phases and speciation of dissolved metals and other ions. Conversely, the availability of inorganic species, such as oxygen, nitrate, ferric iron, and sulfate, can inhibit or promote microbial oxidation of organic carbon.

As another example of the applicability of thermodynamics to biogeochemical systems, consider iron and sulfate reduction. Dissolved iron in groundwater is a major groundwater quality issue. Under many circumstances, high concentrations of dissolved iron can only occur if there is little or no sulfate reduction, because ferrous iron can react with sulfide to form solid phases [*Chapelle and Lovley*, 1992]. If the causes of iron and sulfate reduction are microbial, sulfate reduction is only observed after ferric iron is depleted. This is due to competition for fermentation products (e.g., acetate, formate, and hydrogen) that both iron reducers and sulfate reducers require for metabolism. The iron reducers out-compete the sulfate reducers for the fermentation products

because iron reduction releases a greater amount of energy than sulfate reduction [*Chapelle and Lovley*, 1992]. Even though the reactions discussed above and other processes of concern, such as the biodegradation of synthetic organic compounds, are rate-limited, thermodynamics provides a framework for understanding the feasibility and consequences of any biogeochemical reaction.

The best of both worlds

The microbiologically-based and geochemically-based modeling approaches outlined above both offer advantages. The microbiological approach offers conceptual advantages because the dominant processes are modeled as the rate-limited, biological processes that they are. The geochemical approach has the advantage of using the free energy information provided by thermodynamics to control reaction feasibility and calculate the changes in geochemistry that result from the reactions. Because each approach offers certain advantages, it is beneficial, from a simulation perspective, to combine aspects of each approach into the single model developed for this dissertation. The approach taken here is to insert the rate-limited formulations of the microbiological approach into the thermodynamic framework provided by the geochemical approach. To do this, two major hurdles related to the geochemical approach needed to be overcome.

The first hurdle in applying the combined thermodynamic/kinetic approach is related to the large difference in free energy changes associated with the dominant redox reactions. This problem is avoided in the microbiological

approach because empirical reaction inhibition is used instead of thermodynamics to decide reaction feasibility. The large range in free energy changes for the different redox reactions translates to equilibrium constants that span tens of orders of magnitude. This in turn leads to a range of concentrations that also spans tens of orders of magnitude. The large differences in concentrations lead to extremely ill-conditioned Jacobian matrices when the commonly used Newton-Raphson numerical scheme is employed.

Most geochemical codes do not solve for the concentration of complexed species (i.e., non-component species) within the Newton-Raphson solver. Instead, complexed species can be calculated simply as a function of a component set. The only requirement for a component set is that it is linearly independent. Techniques such as basis switching [e.g., *Lichtner*, 1992; *Bethke*, 1996; *Steefel and Yabusaki*, 1996] can be used to eliminate some of the numerical problems. Basis switching works by eliminating components whose concentrations become very small. When a component is eliminated, a new component must be added to form a different linearly independent set of components. A new component set means that the chemical reactions that form the species set must be re-written in terms of the new components.

While basis switching is not difficult to do computationally, there is a major drawback of this technique when the geochemical code is coupled to a solute transport code. If basis switching is to be used, each and every chemical species must have its own transport equation. The number of chemical species in

a typical field problem can become quite large, easily exceeding fifty or more species.

If basis switching is not used (i.e., the component set remains fixed), then it is possible to greatly reduce the number of solute transport equations needed to simulate a particular system by making the components the dependent variables in the transport equations, rather than each chemical species. The concentration of the equilibrium species can be easily calculated outside of the solute transport simulator, since they are simply functions of the component set. The compartmentalized approach developed for this dissertation facilitates the use of a fixed component set by using reaction networks that do not contain insignificant reactions. Each aqueous kinetic species must still have its own solute transport equation.

The second hurdle in applying the combined thermodynamic/kinetic approach is the more significant challenge. Most geochemical codes do not have the ability to simulate kinetics. Those that do have kinetic capabilities impose thermodynamic equilibrium on all competing redox reactions. The code developed for this study has the ability to apply either a rate-limited or thermodynamically-limited solution to the redox systems considered in this study.

Three of the models reviewed in Chapter 3 are capable of simulating some form of a rate-limited process. The rate-limited processes in these models produce reactants that are then distributed among a separate set of equilibrium

reactions. The three models are (i) KEMOD [*Yeh et al.* 1998], (ii) the *Parkhurst and Appelo* [1997] model, and (iii) the model of *Keating and Bahr* [1998]. No model that I am aware of is capable of simulating multiple, competitive, kinetic reactions that are subject to kinetic and thermodynamic constraints.

The models that are available constrain the user to calculating the competition between redox reactions based on either (i) thermodynamics only or (ii) kinetics only (i.e., empirical reaction inhibition). I am unaware of any model that addresses the question of whether the lower-energy redox reaction (i.e., the loser in the thermodynamic competition) is rate-limited. Table 1.1 provides a summary of previous work that has coupled redox reactions with models of solute transport and illustrates key differences between them and the simulation protocols developed for this dissertation.

Cape Cod Field Site

The Cape Cod site has been a major focus of research for the U.S. Geological Survey for more than fifteen years. It is currently part of the Toxic Substances Hydrology Program [e.g., *Morganwalp and Aronson*, 1996]. The site is located on the western part of Cape Cod, Massachusetts (Figure 1.1). It is situated on a Pleistocene age glacial outwash plain composed mainly of sand and gravel. The upper 25-40 m of the aquifer is composed of well sorted, medium to very coarse sand with some gravel, underlain by fine to very fine sand and silt.

Table 1.1. Summary of redox models in which chemical reactions were coupled with mass transport, showing how this work differs from previous efforts.

Reference	Organic-Inorganic Link	Redox Variable Used	General Reaction Kinetics	Spatial Dimensions	Lower-Energy Redox Reactions Treated as Kinetic or Equilibrium	Thermodynamic Reaction Inhibition (with kinetics)
László and Székely [1989]		X		2		
Liu and Narasimhan [1989a; b]		X		2		
Postma et al. [1991]		X		1		
Yeh and Tripathi [1990, 1991]		X		2		
Engesgaard and Kipp [1992]		X		1		
Lensing et al. [1994]	X		X	1		
McNab and Narasimhan [1994]	X	X	X	2		
Walter et al. [1994a; b]		X		2		
Schäfer and Therrien [1995]	X		X	3		
Yeh and Salvage [1995]		X	X	2		
Furrer et al. [1996]	X		X	1		
Lee [1996]	X	X		1		
Van Cappellen and Gaillard [1996]	X		X	1		
Wunderly et al. [1996]		X		2		
Parkhurst and Appelo [1997]	X	X	X	1		
Keating and Bahr [1998]		X		2		
This work	**X**		**X**	**2**	**X**	**X**

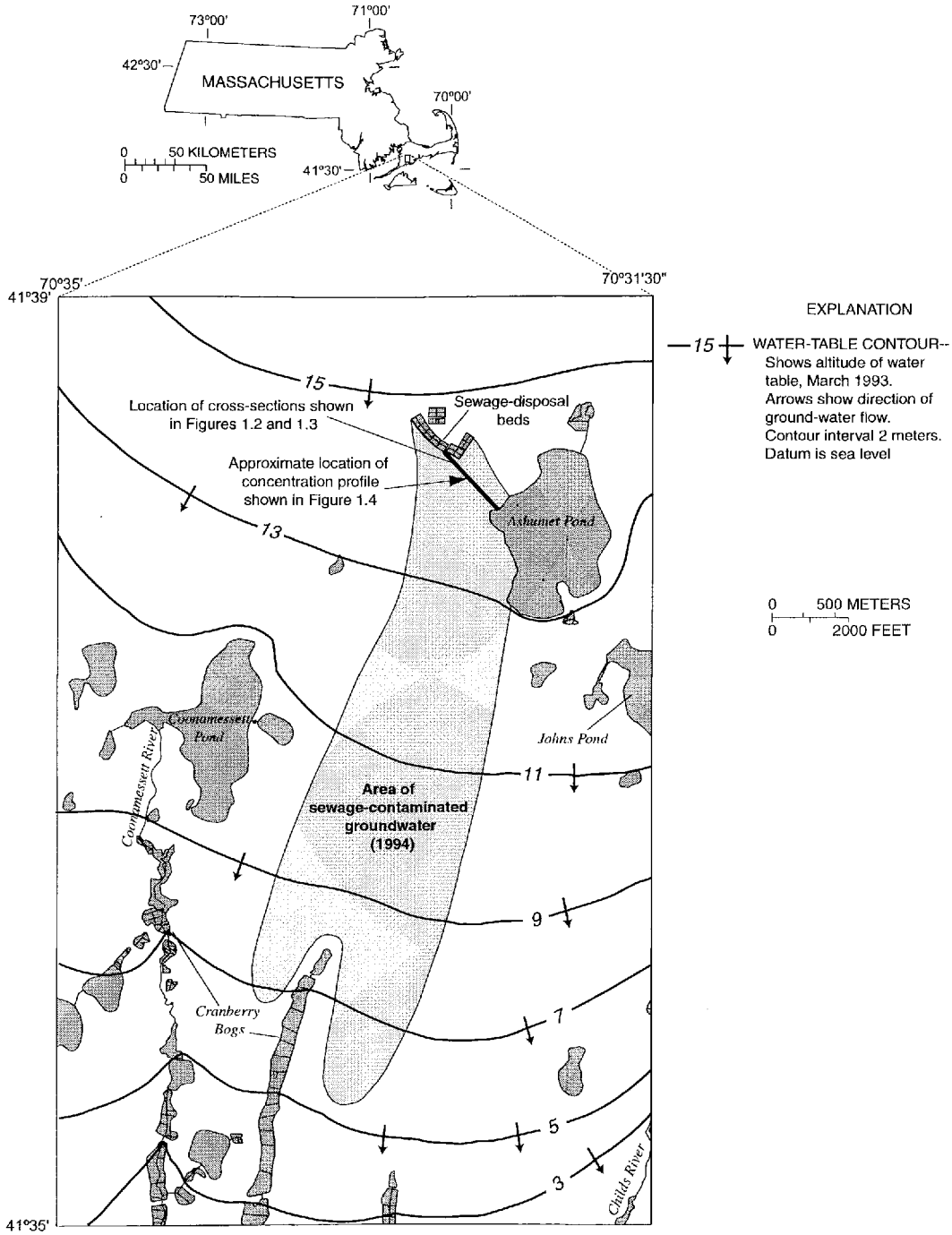

Figure 1.1. Map of the Cape Cod field site showing the extent of sewage contamination. The location of the redox zones that motivated this dissertation (see Figures 1.2 and 1.3) is between the sewage-disposal beds and Ashumet Pond. The location of the concentration versus depth profiles illustrated in Figure 1.4 is also shown. Modified from *Hess et al.* [1999].

The outwash typically contains less than 1% silt and clay [*Barber*, 1987]. The sediments are composed roughly of 90% quartz and feldspar and 10% accessory minerals like mica, glauconite, iron oxides, and ferromagnesian aluminosilicates [*Barber*, 1987; *LeBlanc et al.*, 1991]. Most sediment grains are coated with Fe, Al, and Mn hydroxypolymers [*Coston et al.*, 1995].

Groundwater at the Cape Cod site occurs under unconfined conditions. The water table slopes generally to the south and southwest except where influenced by ponds. The only natural source of recharge to the aquifer is precipitation; recharge is approximately 45% of the total annual precipitation, or about 0.5 m yr^{-1} [*LeBlanc et al.*, 1986]. The elevation of the water table fluctuates on average about 1 m annually due to seasonal variations in recharge and precipitation [*LeBlanc et al.*, 1991]. Groundwater flow is essentially horizontal and the average linear velocity of the groundwater in the sand and gravel is 0.41 m d^{-1} [*LeBlanc et al.*, 1991].

The mean saturated hydraulic conductivity (K) for the Cape Cod site has been estimated by several methods. Grain size distribution and computer model calibration yielded values for K of 5×10^{-4} m s^{-1} to 1.1×10^{-3} m s^{-1} [*LeBlanc*, 1984a, b; *Guswa and LeBlanc*, 1985]. An aquifer test 2.2 km downgradient from the site of a large-scale natural gradient tracer test gave a mean horizontal K of 1.3×10^{-3} m s^{-1} and a ratio of horizontal to vertical K varying from 2:1 to 5:1 [*Garabedian et al.*, 1988]. Borehole flowmeter tests and permeameter tests indicated that K varies by about one order of magnitude [*Wolf*, 1988; *Hess*, 1989;

Rehfeldt et al., 1989; *Wolf et al.*, 1991]. The variability in K is due to the interbedded lenses and layers of sand and gravel that characterize the glaciofluvial deposit [*LeBlanc et al.*, 1991]. The small value of vertical anisotropy in K obtained from the above aquifer test is consistent with the anisotropy value used in a three-dimensional groundwater flow model for the Cape Cod aquifer [*Guswa and LeBlanc*, 1985].

The effective porosity at the Cape Cod site as estimated from several small-scale tracer tests [*Barlow*, 1987; *Garabedian et al.*, 1988; *LeBlanc et al.*, 1991] and spatial moments analysis from the large-scale tracer test [*Garabedian et al.*, 1991] is 0.39. Spatial moments analysis from the large-scale tracer test also yielded values of longitudinal dispersivity of 0.96 m, horizontal transverse dispersivity of 1.8×10^{-2} m, and vertical transverse dispersivity of 1.5×10^{-3} m [*Garabedian et al.*, 1991]. Similar values were also obtained by applying stochastic transport theories to the large-scale tracer test data [*Hess et al.*, 1992].

The Cape Cod site sewage treatment facility has provided secondary treatment to sewage produced at the Otis Air National Guard Base since 1936. The treated sewage is discharged to rapid-infiltration sand beds, which has given rise to a plume of sewage-contaminated groundwater that is now about 5500 m long, 1300 m wide, and 40 m thick [*Savoie and LeBlanc*, 1998]. Recharge from precipitation results in a wedge of pristine groundwater on top of the sewage plume that increases in thickness with distance downgradient [*LeBlanc et al.*, 1991].

Groundwater Chemistry at the Cape Cod Site

The uncontaminated groundwater at the Cape Cod site is low in dissolved solids because the aquifer is composed of sand and gravel that is predominantly quartz and feldspar derived from crystalline bedrock. The alkalinity of the groundwater is low due to the absence of carbonate minerals [*LeBlanc*, 1984a]. The *p*H is typically about 5.5, reflecting that the uncontaminated groundwater is derived from rain water that has equilibrated, or nearly equilibrated, with $CO_2(g)$ in the unsaturated zone and subsequent weathering reactions [*Lee*, 1997].

Analysis of groundwater samples collected at the Cape Cod site in 1978 and 1979 showed that the concentrations of most dissolved substances in the plume are intermediate between the concentrations in the treated sewage and the concentrations in the uncontaminated groundwater [*LeBlanc*, 1984a]. Samples collected in 1994 indicated that many conservative constituents have similar concentrations in both the plume and the sewage effluent [*Savoie and LeBlanc*, 1998].

Sewage Contamination and Geochemical Zones at the Cape Cod Site

Sewage contamination at the Cape Cod site has led to the development of distinct geochemical zones. Groundwater chemistry in these zones is strongly influenced by redox reactions. The zones extend horizontally downgradient from the contamination source and vertically down from the water table. These

zones are (i) the oxic zone, (ii) the suboxic zone, and (iii) the anoxic zone. The leading edge of the anoxic zone does not coincide with the leading edge of the sewage plume. Rather, the leading edge of the anoxic zone lies several kilometers upgradient of the leading edge of the sewage plume. Schematically, the sewage plume is like an elongated onion, with an anoxic core surrounded by rinds or layers of suboxic and oxic groundwater (Figures 1.2, 1.3, and 1.4).

Figure 1.4 shows concentration versus depth profiles for several redox-sensitive constituents at a location along the cross-sections shown in Figures 1.2 and 1.3. The left-most panel of Figure 1.4 shows how *p*H varies from pristine groundwater (approximately 5.5) through the sewage plume (peak of approximately 6.5). The sewage plume itself is delineated by the boron profile. The middle and right-most panels show how oxygen, dissolved manganese, dissolved iron, and nitrate vary between the oxic, suboxic, and anoxic zones. Nitrate and dissolved manganese are present in the suboxic zones, where dissolved iron is absent. Nitrate is absent in the anoxic zone, where dissolved manganese and dissolved iron are present at elevated concentrations. The general topology of Figure 1.4 has also been observed wherever the anoxic zone is present in the area covered by Figures 1.2 and 1.3 [*D. B. Kent*, personal communication, 1997].

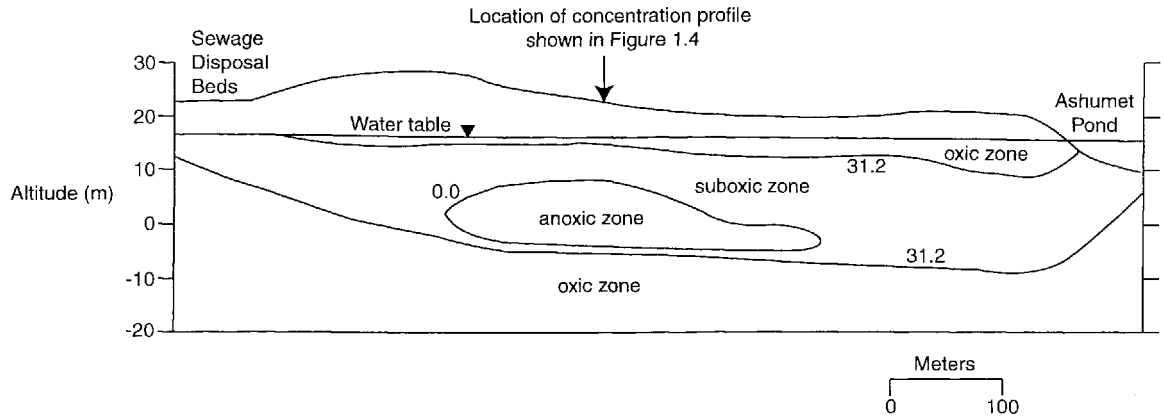

Figure 1.2. Cross-section showing oxygen concentrations. The location of the concentration versus depth profile depicted in Figure 1.4 is also shown. The concentration units are µM. Modified from *Walter et al.* [1996].

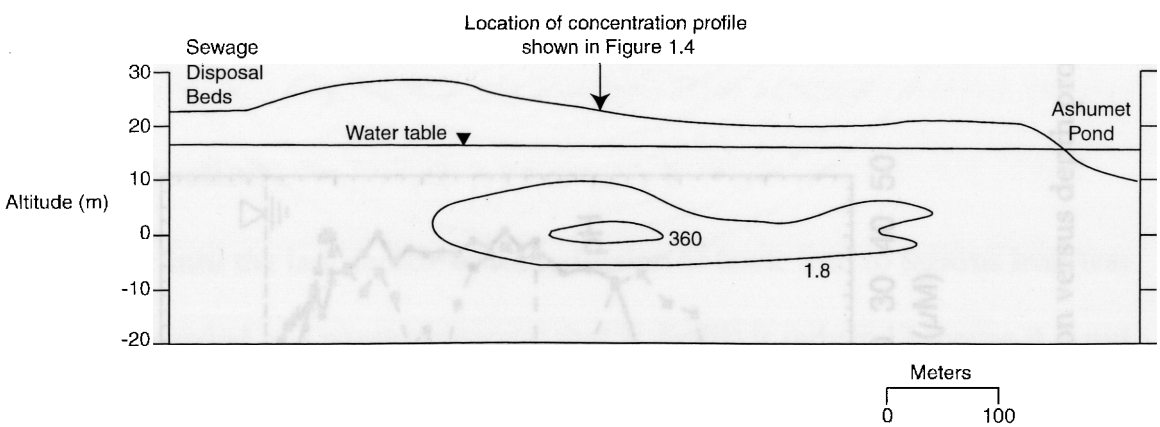

Figure 1.3. Cross-section showing dissolved iron concentrations. The location of the concentration versus depth profile depicted in Figure 1.4 is also shown. The concentration units are µM. Modified from *Walter et al.* [1996].

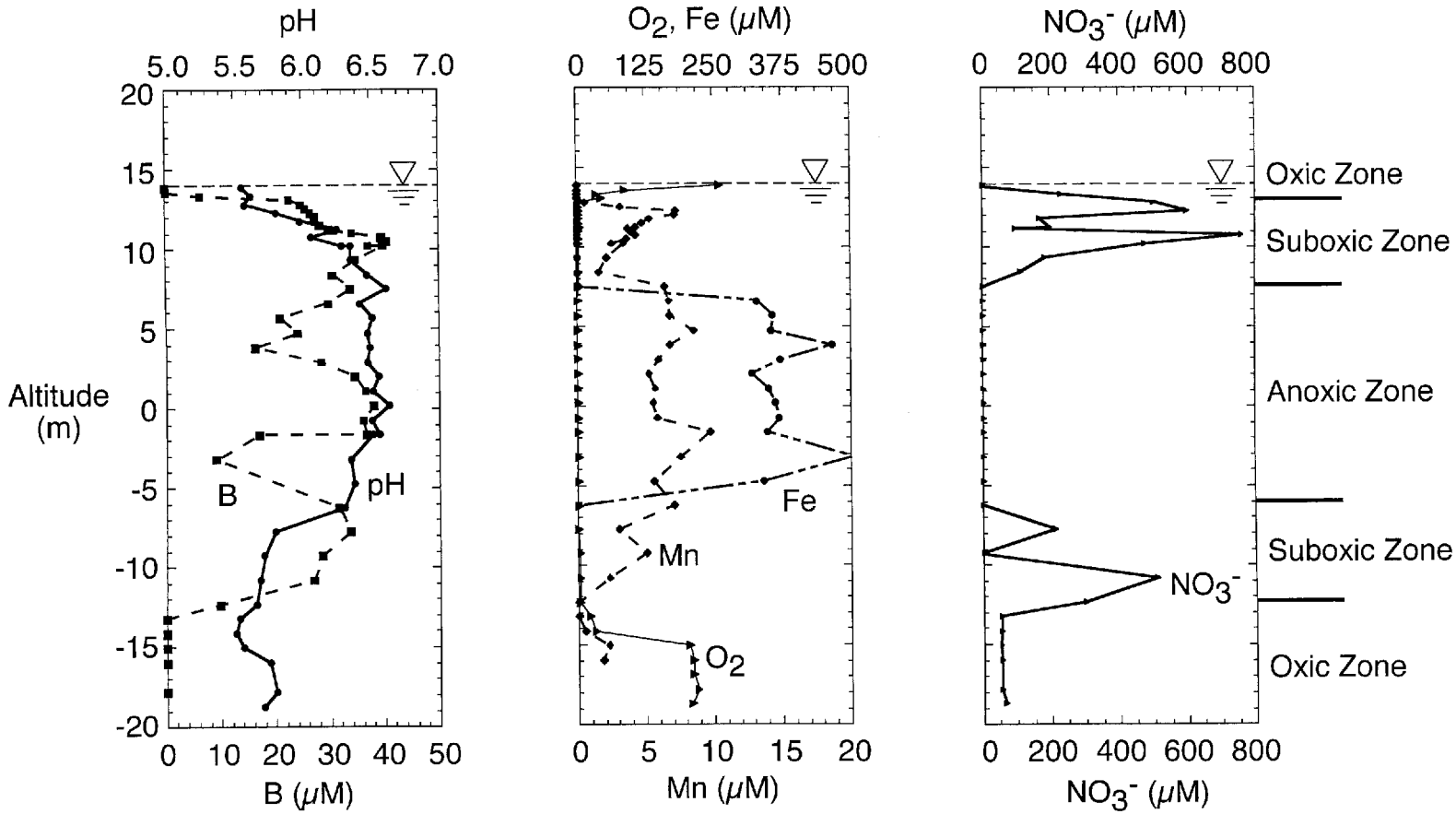

Figure 1.4. Concentration versus depth profiles showing the redox zones at the Cape Cod site. Modified from *Kent et al.* [1994].

Treatment of Various Model Components

Reaction Rates

Thermodynamic theory and field observations show that there are several different electron acceptors available in most aquifers to couple to the oxidation of organic carbon. In most cases, different populations of microbes catalyze organic carbon oxidation reactions with different electron acceptors. Thus, each redox reaction potentially has different rate parameters. In addition, the rate and extent of biodegradation depends upon the type and quantity of electron acceptor [*Vroblesky and Chapelle*, 1994; *Borden et al.*, 1995]. There is a considerable body of literature with regard to degradation rates of various organic substrates mediated by various microorganisms [e.g., *Vogel et al.*, 1987; *Mihelcic and Luthy*, 1988a, b; *Beller et al.*, 1992]. For the effort reported here, representative rate expressions and constants were needed.

Iron Reduction

Up until the last decade or so, reduction of ferric iron to ferrous iron was usually regarded as a passive process; that is, Fe(III) is reduced because it is out of equilibrium with the redox potential of the groundwater [e.g., *Back and Barnes*, 1965; *Edmunds et al.*, 1987]. For instance, if sulfate reduction were occurring in an aquifer, the redox potential would be low enough, based upon thermodynamics, for Fe(III) to be reduced to Fe(II). The redox potential in this case would be too

low for Fe(III) to be the stable form of iron. However, it is now known that iron reducing microorganisms exist that can completely mineralize certain organic compounds [*Arnold et al.*, 1986, 1988; *Lovley et al.*, 1989, 1994; *Lovley and Lonergan*, 1990; *Lovley*, 1991, 1993; *Baedecker et al.*, 1993; *Cozzarelli et al.*, 1994]. The iron reducers produce stoichiometric amounts of Fe(II) as a byproduct of the oxidation of organic carbon. *Lovley* [1991] identified a species of bacteria that gains energy for growth by coupling the oxidation of acetate to the reduction of ferric iron. *Lovley* isolated the bacteria and has written stoichiometric reactions for the complete process. *Arnold et al.* [1986, 1988] have observed reductive dissolution of ferric iron solid phases by a different microbe.

Despite the strong evidence that microbial mediation is the dominant mechanism for ferric iron reduction, abiotic reduction of ferric iron, at least under sulfate-reducing conditions, cannot be neglected. In a study of toluene degradation, *Beller et al.* [1992] found that ferric iron reduction was not directly coupled to toluene degradation, but was most likely an abiotic reaction between ferric iron and biogenic hydrogen sulfide. In addition, *Cozzarelli et al.* [1995] found that ferric iron dissolution occurred in sterile controls in some of their microcosm experiments. *Cozzarelli et al.* theorized that the most likely mechanism was the abiotic reductive dissolution of amorphous ferric iron by sulfide.

Dissolved Organic Carbon

In the majority of circumstances, dissolved organic carbon (DOC) is a complicated mixture of compounds with varying degrees of reactivity. However, field data are frequently reported as a single value, giving the composite concentration of all the DOC. When the reported DOC concentration is consistently low across a study area, it is likely that it is a highly recalcitrant, naturally occurring fraction [*Essaid et al.*, 1995]. One approach to dealing with the complexity of DOC is to assume representative compounds as surrogates for broad classes of, say, organic acids. *Furrer et al.* [1990] used oxalic acid to represent strong organic acids that dissociate readily to form stable complexes and acetic acid for those that do not form stable complexes. To include a recalcitrant fraction of DOC, *Furrer et al.* [1990] included ten moles of "inert" DOC for every mole of "active" DOC, based on the difference between the average charge density of naturally occurring DOC and that of acetate and oxalate.

For this dissertation, all the reactive DOC was lumped together and defined as the chemical entity "CH_2O". Thermodynamic data for the chemical entity "CH_2O" were taken from *Morel and Hering* [1993]. The use of "CH_2O" and its thermodynamic data is not meant to imply that such a compound is actually present in the aquifer at the Cape Cod site. "CH_2O" was simply used as a surrogate variable because detailed information about the DOC at the Cape Cod site is lacking.

Organization of the Dissertation

The work described in this dissertation was performed with the goal of submitting individual chapters to scholarly journals. As such, the overall flow of ideas is divided into sections. For example, the reader may find that while reading the description in Chapter 2 of how the thermodynamic/kinetic problem was handled, it is useful to look ahead to Chapter 3 to see a flow chart of the complete model structure. Chapters 2 and 3 are designed to be stand-alone journal articles. The journal article format required that introductory material be placed in Chapters 2 and 3 so that a reader would be able to read either chapter and obtain a general overview of redox zone development and previous simulation efforts.

Chapter 1 is an introduction to the overall effort. It contains material on the general motivation for the study, a review of previous modeling approaches, a discussion of how some basic processes are handled in the modeling approaches developed for this dissertation, and a review of the Cape Cod site on which the simulations within this dissertation were based.

Chapter 2 describes a new methodology, called the compartmentalized approach, that solves the chemical equations describing redox zone development as a function of time and energy yield in a batch system. The new methodology uses thermodynamics to select competing redox reactions. Although chemical equilibrium concepts are quite important, the dominant reactions that were

simulated are mediated by microbes. Therefore, a kinetic framework was imposed on the reactions to account for the rate limitations that are implicit in biological processes. The compartmentalized approach is capable of treating redox reactions as being either thermodynamically-inhibited or kinetically-inhibited. The distinction is made automatically within the model as a function of local geochemical conditions. The description of the combined thermodynamic and kinetic method is accomplished through the use of a relevant example. A slightly modified version of Chapter 2 has recently been published in *Water Resources Research* [*Abrams et al.*, 1998]. I was the lead author of and primary contributor to this paper.

Chapter 3 describes the integration of the compartmentalized approach into a solute transport framework. After an introduction to the chapter, the compartmentalized approach is briefly reviewed and generalized. An alternative formulation for developing the "compartmentalized" equations is presented and then shown to be equivalent to the approach taken in Chapter 2. The equivalent formulation has advantages when the compartmentalized approach is applied within a solute transport framework. The chief advantages are (i) the reduction in the number of solute transport equations that need to be solved and (ii) the elimination of spatial discontinuities in certain solute transport equations that would be caused by the formulation described in Chapter 2. Two one-dimensional simulations are presented. The first is a test simulation that was used during code development. The second is a field-scale

simulation that is representative of conditions at the Cape Cod site. Two two-dimensional simulations are presented in the same spirit as the one-dimensional simulations. A slightly modified version of this chapter will be submitted for journal publication.

Chapter 4 discusses ways in which the method developed in Chapters 2 and 3 can be extended and possible future directions are explored. The extensions include material that is general in nature and material that would enable the model user to perform history matching and predictions at particular sites.

Chapter 5 provides a final summary and presentation of the major conclusions and contributions of this dissertation.

CHAPTER 2

DEVELOPMENT AND TESTING OF A REACTION NETWORK MODEL FOR REDOX ZONES IN CONTAMINATED AQUIFERS

Abstract

The sequential use of various electron acceptors, which is governed by the energy yield of each reaction, gives rise to redox zones. The large differences in energy yields between the various redox reactions lead to systems of equations that are extremely ill-conditioned. These equations are very difficult to solve, especially in the context of coupled fluid flow, solute transport, and geochemical simulations. A general, rational method was developed to solve such systems, where the dominant reactions are focused upon and compartmentalized, in a manner that is analogous to the redox zones that are often observed in the field. The compartmentalized approach allows one to easily solve a complex geochemical system as a function of time and energy yield, laying the foundation for ongoing work in which the reaction network for the development of redox zones is coupled to a model of subsurface fluid flow and solute transport. This new method (i) solves the numerical system without evoking a redox parameter, (ii) improves the numerical stability of redox systems by choosing which

compartment, and thus which reaction network, to use based upon the concentration ratios of key constituents, (iii) simulates the development of redox zones as a function of time without the use of inhibition factors or switching functions, and (iv) can reduce the number of transport equations that need to be solved in space and time. It is shown, through the use of various model performance evaluation statistics, that the appropriate compartment choice under different geochemical conditions leads to numerical solutions without significant error.

Introduction

The work described in this Chapter forms the foundation for the development of a protocol for simulating the development of redox zones in contaminated aquifers; i.e., coupled modeling of fluid flow, solute transport, and geochemical reactions. In this study, the degradation of dissolved organic carbon, occurring via biogeochemical reactions, is focused upon as the driving force for redox zone formation.

Redox reactions that describe organic carbon degradation must be viewed in both an inorganic and organic chemical framework. The process of biodegradation ultimately converts organic carbon to inorganic carbon and changes the oxidation state of many inorganic compounds. This occurs because the active microbes mediate oxidation/reduction (redox) reactions between

organic carbon (electron donor) and various inorganic electron acceptors [*Lovley et al.*, 1994]. These redox reactions involve hydrogen ions, and thus they can affect *p*H. Most of these redox reactions also cause changes in carbonate alkalinity. Changes in the oxidation state of inorganic constituents can cause (i) anoxic conditions, (ii) removal of undesirable inorganic contaminants (e.g., nitrate), (iii) precipitation/dissolution of solid phases, and (iv) changes in toxicity and mobility of many hazardous dissolved metals.

In many aquifers, electron acceptors such as oxygen, manganese oxides, and iron oxyhydroxides are naturally occurring. Electron acceptors such as nitrate, sulfate, and additional dissolved oxygen are introduced to aquifers via anthropogenic contamination and natural aquifer recharge. Other than natural sources, organic carbon is introduced into aquifers either in the aqueous phase or as a nonaqueous phase liquid which subsequently dissolves. Thus, modeling organic carbon degradation in aquifers is a groundwater flow and solute transport problem, in addition to an organic and inorganic chemistry problem.

Redox Zonation

The development of redox zones in aquifers has been discussed by many authors [*Baedecker and Back*, 1979a, b; *Champ et al.*, 1979; *Edmunds et al.*, 1982, 1984; *Jackson and Patterson*, 1982; *Barcelona et al.*, 1989; *Lyngkilde and Christensen*, 1992; *Baedecker et al.*, 1993; *Bennett et al.*, 1993; *Eganhouse et al.*, 1993; *Cozzarelli et al.*, 1994; *Lovley et al.*, 1994]. These studies show that up to five redox zones can

develop: (i) zone of oxygen reduction, (ii) zone of denitrification and manganese reduction, (iii) zone of iron reduction, (iv) zone of sulfate reduction, and (v) zone of methane production. Each zone is a result of oxidation of organic matter by the oxidant that will yield the greatest free energy change per mole of organic carbon oxidized [*Champ et al.*, 1979; *Froelich et al.*, 1979]. When this oxidant is depleted, the next most efficient oxidizer is used until there is no more organic carbon or oxidants left.

Three different redox zones have been identified within the sewage plume at the U.S. Geological Survey's Cape Cod research site in Massachusetts; i.e., oxic, suboxic, and anoxic zones [*LeBlanc*, 1984a; *Kent et al.*, 1994]. It should be pointed out that neither sulfide nor methane have been observed at the Cape Cod site, even though sulfate is present. The anoxic zone at Cape Cod does contain dissolved iron, thus the most relevant redox reactions are oxygen reduction, denitrification, manganese reduction, and iron reduction [*Smith and Duff*, 1988; *Smith et al.*, 1991a; *Kent et al.*, 1994]. The term "suboxic" is applied to the zone of denitrification and manganese reduction because of the persistence of small concentrations of dissolved oxygen. Figure 2.1 is a conceptualization of the redox zones in a vertical slice through a longitudinal profile of the Cape Cod site aquifer, oriented along a hypothetical flow plane.

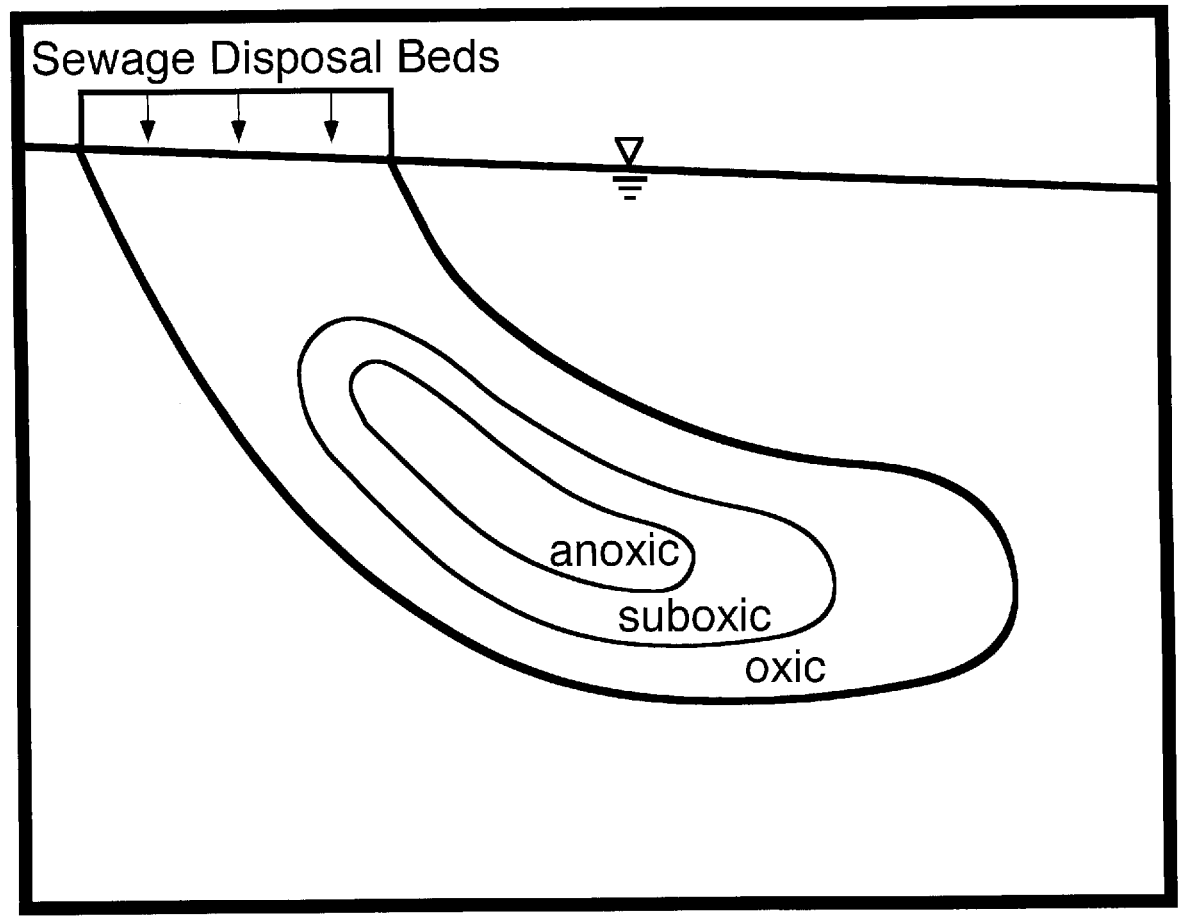

Figure 2.1. Conceptual illustration of the redox zones in a vertical slice down the long profile of the plume at the Cape Cod site, oriented along a hypothetical flow plane.

Simulation Approaches

In theory, the coupling of groundwater flow, solute transport, and geochemical reactions is rather straightforward. Reactive transport models that can include the necessary chemical reactions have been described in the literature [e.g., *Liu and Narasimhan*, 1989a, b; *Yeh and Tripathi*, 1990, 1991; *Engesgaard and Kipp*, 1992; *Lichtner*, 1992; *McNab and Narasimhan*, 1994; *Steefel and Lasaga*, 1994; *Walter et al.*, 1994a, b; *Van Cappellan and Gaillard*, 1996; *Wunderly*, 1996]. In practice, however, the large differences in energy yield between the various redox reactions lead to seriously ill-posed numerical problems. The thermodynamic equilibrium constants for redox reactions, which are functions of their energy yield, span tens of orders of magnitude. This leads to a chemical system in which concentrations, the dependent variables, range from their maximum field value to infinitesimally small. The result is the creation of extremely ill-conditioned Jacobian matrices when the commonly-used Newton-Raphson method is employed.

The notion of "redox zones" leads to the idea that when attempting to simulate solute transport and chemical reactions in such aquifers, perhaps it is possible to ignore certain reactions under certain conditions. If this is true, then it follows that the range of values in subsequent Jacobians will be much smaller. This in turn leads to systems of equations that are much more numerically stable. Techniques such as basis switching improve numerical stability by rewriting chemical reactions in terms of dominant species, without altogether eliminating

insignificant reactions [*Lichtner*, 1992; *Bethke*, 1996; *Steefel and Yabusaki*, 1996]. In this chapter, a method of compartmentalizing the dominant redox reactions is described that allows one to embed kinetics within a thermodynamic framework without encountering the numerical problems created by using thermodynamics. The method presented in this chapter can reduce the number of transport equations that need to be solved in space and time by reducing the number of chemical entities under consideration. In Chapter 3, the reaction network for the development of redox zones is coupled to a solute transport simulator. This new method facilitates (i) further understanding of redox processes, both organic and inorganic, and (ii) an ability to test hypotheses for processes that have occurred, and are occurring, at many field sites.

Model Development and Applications

Chemical Reactions

The basic strategy for solving geochemical problems numerically is straightforward. Mass action expressions are first written for each chemical reaction. Together with mass balance equations and charge balance equations (implicit or explicit) these equations constitute a system of N nonlinear equations in N unknowns. This system of equations is typically solved using the Newton-Raphson method. There are, however, nuances to the particular way in which redox reactions are written. More specifically, the issue is how the concentration

of electrons ($[e^-]$) is treated mathematically. *Liu and Narasimhan* [1989a] provide a thorough review of the five most common methods for treating redox reactions. In general, each of these five methods employ a *redox parameter* that describes the *redox state* or *redox potential* (e.g., *p*E, where *p*E = $-\log[e^-]$) of the geochemical system. When redox parameters are used, redox reactions are written as half-reactions (i.e., one half-reaction representing oxidation and another representing reduction, rather than one overall reaction representing the coupled chemical process).

It is possible to include $[e^-]$ in the set of unknowns, but the numerics are arduous because $[e^-]$ can easily span twenty or more orders of magnitude. In addition, there are two, more significant conceptual problems when $[e^-]$ is an unknown. Free, or aqueous, electrons do not exist in solution. If $[e^-]$ is an unknown, then in a solute transport framework, electrons, or another variable representing the redox state of the water, must be transported; this is conceptually incorrect. Second, it is well known that there is no true *p*E for a natural water. The platinum electrode, which is widely used for field determinations of redox potential, is insensitive to many important redox couples [*Stumm and Morgan*, 1981]. Calculated *p*Es are representative of equilibrium among redox couples, a situation that is rarely achieved in nature [*Lindberg and Runnells*, 1984; *Liu and Narasimhan*, 1989a]. For example, values of *p*E for the suboxic zone of the sewage plume at the Cape Cod site, calculated

from the concentrations of various redox-sensitive constituents, range from 5.5 to 14.1 [*Kent et al.*, 1994].

The conceptual difficulties with using *p*E, or another variable representing the redox state, motivated the use of an approach without such a variable. In the approach taken here, all redox reactions are written as full reactions with an electron donor (i.e., dissolved organic carbon in this dissertation) coupled explicitly to an electron acceptor. *Lichtner* [1992], for example, employed a similar approach for handling redox reactions. In this manner, one is not forced to calculate values for hypothetical chemical entities, nor is one confined to imposing an indeterminate property, such as *p*E, on the geochemical system.

A reaction network was hypothesized (see Table 2.1) to represent the major geochemical processes that led to the development of the three redox zones at the Cape Cod site. These processes are oxygen reduction, denitrification, manganese reduction, and iron reduction. Table 2.2 shows how the mass balance equations were formulated using values from the Cape Cod field data. Aqueous complexes that contributed less than 1% to the mass balance of the relevant component and solids that were undersaturated were deleted from the reaction network. The mass action and mass balance equations shown in Table 2.2 provide the 17 algebraic equations necessary to solve for the 17 unknowns in this example.

Table 2.1. Reaction network used to simulate the development of redox zones and evaluate the compartmentalized approach. The brackets denote how the four redox reactions were grouped into oxic, suboxic, and anoxic compartments.

Redox Reactions

Oxic

$$O_2(aq) + \text{"}CH_2O\text{"} = CO_3^{2-} + 2\,H^+$$

$$2\,NO_3^- + \frac{5}{2}\,\text{"}CH_2O\text{"} = N_2(aq) + \frac{5}{2}\,CO_3^{2-} + 3\,H^+ + H_2O$$

Suboxic

$$MnO_2(s) + \frac{1}{2}\,\text{"}CH_2O\text{"} + H^+ = Mn^{2+} + \frac{1}{2}\,CO_3^{2-} + H_2O$$

Anoxic

$$Fe(OH)_3(s) + \frac{1}{4}\,\text{"}CH_2O\text{"} + \frac{3}{2}\,H^+ = Fe^{2+} + \frac{1}{4}\,CO_3^{2-} + \frac{5}{2}\,H_2O$$

pH Buffering Reactions

$$H_2O = H^+ + OH^-$$

$$H_2CO_3 = CO_3^{2-} + 2\,H^+$$

$$HCO_3^- = CO_3^{2-} + H^+$$

Aqueous Speciation Reactions

$$MnOH^+ + H^+ = Mn^{2+} + H_2O$$

$$MnHCO_3^+ = Mn^{2+} + CO_3^{2-} + H^+$$

$$Fe(OH)_2^\circ + 2\,H^+ = Fe^{2+} + H_2O$$

$$Fe(OH)^+ + H^+ = Fe^{2+} + H_2O$$

Table 2.2. Equations and chemical composition used for model development.

Mass Action Equations

$[O_2(aq)] = [CO_3^{2-}][H^+]^2["CH_2O"]^{-1}10^{-68.38}$

$[NO_3^-] = ([N_2(aq)][CO_3^{2-}]^{2.5}[H^+]^3["CH_2O"]^{-2.5}10^{-163.5})^{0.5}$

$[Mn^{2+}] = [CO_3^{2-}]^{-0.5}[H^+]["CH_2O"]^{0.5}10^{32.84}$

$[Fe^{2+}] = [CO_3^{2-}]^{-0.25}[H^+]^{1.5}["CH_2O"]^{0.25}10^{11.92}$

$[H^+] = [OH^-]^{-1}10^{-13.99}$

$[H_2CO_3] = [CO_3^{2-}][H^+]^2 10^{6.35}$

$[HCO_3^-] = [CO_3^{2-}][H^+]10^{10.32}$

$[MnOH^+] = [Mn^{2+}][H^+]^{-1}10^{-10.0}$

$[MnHCO_3^+] = [Mn^{2+}][CO_3^{2-}][H^+]10^{-12.1}$

$[Fe(OH)_2^\circ] = [Fe^{2+}][H^+]^{-2}10^{-20.57}$

$[Fe(OH)^+] = [Fe^{2+}][H^+]^{-1}10^{-9.5}$

Mass Balance Equations

$$T_{H^+} = [H^+] - [OH^-] + 2[H_2CO_3] + [HCO_3^-] + 2[O_2(aq)] - 3[N_2(aq)] - [MnO_2(s)] - 1.5[Fe(OH)_3(s)] - [MnOH^+] + [MnHCO_3^+] - 2[Fe(OH)_2^\circ] - [Fe(OH)^+]$$
$$= -ALK + 2[CO_2]_T + 2[O_2]_T - [MnO_2(s)]_T - 1.5[Fe(OH)_3(s)]_T$$

$$T_{CO_3^{2-}} = [CO_3^{2-}] + [H_2CO_3] + [HCO_3^-] + [O_2(aq)] - 2.5[N_2(aq)] + 0.5[MnO_2(s)] + 0.25[Fe(OH)_3(s)] + [MnHCO_3^+]$$
$$= [CO_2]_T + [O_2]_T + 0.5[MnO_2(s)]_T + 0.25[Fe(OH)_3(s)]_T$$

$$T_{NO_3^-} = [NO_3^-] + 2[N_2(aq)] = [NO_3^-]_T$$

$$T_{Mn^{2+}} = [Mn^{2+}] + [MnO_2(s)] + [MnOH^+] + [MnHCO_3^+] = [MnO_2(s)]_T$$

$$T_{Fe^{2+}} = [Fe^{2+}] + [Fe(OH)_3(s)] + [Fe(OH)_2^\circ] + [Fe(OH)^+] = [Fe(OH)_3(s)]_T$$

$$T_{"CH_2O"} = ["CH_2O"] - [O_2(aq)] + 2.5[N_2(aq)] - 0.5[MnO_2(s)] + 0.25[Fe(OH)_3(s)]$$
$$= ["CH_2O"]_T - [O_2]_T - 0.5[MnO_2(s)]_T - 0.25[Fe(OH)_3(s)]_T$$

Chemical Composition (derived from field data)

$ALK = 6 \times 10^{-5}$

$[CO_2]_T = 5 \times 10^{-4}$

$[O_2]_T = 2.5 \times 10^{-4}$

$[NO_3^-]_T = 2.3 \times 10^{-4}$

$[MnO_2(s)]_T = 1 \times 10^{-5}$

$[Fe(OH)_3(s)]_T = 1 \times 10^{-3}$

$["CH_2O"]_T = 0$

Notes: ALK is the carbonate alkalinity.
T_j is the total analytical concentration of model components.
The subscript $_T$ designates the chemical entities whose concentrations are known before any reactions occur (i.e., the chemical "recipe" of the system).

Compartmentalized Approach

Description

The causes of the numerical difficulties have been discussed that occur when, for example, all the reactions shown in Table 2.1 are included in a simulation. The numerical instability can be circumvented to some degree by making good initial guesses for the dependent variables. These difficulties are apparent in batch simulations, but are even more apparent in the context of solute transport because the entire range of possible concentrations will be encountered at one time or another during the course of a transient solute transport simulation. This makes the selection of good initial guesses throughout a spatial and temporal domain difficult, since the extent of reaction cannot be known *a priori*. In addition, if all reactions are included, a larger number of transport equations is needed than if some reactions can be eliminated.

Redox zones can be defined by the redox-sensitive species, and thus the redox reactions, that dominate. Therefore, it is reasonable to assume that there are always some redox reactions that dominate over others, and that some redox reactions can be ignored under certain conditions without incurring significant error. *Keating* [1995] and *Keating and Bahr* [1998] used a technique in which all potential redox reactants were present initially, but certain redox reactions were removed from the reaction set if the concentrations of relevant reactants became limiting.

It is hypothesized in this chapter that "compartments" can be developed, analogous to redox zones, in which each compartment contains the dominant redox reactions within its respective zone, but all potential redox reactions do not need to be included initially. The compartments have no spatial context; they should be thought of as different stages in reaction progress.

For the current example, there are two redox reactions in each compartment (Figure 2.2). The decision to switch from one compartment, or stage, to the next is based upon the relative proportion of the most energetic oxidant with respect to the least energetic oxidant in that compartment. For example, the reaction network for the compartment representing the oxic zone will be used until the concentration of dissolved oxygen is less than a specified percent of the available nitrate. When this occurs, the reaction network representing the suboxic zone will be used until the concentration of nitrate is less than a specified percent of the available manganese oxide. At this point, the reaction network for the compartment representing the anoxic zone will be used. The decision variable for switching (i.e., the cut-off value) does not need to be the same for switching between compartments two and three as it is for switching between compartments one and two.

Reactions that occur in compartments one and two affect the chemistry of compartments two and three, respectively, and all the compartments use different components, species, and reaction sets. Thus, information that is specific to a given reaction network (e.g., mass balances) could be "lost" upon the

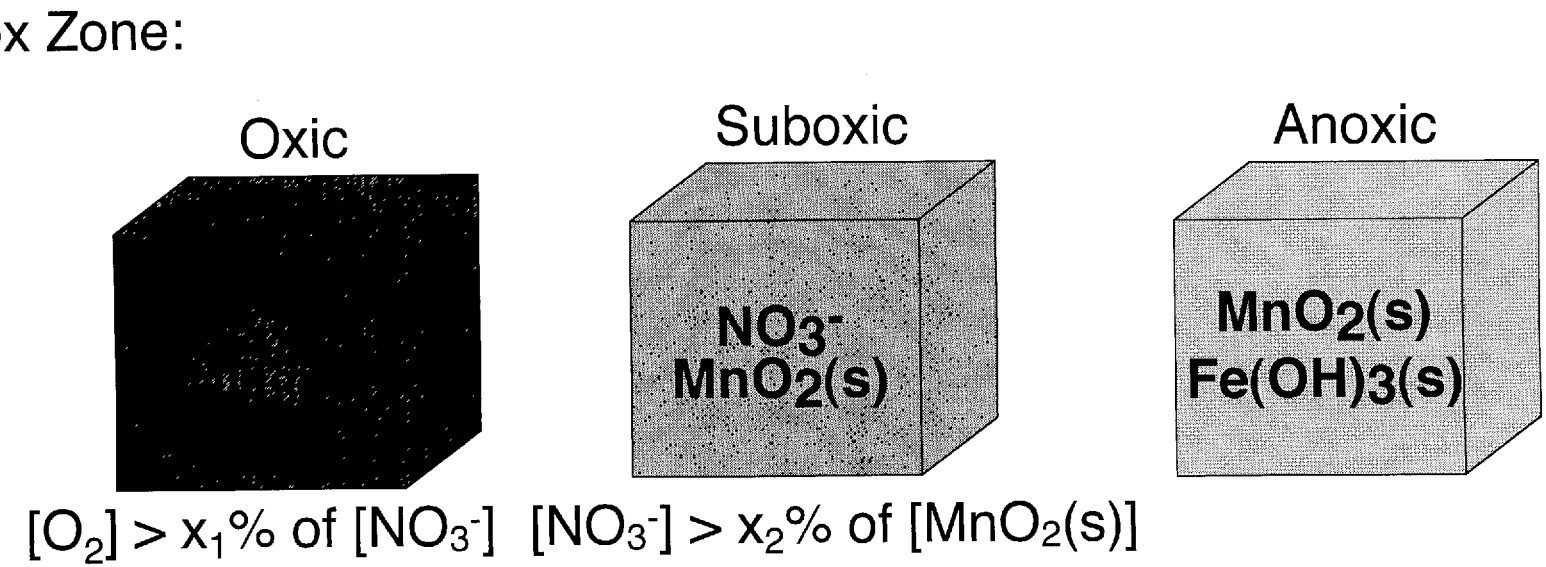

Figure 2.2. Schematic representation of the compartmentalized approach. Each compartment is defined by two redox reactions. Only one compartment is active at a time. The criteria that must be satisfied for a compartment to be active are shown, where x_1 *and* x_2 are the cut-off values for switching between compartments. When neither criterion is satisfied only the anoxic compartment is active.

switch between compartments. Therefore, the potentially "lost" information must be passed to the next compartment to update the starting state for the next reaction network. In contrast with techniques such as basis switching [e.g., *Bethke*, 1996], no chemical reactions need to be rewritten and no equilibrium constants need to be altered; insignificant reactions are merely dropped from the reaction network as new ones are added.

Test problem

A batch simulation problem was developed against which to test the compartmentalized approach. The test problem was based upon representative conditions at the Cape Cod site. The test problem was first solved without compartmentalizing the reactions, i.e., all the reactions shown in Table 2.1 were used in each redox zone and all 17 equations shown in Table 2.2 were solved simultaneously during the entire course of the simulation. The composition of the batch system (i.e., the known quantities) was derived from field data and is shown, along with the starting alkalinity, in Table 2.2. The results for the test problem without reaction compartmentalization are shown in Figure 2.3, which was generated with HYDRAQL [*Papelis et al.*, 1988], a descendent of MINEQL [*Westall et al.*, 1976]. Figure 2.3a shows the distribution of redox-sensitive species and the development of redox zones as a function of the amount of DOC reacted, as predicted by thermodynamics. Figure 2.3b shows the changes in *p*H and alkalinity as the simulation proceeds. The simulation results in Figure 2.3 were

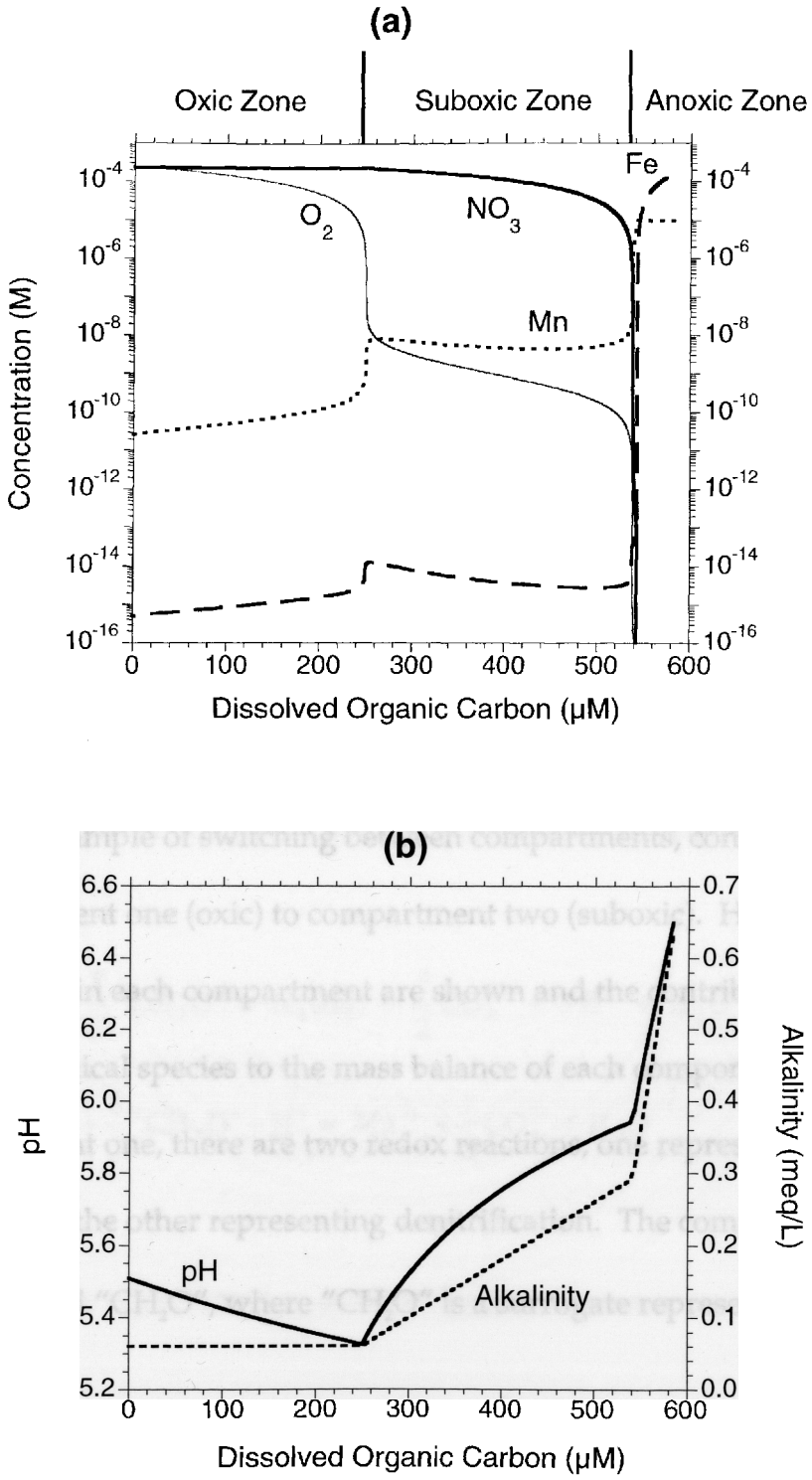

Figure 2.3. Distribution diagram generated without reaction compartmentalization showing (a) concentrations of redox-sensitive species and (b) *p*H and alkalinity as a function of DOC reacted. The oxic, suboxic, and anoxic zones are also shown.

realized with some difficulty. To construct the first portion of the diagram, from 0 μM DOC to about 540 μM, required DOC increments of 10^{-1} μM to ensure convergence (10^3 titration steps to react 100 μM of DOC). Beyond 540 μM (i.e., the anoxic/iron zone) the required DOC step to ensure convergence was 10^{-4} μM (i.e., 10^6 titration steps to react 100 μM of DOC).

Application of the compartmentalized approach to the test problem

The implementation of the compartmentalized approach employed here to solve the test problem uses HYDRAQL to simulate the simplified reaction networks within each compartment (see Table 2.1 and Figure 2.2).

As an example of switching between compartments, consider the switch from compartment one (oxic) to compartment two (suboxic). Here only the redox reactions in each compartment are shown and the contribution of individual chemical species to the mass balance of each component is not shown. For compartment one, there are two redox reactions, one representing aerobic respiration and the other representing denitrification. The components are H^+, CO_3^{2-}, NO_3^-, and "CH_2O", where "CH_2O" is a surrogate representing all the reactive DOC:

$$O_2(aq) + \text{"}CH_2O\text{"} = CO_3^{2-} + 2H^+ \tag{2.1}$$

$$2NO_3^- + \frac{5}{2}\text{"}CH_2O\text{"} = N_2(aq) + \frac{5}{2}CO_3^{2-} + 3H^+ + H_2O \tag{2.2}$$

The mass balance equations are:

$$T^1_{H^+} = -\mathrm{ALK} + 2[\mathrm{CO_2}]_\mathrm{T} - 2[\mathrm{O_2}]_\mathrm{T} \tag{2.3}$$

$$T^1_{CO_3^{2-}} = [\mathrm{CO_2}]_\mathrm{T} + [\mathrm{O_2}]_\mathrm{T} \tag{2.4}$$

$$T^1_{NO_3^-} = [\mathrm{NO_3}]_\mathrm{T} \tag{2.5}$$

$$T^1_{"CH_2O"} = ["\mathrm{CH_2O}"]_\mathrm{T} - [\mathrm{O_2}]_\mathrm{T} \tag{2.6}$$

The components in compartment two are H^+, CO_3^{2-}, NO_3^-, Mn^{2+}, and "CH_2O".

Aerobic respiration no longer occurs and manganese reduction has been added:

$$2\,\mathrm{NO_3^-} + \frac{5}{2}\,"\mathrm{CH_2O}" = \mathrm{N_2}(aq) + \frac{5}{2}\mathrm{CO_3^{2-}} + 3\,\mathrm{H^+} + \mathrm{H_2O} \tag{2.7}$$

$$\mathrm{MnO_2}(s) + \frac{1}{2}\,"\mathrm{CH_2O}" + \mathrm{H^+} = \mathrm{Mn^{2+}} + \frac{1}{2}\mathrm{CO_3^{2-}} + \mathrm{H_2O} \tag{2.8}$$

The mass balance equations (i.e., as if there never were a compartment one) are:

$$T^2_{H^+} = -\mathrm{ALK} + 2[\mathrm{CO_2}]_\mathrm{T} - [\mathrm{MnO_2}(s)]_\mathrm{T} \tag{2.9}$$

$$T^2_{CO_3^{2-}} = [\mathrm{CO_2}]_\mathrm{T} + 0.5[\mathrm{MnO_2}(s)]_\mathrm{T} \tag{2.10}$$

$$T^2_{NO_3^-} = [\mathrm{NO_3}]_\mathrm{T} \tag{2.11}$$

$$T^{2}_{Mn^{2+}} = [\mathrm{MnO_2}(s)]_{\mathrm{T}} \tag{2.12}$$

$$T^{2}_{"CH_2O"} = ["\mathrm{CH_2O}"]_{\mathrm{T}} - 0.5[\mathrm{MnO_2}(s)]_{\mathrm{T}} \tag{2.13}$$

If there is a switch from compartment one to compartment two, then the mass balance equations for compartment two must be modified to account for the effects of the compartment one reactions on the chemistry of compartment two. This prevents the reaction information of compartment one from being lost:

$$T^{2\,\mathrm{modified}}_{H^+} = T^{2}_{H^+} + 2 * ([\mathrm{O_2}(aq)] \text{ used in Compartment 1}) \tag{2.14}$$

$$T^{2\,\mathrm{modified}}_{CO_3^{2-}} = T^{2}_{CO_3^{2-}} + 1 * ([\mathrm{O_2}(aq)] \text{ used in Compartment 1}) \tag{2.15}$$

$$T^{2\,\mathrm{modified}}_{NO_3^-} = [\mathrm{NO_3}]_{\mathrm{T}} \tag{2.16}$$

$$T^{2\,\mathrm{modified}}_{Mn^{2+}} = [\mathrm{MnO_2}(s)]_{\mathrm{T}} \tag{2.17}$$

$$\begin{aligned} T^{2\,\mathrm{modified}}_{"CH_2O"} = T^{2}_{"CH_2O"} &+ 1.25 * ([\mathrm{NO_3^-}] \text{ used in Compartment 1}) \\ &- 1 * ([\mathrm{O_2}(aq)] \text{ remaining in Compartment 1}) \end{aligned} \tag{2.18}$$

The results from the compartmentalized simulation, using a cut-off value of 1% for both instances of compartmental switching, are plotted in Figure 2.4 as an overlay on top of Figure 2.3a (Figure 2.3a is considered to be the correct answer). Clearly, the match between the simulation approaches is nearly perfect; differences are not discernible when plotted in this manner. This result is pleasing, but a rigorous statistical evaluation is more appropriate than a simple

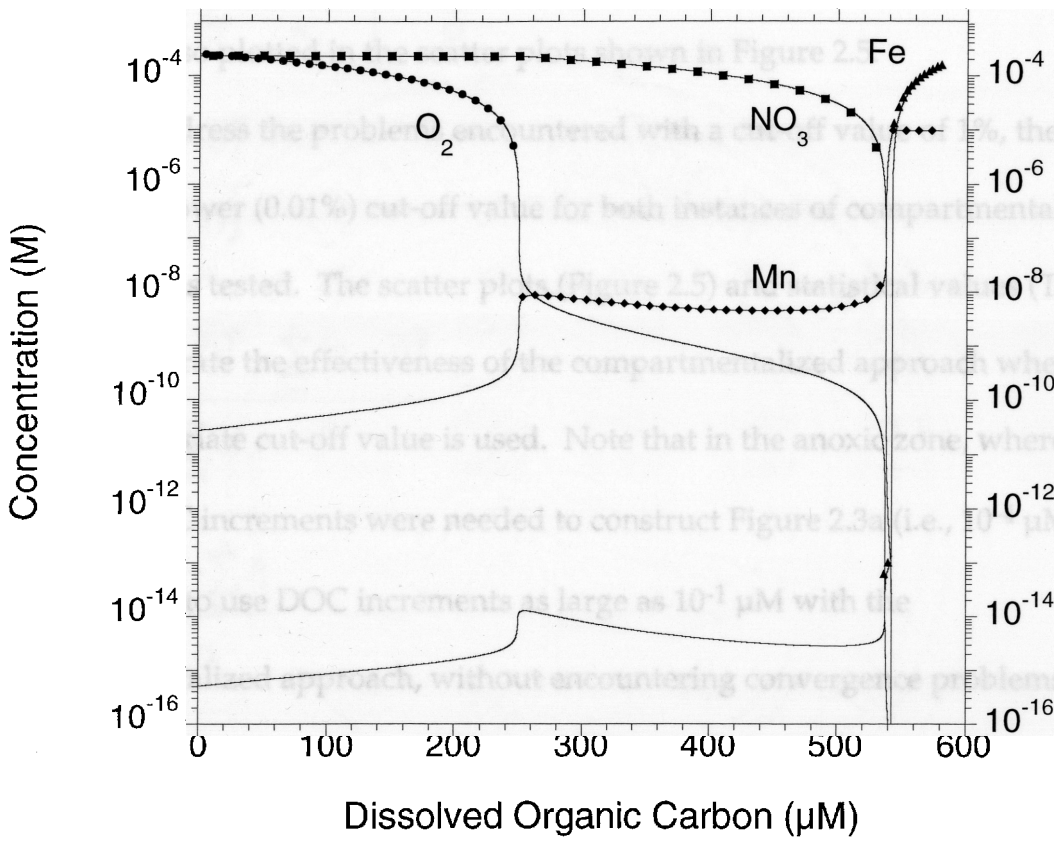

Figure 2.4. Comparison of a 1% cut-off (plot symbols) with the results shown in Figure 2.3. Only a portion of the symbols are plotted, to avoid clutter. The sequence of symbols truncates as a function of the cut-off value.

visual comparison. To do this, five model performance evaluation statistics, shown in Tables 2.3 and 2.4, were used to evaluate quantitatively the compartmentalized approach against the model that includes all redox reactions all the time. Note that although the root mean square error (%) is quite high for Mn and Fe, the other statistics appear to have reasonably good values. The results are also plotted in the scatter plots shown in Figure 2.5.

To address the problems encountered with a cut-off value of 1%, the impact of a lower (0.01%) cut-off value for both instances of compartmental switching was tested. The scatter plots (Figure 2.5) and statistical values (Table 2.4) demonstrate the effectiveness of the compartmentalized approach when the more appropriate cut-off value is used. Note that in the anoxic zone, where the smallest DOC increments were needed to construct Figure 2.3a (i.e., 10^{-4} μM), it was possible to use DOC increments as large as 10^{-1} μM with the compartmentalized approach, without encountering convergence problems.

Kinetic Framework

Description

Thermodynamics provides the driving force for simulating the geochemical reactions that represent biodegradation. Clearly, consideration of these reactions as equilibrium reactions is inappropriate because they represent biologic processes, which do not occur instantaneously. Furthermore, for the redox reactions under consideration, equilibrium lies extremely far to the right,

Table 2.3. Statistical formulas used to evaluate the compartmentalized approach.

$$\mathrm{ME} = \mathrm{Max}\left|P_i - O_i\right| \qquad i = 1, n$$

$$\mathrm{RMSE}(\%) = \left[\sum_{i=1}^{n} \frac{(P_i - O_i)^2}{n}\right]^{0.5} \cdot \frac{100}{\overline{O}}$$

$$\mathrm{CD} = \frac{\sum_{i=1}^{n} \left(O_i - \overline{O}\right)^2}{\sum_{i=1}^{n} \left(P_i - \overline{O}\right)^2}$$

$$\mathrm{EF} = \frac{\sum_{i=1}^{n} \left(O_i - \overline{O}\right)^2 - \sum_{i=1}^{n} \left(P_i - \overline{O}\right)^2}{\sum_{i=1}^{n} \left(O_i - \overline{O}\right)^2}$$

$$\mathrm{CRM} = \frac{\sum_{i=1}^{n} O_i - \sum_{i=1}^{n} P_i}{\sum_{i=1}^{n} O_i}$$

Note: P_i are the values from the compartmentalized approach, O_i are the values from the standard modeling approach, n is the number of data, $\overline{O}$ is the mean of the standard modeling approach results. The lower limit for the ME (maximum error), RMSE (root mean square error), and CD (coefficient of determination) statistics is zero. The maximum value for EF (modeling efficiency) is one. Both EF and CRM (coefficient of residual mass) can become negative. If EF is less than zero, the compartmentalized approach values are worse than simply using the mean of the standard modeling approach results. See *Loague and Green* [1991] for a more detailed description of these statistics.

Table 2.4. Statistical values for two different cut-off criteria.

Sample size(n) and model performance statistics	O_2	NO_3	Mn	Fe	pH	ALK	Perfect model
				Cut-Off = 1%			
n	2479	5353	3329	455	5808	5808	
ME	0.0000	0.0000	0.0000	0.0000	0.0342	0.0000	0.0000
RMSE (%)	0.0000	0.7596	40.7861	12.6620	0.1625	3.2810	0.0000
CD	1.0000	0.9821	0.9556	0.9171	0.9588	0.9400	1.0000
EF	1.0000	0.9997	0.9760	0.9726	0.9987	0.9983	1.0000
CRM	0.0000	0.0056	-0.0532	-0.1183	-0.0009	-0.0146	0.0000
				Cut-off = 0.01%			
n	2514	5378	3318	454	5832	5832	
ME	0.0000	0.0000	0.0000	0.0000	0.0001	0.0000	0.0000
RMSE (%)	0.0000	0.0011	0.0006	0.0000	0.0002	0.0013	0.0000
CD	1.0000	1.0000	1.0000	1.0000	0.9999	1.0000	1.0000
EF	1.0000	1.0000	1.0000	1.0000	1.0000	1.0000	1.0000
CRM	0.0000	0.0000	0.0000	0.0000	0.0000	0.0000	0.0000

Changing the cut-off from 1% to 0.01% resulted in a significant improvement in model performance (e.g., RMSE for Mn improved from 40.786% to 0.0006% with the change in tolerance). See Table 2.3 for explanations of the model performance statistics.

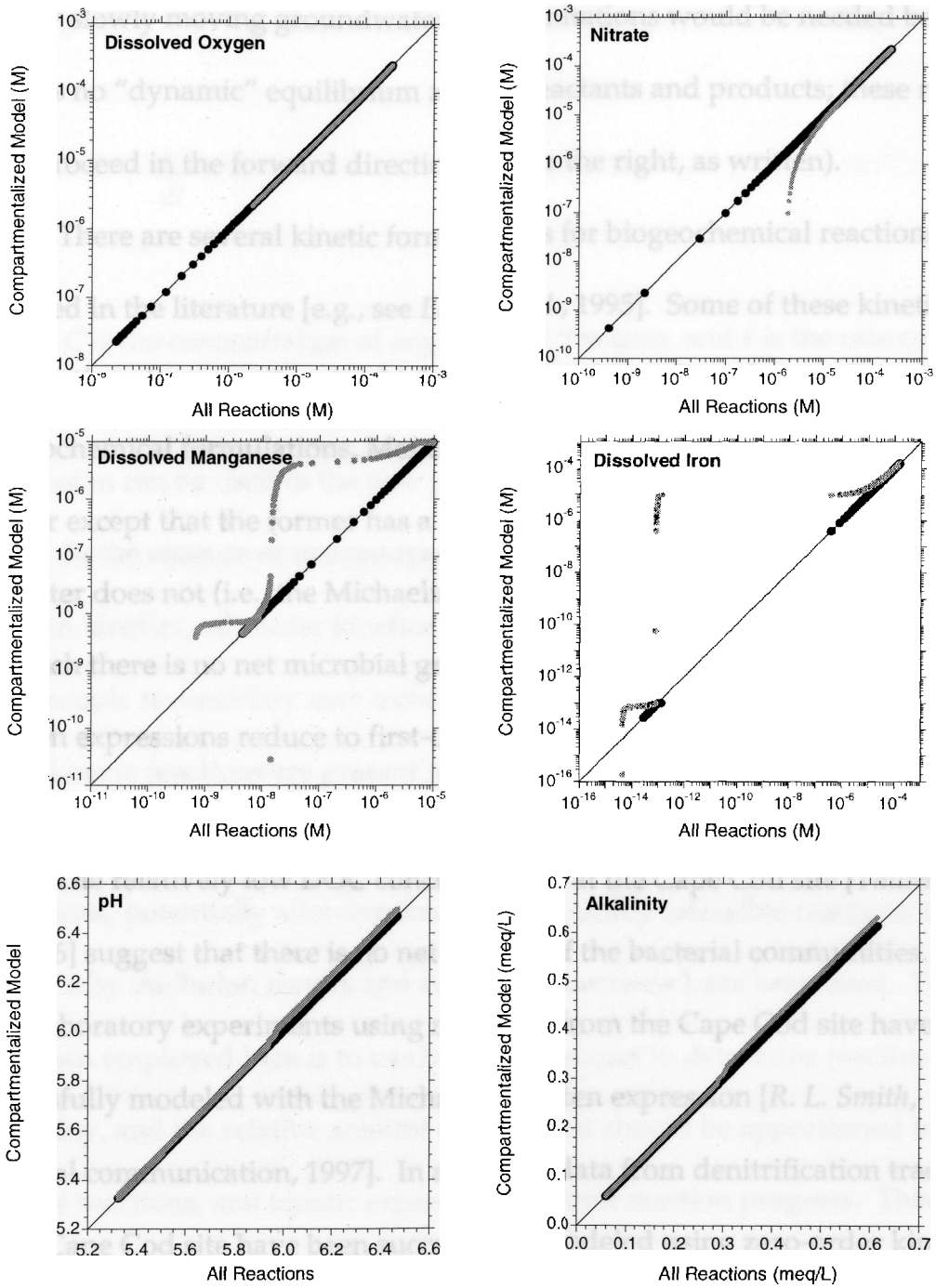

Figure 2.5. Scatter plots comparing the compartmentalized approach with the approach in which all reactions are used in each redox zone. Results with a cut-off value of 1% (gray plot symbols) and 0.01% (black plot symbols) are shown.

as the reactions are written (Table 2.1). So even if these reactions were occurring in very slowly moving groundwater, rate limitations would be needed because there is no "dynamic" equilibrium among reactants and products; these reactions only proceed in the forward direction (i.e., to the right, as written).

There are several kinetic formulations for biogeochemical reactions reported in the literature [e.g., see *Essaid et al.*, 1995]. Some of these kinetic formulations incorporate microbial dynamics while others do not. Two biogeochemical formulations, Monod and Michaelis-Menten, are mathematically similar except that the former has a term for the concentration of microbes while the latter does not (i.e., the Michaelis-Menten form is appropriate for situations in which there is no net microbial growth). Both the Monod and Michaelis-Menten expressions reduce to first-order kinetics at low reactant concentrations and to zero-order kinetics at high reactant concentrations.

The relatively low DOC concentrations at the Cape Cod site [*Thurman et al.*, 1986] suggest that there is no net growth of the bacterial communities. Data from laboratory experiments using materials from the Cape Cod site have been successfully modeled with the Michaelis-Menten expression [*R. L. Smith*, personal communication, 1997]. In addition, data from denitrification tracer tests at the Cape Cod site have been successfully modeled using zero-order kinetics [*Smith et al.*, 1996]. For these reasons, Michaelis-Menten kinetics are employed in ongoing work with coupled solute transport/geochemical simulations

(for process-based modeling). Zero-order kinetics were used for model development with the batch simulations that are reported in this chapter:

$$\frac{dC}{dt} = -k \tag{2.19}$$

where C is the concentration of any reactant, t is time, and k is the rate constant. The zero-order kinetic formulation is used solely for simplicity; any rate expression can be used in the new model.

In the absence of thermodynamic constraints, Monod kinetics, Michaelis-Menten kinetics, nth-order kinetics, and kinetic expressions based upon microscopic reversibility may incorrectly simulate reaction progress if two or more kinetic reactions are present in a reaction set. This is because the simulated kinetic reactions will proceed as a function of time regardless of the geochemical conditions, potentially allowing thermodynamically infeasible reactions to occur. This is why inhibition factors and switching functions have been used. The approach employed here is to use thermodynamics to determine reaction feasibility, and the relative amount of DOC that should be apportioned to the feasible reactions, and kinetic expressions to limit reaction progress. This approach contrasts with that of *Keating* [1995] and *Keating and Bahr* [1998], who used a strictly equilibrium formulation for all chemical reactions and a time-dependent source of electrons to control the progress of redox reactions.

As an example, consider the oxic compartment, where oxygen reduction and denitrification can occur and denitrification represents the lower-energy reaction. Each reaction can be assigned a different rate, but for the sake of this description, it is assumed that (i) the two redox reactions proceed at the same rate, (ii) oxygen and nitrate concentrations are initially the same, and (iii) DOC is present in excess (i.e., the time step is small enough so that all the available DOC is not reacted within one time step). The third assumption is important because it ensures that the oxygen concentration (in this example) will not be artificially large due to DOC limitations.

According to kinetics (i.e., without any form of reaction suppression), at the end of a time step a certain amount of DOC will have reacted, reducing the concentrations of oxygen and nitrate equally and leaving some free DOC unreacted. Since the system is not DOC limited, it is assumed that the kinetically-derived concentration of oxygen is correct, but that the kinetically-derived concentration of nitrate must be checked for thermodynamic feasibility. To do this, a thermodynamic (i.e., equilibrium) simulation is performed in which enough DOC is added to the system to lower the oxygen concentration to the same value as the kinetically-derived concentration. If the same amount of DOC that was consumed by oxygen in the kinetic simulation is required, then thermodynamics indicates that the denitrification reaction should be completely suppressed under the specified geochemical conditions. If more DOC is required, then denitrification is only partially suppressed. In either case, if the

concentration of nitrate is higher in the thermodynamic simulation, then the kinetic simulation is incorrect and the thermodynamic result is used. If the concentration of nitrate in the thermodynamic simulation is equal to or lower than the kinetic simulation, then the kinetic simulation is correct and it is used.

Incorporation of the compartmentalized approach

The compartmentalized approach was incorporated within a kinetic framework to simulate the development of redox zones as a function of time in a batch system. KEMOD [*Yeh et al.*, 1993, 1998], the mixed kinetic-equilibrium geochemistry module of HYDROGEOCHEM 2.1 [*Yeh and Salvage*, 1995], was adapted to perform the kinetic and thermodynamic calculations according to the procedure described above. The basic numerical solution strategy for KEMOD is similar to that of HYDRAQL [*Papelis et al.*, 1988] and MINEQL [*Westall et al.*, 1976], except that KEMOD has the ability to include elementary kinetics reactions based upon microscopic reversibility. I modified KEMOD so that it could solve irreversible, *n*th order kinetics. The reactions used are shown in Table 2.1. In the kinetic framework, all four redox reactions are treated as irreversible, zero-order kinetic reactions that proceed from left to right, as written. The *p*H buffering and speciation reactions are treated as equilibrium reactions. The equations are the same as those shown in Table 2.2 except for the addition of equations of the form of (2.19) to represent the rate limitations imposed on the redox reactions. The kinetic equations are not used for the thermodynamic calculation, and the mass

action equations (for the redox reactions) are not used for the kinetic calculation. The initial conditions are the same as the starting state of the equilibrium simulation shown in Figure 2.3 except DOC is present in excess over the concentrations of all the redox-sensitive reactants. Thermodynamics would thus predict instant utilization and exhaustion of all redox reactants.

Since reaction progress is limited by kinetic constraints, the redox reactants are not exhausted immediately but rather the redox zones develop as a function of time. No form of empirical reaction inhibition is used to suppress reactions. Redox reactions that are in the same compartment can both occur simultaneously if the geochemical conditions are appropriate (e.g., in compartment one, under low oxygen but relatively higher nitrate concentrations). If the geochemical conditions are not appropriate for simultaneous redox reactions, the lower-energy reaction is automatically suppressed by the thermodynamic constraints. There is always overlap between sequential redox reactions (e.g., denitrification can occur in the oxic and suboxic compartments).

The results from the thermodynamic/kinetic simulation are plotted in Figure 2.6 as a function of dimensionless time (t/t_{max}). The simulation was run from an initial condition of *p*H 5.5 to a final *p*H of 6.5, as in Figure 2.3. The curves in Figure 2.6 truncate abruptly due to compartmental switching (i.e., the cut-off criteria are enforced). The development of redox zones as a function of time is clearly shown. Throughout the reaction space, lower-energy redox

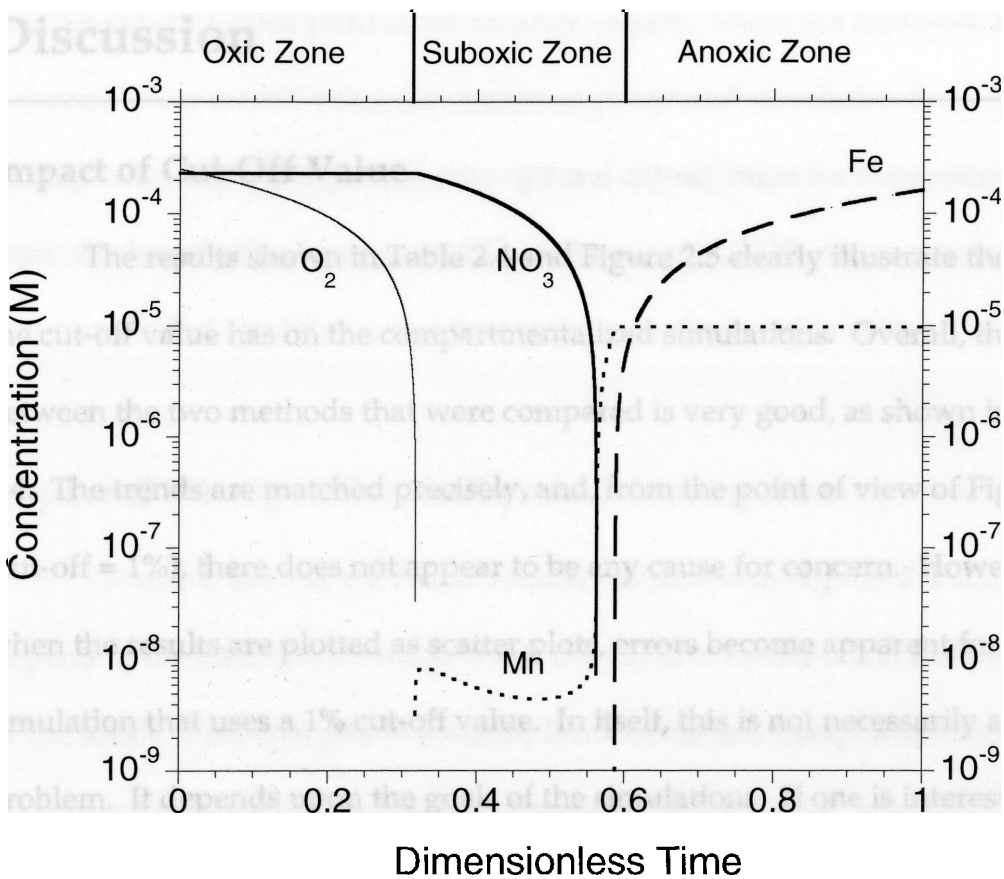

Figure 2.6. Development of redox zones and distribution of redox-sensitive species as a function of time. Suppression of lower energy reactions is accomplished through thermodynamic constraints.

reactions are suppressed by higher-energy redox reactions due to the thermodynamic constraints. Reaction progress is limited by the kinetic constraints.

Discussion

Impact of Cut-Off Value

The results shown in Table 2.4 and Figure 2.5 clearly illustrate the impact the cut-off value has on the compartmentalized simulations. Overall, the match between the two methods that were compared is very good, as shown in Figure 2.4. The trends are matched precisely, and, from the point of view of Figure 2.4 (cut-off = 1%), there does not appear to be any cause for concern. However, when the results are plotted as scatter plots, errors become apparent for the simulation that uses a 1% cut-off value. In itself, this is not necessarily a problem. It depends upon the goals of the simulations. If one is interested in general trends in the development of redox zones, then a cut-off value of 1% is probably fine. If, however, one is interested in tracking a particular chemical entity, then the ability to simulate its appearance/disappearance with reasonable accuracy is highly dependent on the cut-off value.

The best cut-off value for a particular situation is dependent on a number of factors, including the use of different redox reactions (e.g., employing different organic compounds instead of solely using "CH_2O" to represent all of the

available DOC). For instance, the free energy yield associated with the degradation of, say, toluene, may produce curves with different slopes. These slopes may also be different for different oxidants. In general, however, there is a correlation between desired accuracy and magnitude of the cut-off value; smaller cut-off values yield more accurate results. There is a trade-off, however, between lower cut-off value (i.e., more accuracy) and simulation time. No attempt was made to determine the optimal cut-off value for the system studied here. Such an optimal value would be a function of DOC increment size, desired accuracy, initial conditions, and the reactions under consideration.

Impact of Site-Specific Geochemical Assumptions

Characteristics of the redox boundaries shown in Figures 2.3 and 2.6 depend upon assumptions made about the initial conditions and the free energy of the solids. Free energies of hydrous ferric oxide and manganese oxide were taken from published compilations [*Morel and Hering*, 1993]. Iron and manganese oxides on aquifer sediments from the Cape Cod site exist as complex hydroxypolymer coatings; the actual free energies are unknown and iron and manganese likely exist as solids with a range of compositions [*Coston et al.*, 1995]. Inclusion of a range of compositions for each class of solids would affect overall reactivity, which would affect the minimum computed concentrations of dissolved iron and dissolved manganese and the positions of the redox

boundaries. Maximum computed concentrations of dissolved iron and dissolved manganese depend on the initial conditions.

Characteristics of the evolution of *p*H and alkalinity shown in Figure 2.3 also depend on site-specific geochemical assumptions. Stoichiometric coefficients for both the hydrogen ion and carbonate species in the redox reactions differ somewhat for different organic compounds. Thus, use of different organic compounds in the computations would yield different *p*H and alkalinity trajectories. Inclusion of *p*H buffers in addition to those of the carbonate species would also influence the *p*H trajectory. Surface complexation reactions between surface sites on the aquifer sediments and hydrogen ions would provide additional *p*H buffering [*Stollenwerk*, 1995]. The result of additional buffers would be that greater quantities of organic matter and electron donors would be required to achieve the *p*H values shown on Figure 2.3.

Comparison with Field Observations

The simulations reported here were performed over the *p*H range 5.5 to 6.5 to represent the range of field conditions from pristine groundwater to the average conditions found in the core of the upgradient portion of the sewage plume at the Cape Cod site. Qualitatively, the simulation results agree with field observations, as can be seen by comparing Figures 2.3 and 2.6 with Figure 1.4. The simulation results in Figures 2.3a and 2.6 show the presence of an oxic zone with high concentrations of dissolved oxygen and nitrate, a suboxic zone with

high concentrations of nitrate and elevated dissolved manganese, and an anoxic zone with high concentrations of dissolved manganese and dissolved iron. Figure 2.3b shows the increases in *p*H associated with the suboxic and anoxic zones as seen in Figure 1.4.

The theoretically-based equilibrium constants, which represent the Gibbs free energy of reaction, determine the most favorable reactions. For example, in the *p*H range observed at the Cape Cod site, the thermodynamically-based model predicts that iron reduction will not commence, and thus no iron zone will form, until all of the available manganese has been reduced. This is because the energy released by manganese reduction is so much greater than the energy released by iron reduction. A similar situation was described by *Chapelle and Lovley* [1992] in which sulfate reduction was observed only after ferric iron was depleted.

The simulation results shown in Figures 2.3 and 2.6 represent what would occur in a batch system. Figure 1.4 represents one snapshot in time of a vertical profile, at one location, in the transient Cape Cod groundwater flow system. As such, the simulation results are only comparable to field data in a qualitative sense. Figure 1.4 may, however, represent a steady-state in which concentrations are not changing with time, even though thermodynamic equilibrium is not achieved. This could occur because reactants and products are constantly flowing in and out of any given control volume. Thus, a quantitative model

evaluation against field data can only be realized in the context of solute transport simulations.

Simultaneous Occurrence of Redox Reactions

An important aspect of any model that simulates sequential, microbially-mediated redox reactions is the recognition that under certain geochemical conditions, competing reactions may occur simultaneously (e.g., incomplete suppression of a lower-energy reaction). The compartmentalized approach allows for this possibility by always having two redox reactions in each compartment and by overlapping reactions between compartments (e.g., denitrification is included in the oxic and suboxic compartments and manganese reduction is included in the suboxic and anoxic compartments).

Figure 2.6 shows, for example, denitrification and manganese reduction occurring simultaneously in the micromolar range. The time over which this occurs appears to be rather small, but this is a function of the kinetic formulation (i.e., zero-order kinetics). If first-order kinetics were used in the low concentration ranges, as it is with Michaelis-Menten kinetics, the time over which simultaneous redox reactions occur would be greater.

Conclusions

Redox zones often develop in contaminated aquifers as a response to microbes oxidizing dissolved organic carbon coupled to the reduction of the electron acceptor that yields the greatest amount of free energy. Thermodynamics provides a basis for predicting under what conditions a given reaction, or microbial process, will occur. With this tool, the development of redox zones can be simulated on a firmer theoretical basis, reducing the amount of calibration that must be done (e.g., inhibition factors). Furthermore, the qualitative description of sequential redox reactions and the development of redox zones can be quantified using thermodynamics.

The large differences in energy yields between the various redox reactions lead to systems of equations that are ill-conditioned. This difficulty was circumvented by developing a rational method to eliminate insignificant reactions while maintaining the integrity of the numerical solution. This was done by compartmentalizing the reaction networks in a manner that is conceptually based on the redox zones themselves. The reactions that give rise to a particular zone are focused upon, while those that are not important, due to reactant availability and energetic efficiency, are ignored. When the cut-off criteria are selected appropriately (i.e., the switch between compartments is done properly) no significant errors are generated. In addition, it is possible to reduce

the number of transport equations required to simulate solute transport coupled with geochemical reactions.

When the compartmentalized approach is placed within a kinetic framework, the development of redox zones can be simulated as a function of time. The method of incorporating kinetics allows the use of any kinetic formulation to constrain reaction progress, while still using thermodynamics to prevent reactions from occurring under infeasible conditions. The compartmentalized approach lays the foundation for Chapter 3, in which the reaction network for the development of redox zones is coupled to a model of subsurface fluid flow and solute transport based upon the Cape Cod site.

Chapter 3

Incorporation of a Compartmentalized Reaction Network Model into a Solute Transport Framework for the Development of Redox Zones at Field Scales

Abstract

This chapter takes the concepts presented in Chapter 2 and embeds them within a solute transport framework. The compartmentalized approach, as described in Chapter 2, was developed to simulate the geochemical evolution of a particular batch system. In this chapter, the compartmentalized approach is generalized to facilitate the description of its incorporation into a solute transport simulator. It is then shown that there is an equivalent formulation that removes any discontinuities that may occur when switching compartments. In Chapter 2, the rate-limited redox reactions were modeled with zero-order kinetics. In this chapter, they were simulated with a modified Monod relationship that allows either the organic substrate or the electron acceptor to be the rate limiting reactant. The sequential iteration approach (SIA), a technique that allows the

number of solute transport equations to be reduced, is adopted to solve the coupled geochemical/solute transport problem. It is shown that when the compartmentalized approach is embedded within the SIA, with the total analytical concentration of each component as the dependent variable in the transport equation, it is possible to reduce the number of transport equations even further than with the unmodified SIA. Two one-dimensional, coupled geochemical/solute transport simulations are presented in which redox zones dynamically evolve in time and space. The first simulation was used to develop and test the code and the second simulation was constructed to approximate field conditions at the Cape Cod site. Two two-dimensional coupled geochemical/solute transport simulations are also presented. In addition to demonstrating that the compartmentalized solute transport model functions in two dimensions, the impact of transverse dispersion on the development of suboxic transition zones is explored. The compartmentalized approach as described in this chapter enables the coupled geochemical/solute transport problem for the development of redox zones to be simulated under both kinetic and thermodynamic constraints.

Introduction

Aquifers that become contaminated with organic carbon have the potential to develop zones within the contaminant plume in which the groundwater chemistry is drastically different than in surrounding zones. Often, the major differences between zones are the concentrations of redox-sensitive compounds, also known as electron acceptors and donors, such as dissolved oxygen, nitrate, and dissolved manganese and iron. In such cases, these areas are termed *redox zones*. Redox zones arise because the oxidation of dissolved organic carbon (DOC) occurs via sequential, microbially-mediated redox reactions that differ widely in the amount of energy liberated by the reactions. Since the energy yields differ so greatly, the microbial consortia that can mediate a higher-energy reaction will greatly dominate over other consortia. For example, aerobic biodegradation will take place until essentially all the dissolved oxygen is depleted, leading to the formation of suboxic and/or anoxic zones. The sequential process continues, with each stage utilizing successively less energetic reactions, until all the available DOC or electron acceptors are depleted.

Since methods such as pump-and-treat or capture-and-containment are frequently insufficient to remediate many contaminated aquifers, a significant amount of research has recently focused on the ability of bacteria to degrade organic compounds. As highlighted in a recent National Research Council book [*NRC*, 1994], the ability to biodegrade many hazardous compounds is dependent

upon the redox conditions of the contaminated subsurface. For example, naphthalene biodegrades under aerobic conditions, but does not degrade, or degrades very slowly, under anaerobic conditions. It is necessary, therefore, to know the redox conditions within a flow field to ensure that bioremediation will be successful.

The transport of heavy metals is also dependent upon redox conditions. Nearly all metals of interest in groundwater problems are influenced by redox conditions [*Freeze and Cherry*, 1979]. Small changes in redox conditions can have drastic effects on the sorptive properties and toxicity of metals. For example, under reducing conditions chromium exists in the plus three oxidation state (Cr(III)), which can be irreversibly sorbed to aquifer solids; in contrast, under oxidizing conditions chromium exists in the plus six oxidation state (Cr(VI)) and is mobile [*Kent et al.*, 1994]. Moreover, Cr(VI) is very toxic, while Cr(III) is less so [*NRC*, 1994]. Arsenic toxicity is also dependent upon oxidation state; As(III) is more toxic than As(V) [*NRC*, 1994]. Thus, an ability to characterize and predict the extent of multiple redox zones is necessary for a process-based understanding of the fate and transport of many chemical substances currently recognized as hazardous.

Mathematical models can be a great aid in the conceptual understanding of the processes behind the development and fate of redox zones in aquifers. They can also be useful predictive tools, in terms of the fate of a particular contaminant or in the context of developing and simulating remediation

strategies. To successfully simulate the development and fate of redox zones in aquifers, it is necessary to construct a model that includes (i) subsurface fluid flow, (ii) solute transport (e.g., advection and dispersion), and (iii) geochemical reactions. This is necessary because none of these processes alone is capable of characterizing the development of redox zones; the zones develop as a consequence of the interaction of these three broad processes.

The Cape Cod Site

Land disposal of secondarily-treated sewage at the Massachusetts Military Reservation near Falmouth, MA (Cape Cod) occurred from 1936 to 1995 and has led to the development of distinct redox zones [*LeBlanc*, 1984a; *Smith and Duff*, 1988; *Kent et al.*, 1994]. The oxic, suboxic, and anoxic zones extend horizontally downgradient from the contaminant source and vertically down from the water table. The anoxic zone at Cape Cod contains dissolved iron but no sulfide; thus the most relevant redox reactions are oxygen reduction, denitrification, manganese reduction, and iron reduction [*Smith and Duff*, 1988; *Smith et al.*, 1991a; *Kent et al.*, 1994]. The nature of the driving force for these microbially-mediated chemical reactions, thermodynamics, in conjunction with the rate of the reactions, gives rise to sharp boundaries between the zones.

Simulation Approaches

Of the many models that have been developed in an effort to characterize and simulate solute transport coupled with biodegradation and/or redox processes, most have either focused on the biological aspects of the problem [e.g., see *Essaid et al.* 1995], or restricted their analysis to simplified problems. In a two-part paper, *Liu and Narasimhan* [1989a, b] presented a model that simulated multiple species reactive transport, including redox reactions. All of the formulations described by *Liu and Narasimhan* required the use of a "redox parameter", such as *p*E. It appears that the kinetic formulations used by *Liu and Narasimhan* were limited to zero-order. Following the work of *Liu and Narasimhan* [1989a, b], *McNab and Narasimhan* [1993] presented a model that was designed to accommodate the degradation of organic compounds. This model included first-order kinetics and linear sorption. Next, *McNab and Narasimhan* [1994] described a model of reactive transport that handled the degradation of organic compounds, but also utilized thermodynamics in conjunction with a "quasi-expert system" to decide reaction feasibility. The 1994 model of *McNab and Narasimhan* used first-order kinetics for organic compounds and all inorganic reactions were considered to be at equilibrium. The decision parameter for the expert system was the *p*E of the system, which was calculated only from the inorganic species.

Within the last five years or so, several models have been developed that can solve general mixed kinetic and equilibrium problems, either in batch or

coupled to solute transport. *Yeh et al.* [1993, 1998] and *Yeh and Salvage* [1995] presented models that could include any number of kinetic reactions, but the kinetic formulations were restricted to mass-action-based expressions. The *Yeh et al.* and *Yeh and Salvage* models provide no mechanism for the inhibition of a lower-energy kinetic reaction in the presence of a higher-energy kinetic reaction, such as denitrification in the presence of appreciable dissolved oxygen. *Parkhurst* [1995] and *Parkhurst and Appelo* [1997] developed a model that can accommodate any user-specified kinetic formulation. The *Parkhurst and Appelo* model stoichiometrically "titrates" DOC into a geochemical system, which is controlled by thermodynamic equilibrium, as a function of time according to user-specified rate expressions. The rate expressions can be designated to operate over user-specified concentration ranges. *Keating* [1995] and *Keating and Bahr* [1998] developed a quasi-kinetic, partial equilibrium model. The *Keating and Bahr* model used equilibrium redox reactions, which could be selectively removed from the reaction network, in conjunction with an internal, time-dependent source of electrons. All currently available models that incorporate kinetics within a thermodynamic framework impose thermodynamic equilibrium on competing redox reactions. Current models do not allow the losers of the thermodynamic competition to be simulated as rate-limited reactions.

This chapter links the geochemical compartmentalized approach described in Chapter 2 with solute transport. The compartmentalized approach provides a simple means to simulate multiple kinetic reactions with different

reaction rates that are constrained by thermodynamics. Competing redox reactions can be either thermodynamically- or kinetically-inhibited, including lower-energy redox reactions that lose the thermodynamic competition with higher-energy redox reactions. The new model described in this chapter can accommodate a realistic number of kinetic reactions that compete for DOC, without the use of empirical reaction inhibition. Each reaction can not only have its own rate parameters, they can have different kinetic formulations, if desired.

Theory

Geochemistry

In this study, the terms *component* and *species* are used in the same manner as in *Westall et al.* [1976]. Components do not necessarily equate to the thermodynamic concept as used in the phase rule; rather, they are defined in the sense that *Rubin* [1983] defined *tenads*. They are chemical entities whose global mass is reaction-invariant. Only physical processes can change the global mass of a component, i.e., advection and dispersion. The most direct comparison is to the *basis* from linear algebra. Components constitute an independent basis set such that all species are formed from linear combinations of the components and no component can be represented by components other than itself. The free component itself is considered a species. The solution to a geochemical problem consists of a concentration value for each species. The solution for an

equilibrium problem is obtained by solving a system of nonlinear mass action equations (one for each non-component species) and linear mass balance equations (one for each component). For a problem that includes kinetic reactions, rate expressions replace the appropriate mass action equation. The total mass for each component is referred to as the total analytical concentration. The total analytical concentration of a particular component is the sum of the concentrations of all species that contain the component, weighted by their stoichiometric coefficients. Since the concentrations of all species are unknown at the outset, the system of equations is closed by specifying a value for the total analytical concentration for each component. Borrowing terminology from *Morel and Hering* [1993], *recipe items* are defined as chemical entities that one might glean from a chemical analysis (e.g., alkalinity, total carbon dioxide, dissolved oxygen, etc.). The recipe items, which provide the value of the total analytical concentration for each component, are written in terms of the chosen component set as:

$$T_j = \sum_{i=1}^{M} s_{ij} x_i = \sum_{i=1}^{R} a_{ij} y_i \qquad j = 1, N_c \tag{3.1}$$

where T_j is the total analytical concentration of component j ($M\ L^{-3}$), M is the number of chemical species, including free components, s_{ij} is the stoichiometric coefficient of component j in species i, x_i is the concentration of species i ($M\ L^{-3}$), R is the number of recipe items, a_{ij} is the stoichiometric coefficient of component j in

recipe item i, y_i is the concentration of recipe item i ($M\ L^{-3}$), and N_c is the number of components.

The compartmentalized approach operates on the premise that some redox reactions dominate over others, allowing less significant reactions to be dropped from the reaction network, as described in Chapter 2. The compartments themselves have no spatial context. They are a function of reaction progress only. The switch from one compartment to the next is governed by a user-specified cut-off criterion. In general, each "compartmentalized" reaction network uses at least some different components and species. The mass balance information (i.e., the total analytical concentration) must, therefore, be passed from one reaction network to the next so that the initial conditions in the new compartment match the final conditions in the old compartment.

To facilitate describing the compartmentalized approach, "driving" and "non-driving" components are defined differently. In general, any number of different organic compounds can be included in the reaction networks. For the redox system of interest in this study, all reactive dissolved organic carbon is lumped together and defined as the component "CH_2O", which is considered to be the driving component. All chemical changes in the system are driven by reactions with "CH_2O". For example, in Chapter 2, small increments of "CH_2O" were added to the simulated system to drive the development of redox zones. For this study, all other components are considered to be non-driving.

As shown in Chapter 2, two redox reactions are present in each compartment. The sequence of reactions and compartments is determined by the energy yield of the redox reactions under consideration. They are ordered from highest to lowest energy. There is always overlap of reactions between compartments. The lower-energy reaction in one compartment is the higher-energy reaction in the next compartment.

The compartmentalized approach for the development of redox zones can be generalized as follows:

$$T_j^n = \sum_{i=1}^{R_n} a_{ij}\, y_i^n + A_j \qquad n = 1, k;\ j = 1, N_c \tag{3.2}$$

$$A_j = \sum_{i=1}^{n-1} s_{(n-i)j}^{h} \left| x_{n-i}^{h,\circ} - x_{n-i}^{h} \right| \qquad \text{if } j \text{ is a non-driving component} \tag{3.3}$$

$$A_j = s_{(n-1)j}^{l} \left| x_{n-1}^{l,\circ} - x_{n-1}^{l} \right| - s_{(n-1)j}^{h} x_{n-1}^{h} \qquad \text{if } j \text{ is the driving component} \tag{3.4}$$

where n is the compartment number, R_n is the number of recipe items in compartment n, y_i^n is the concentration of recipe item i in compartment n, k is the number of compartments, s and x are defined the same as in (3.1) except the superscript h denotes the higher-energy redox species in n, the superscript l denotes the lower-energy redox species in n, and the superscript $^\circ$ denotes the initial concentration. For example, consider the reaction network for compartment two in Chapter 2. The components are H^+, CO_3^{2-}, NO_3^-, and Mn^{2+}.

The redox reactions in this example are denitrification and manganese reduction. Equations (3.2) – (3.4) are written as:

$$T^2_{H^+} = -\mathrm{ALK} + 2[\mathrm{CO_2}]_\Gamma - [\mathrm{MnO_2}(s)]_\Gamma + A_{H^+} \tag{3.5}$$

$$T^2_{CO_3^{2-}} = [\mathrm{CO_2}]_\Gamma + 0.5[\mathrm{MnO_2}(s)]_\Gamma + A_{CO_3^{2-}} \tag{3.6}$$

$$T^2_{NO_3^-} = [\mathrm{NO_3}]_\Gamma + A_{NO_3^-} \tag{3.7}$$

$$T^2_{Mn^{2+}} = [\mathrm{MnO_2}(s)]_\Gamma + A_{Mn^{2+}} \tag{3.8}$$

$$T^2_{"CH_2O"} = ["\mathrm{CH_2O}"]_\Gamma - 0.5[\mathrm{MnO_2}(s)]_\Gamma + A_{"CH_2O"} \tag{3.9}$$

$$A_{H^+} = 2([\mathrm{O_2}(aq)]^\circ - [\mathrm{O_2}(aq)]) \tag{3.10}$$

$$A_{CO_3^{2-}} = [\mathrm{O_2}(aq)]^\circ - [\mathrm{O_2}(aq)] \tag{3.11}$$

$$A_{NO_3^-} = 0 \tag{3.12}$$

$$A_{Mn^{2+}} = 0 \tag{3.13}$$

$$A_{"CH_2O"} = 1.25([\mathrm{NO_3^-}]^\circ - [\mathrm{NO_3^-}]) - ([\mathrm{O_2}(aq)]) \tag{3.14}$$

If the redox reactions are specified as kinetic reactions, which allows the assumption of an excess of the driving component, then (3.4) can be set to zero. It is assumed here that the redox reactions are mediated by microbes and that the overall result of the oxidation of organic carbon at the Cape Cod site can be represented by the four redox reactions shown in Table 2.1. Since the redox reactions represent biogeochemical processes, it is assumed that they are rate-

limited processes, and they are simulated as kinetic reactions. *Bekins et al.* [1998] have shown that biogeochemical reactions, over a range of concentrations, are best represented by a hyperbolic rate expression, such as the Monod or Michaelis-Menten expressions. The Michaelis-Menten expression is mathematically similar to the Monod expression except that the Monod expression typically has a term for the concentration of microbes. The relatively low DOC concentrations at the Cape Cod site [*Thurman et al.*, 1986] suggest that there is no net growth of the bacterial communities. Under these conditions the concentration of microbes can be ignored and the Monod no-growth expression can be written as:

$$\frac{dC}{dt} = -k\frac{C}{k_c + C} \tag{3.15}$$

where C is the concentration of an electron acceptor ($M\ L^{-3}$), k is the maximum reaction rate ($M\ L^{-3}\ T^{-1}$), k_c is the concentration at which the reaction rate is half the maximum rate, the so-called half-saturation constant ($M\ L^{-3}$), and t is time (T). Note that (3.15) reduces to first-order kinetics at low reactant concentrations and to zero-order kinetics at high reactant concentrations.

It is intuitive that the rate of reaction should be a function not only of the concentration of the electron acceptor, but also of the organic substrate. Thus, a modified Monod relationship [*Bailey and Ollis*, 1977; *Molz et al.*, 1986] was adopted:

$$\frac{dC}{dt} = -k\left(\frac{C}{k_c + C}\right)\left(\frac{S}{k_s + S}\right) \tag{3.16}$$

where S is the concentration of organic substrate ($M\ L^{-3}$) and k_s is the half-saturation constant associated with the substrate ($M\ L^{-3}$). This formulation allows either the organic substrate or the electron acceptor to limit the reaction rate, if either of their concentrations are low. For example, when $S << k_s$, the organic substrate term on the right-hand side of (3.16) becomes small and limits the overall reaction rate.

The various microbial communities that mediate the redox reactions shown in Table 2.1 essentially compete for whatever organic carbon is available. The geochemical portion of the simulations utilizes two redox reactions in each compartment, plus aqueous *p*H buffering reactions and appropriate aqueous speciation reactions for that compartment. In a given compartment, simulations in which both electron acceptors and organic substrate are present in excess will show that both reaction rates have finite, positive values. In the absence of any reaction inhibition, both electron acceptors would be consumed. Thermodynamic constraints, however, dictate which reactions should actually occur. The same procedure described in Chapter 2 is used to determine reaction feasibility and the amount of dissolved organic carbon that should be partitioned to each reaction. No empirical reaction inhibition is used in this study.

Solute Transport

Computational strategy

Transport of conservative solutes is usually described by linear partial differential equations, with one written for each solute. Many different schemes have been proposed to couple equilibrium geochemical reactions with solute transport simulators. *Yeh and Tripathi* [1989] reviewed the three general approaches that have been taken and evaluated them in terms of their flexibility, practicality (i.e., CPU time and memory usage), and the ease with which kinetic reactions can be included.

The three approaches described by *Yeh and Tripathi* [1989] differ by the manner in which the equations describing geochemical reactions are coupled to the solute transport equations. The approaches *Yeh and Tripathi* reviewed either (i) solve simultaneously a mixed system of differential and algebraic equations, (ii) solve simultaneously a system of nonlinear partial differential equations, or (iii) iterate sequentially between linear partial differential equations and nonlinear algebraic equations (± ordinary differential equations for kinetics). *Yeh and Tripathi* [1989] concluded that the latter approach, the sequential iteration approach (SIA), holds the most promise for solving a wide range of practical problems. One advantage of the SIA is that the nonlinearities caused by the geochemical equations are removed from the partial differential equations, making the task of solving the solute transport equations much simpler. Another

advantage of the SIA is that it is relatively straightforward to utilize the wide range of already available geochemical codes.

The SIA can be further subdivided. For example, one could use the concentration of each dissolved species as the dependent variable in the solute transport equations. To apply this method, one needs a separate solute transport equation for each dissolved species, a number that can become quite large. Alternatively, one could solve for the total dissolved concentration of each aqueous component in the transport equation [*Theis et al.*, 1982; *Kirkner et al.*, 1984, 1985; *Engesgaard and Kipp*, 1992]. Both of these methods calculate the chemical speciation in a separate chemical module of the computer code, but for the latter approach the solute transport equations have no direct knowledge of the individual chemical species. Clearly, such a method has the potential to significantly reduce the number of solute transport equations needed.

A third variant of the SIA employs the total analytical concentration of each component as the dependent variable in each transport equation. With this method, all forms of the component (i.e., total dissolved, total sorbed, and total precipitated) are summed and used as the dependent variable in the solute transport equations. Again, the chemical speciation is calculated in a separate chemical module. This method is very convenient because, as described above, the known value of the total analytical concentration for each component provides closure for the geochemical system of equations. Furthermore, it is

very easy to include precipitated species and kinetic species with this variant of the SIA [*Yeh and Tripathi*, 1989].

The approach employed in this study is the SIA, with the total analytical concentration of each component as the dependent variable in the solute transport equation. I modified HYDROGEOCHEM 2.1 [*Yeh and Salvage*, 1995] to use the compartmentalized approach described above (and in Chapter 2) and to include no-growth Monod kinetics.

In the unmodified HYDROGEOCHEM 2.1, transport of equilibrium species is achieved by solving the relevant mass action equations at each time step and then utilizing (3.1) to calculate the total analytical concentration of each component, which is then solved for at the next time step with the advection-dispersion equation, given as:

$$\frac{\partial T_j}{\partial t} = -\nabla \cdot \left(\bar{\mathbf{v}} C_j\right) + \nabla \cdot \left(\mathbf{D} \cdot \nabla C_j\right) \qquad j = 1, N_c \tag{3.17}$$

$$C_j = T_j - P_j \tag{3.18}$$

where C_j is the total dissolved concentration of component j ($M\ L^{-3}$), P_j is the total precipitated concentration of component j ($M\ L^{-3}$), $\bar{\mathbf{v}}$ is the average linear velocity vector ($L\ T^{-1}$), and $\mathbf{D}$ is the dispersion coefficient tensor ($L^2\ T^{-1}$). Since the T_js are functions of the C_js, functional relationships need to be defined to link them.

These functional relationships are the mass action and mass balance equations discussed above.

Kinetic species

Kinetic species are not simply functions of the concentrations of the components that form them. Accordingly, each aqueous kinetic species must have its own solute transport equation:

$$\frac{\partial c_i}{\partial t} = -\nabla \cdot (\bar{\mathbf{v}} c_i) + \nabla \cdot (\mathbf{D} \cdot \nabla c_i) + r_i \qquad i = 1, N_k \qquad (3.19)$$

where c_i is the concentration of the ith aqueous kinetic species ($M\,L^{-3}$), r_i is the rate of production of the ith aqueous kinetic species ($M\,L^{-3}\,T$), and N_k is the number of aqueous kinetic species. The contribution of the kinetic species to the total analytical concentration of each relevant component is accounted for with (3.1) before (3.17) and (3.18) are solved.

Equation (3.19) indicates that there is one transport equation for each aqueous kinetic species. Because the number of such species may be different in different compartments, a decision must be made regarding boundary conditions. For example, if one were to drop the kinetic species O_2 from the reaction network upon switching from compartment one to compartment two (i.e., oxic to suboxic), a discontinuity in (3.19) would be created. Moving boundaries would thus be needed for (3.19). The moving boundaries would

separate the regions of an aquifer that are in the compartment one stage of reaction progress from those that are in different compartments.

The approach used here is to simply retain the aqueous kinetic species from previous compartments so that no discontinuity develops and moving boundaries are not needed. This may seem to contradict the original premise of the compartmentalized approach, but it does not. A chief advantage of the compartmentalized approach is the ease with which thermodynamic feasibility can be decided. This is not affected by retaining insignificant kinetic reactions. When checking for thermodynamic feasibility, the insignificant reactions are still ignored; i.e., thermodynamic calculations are not performed for species that are not part of the compartment in question. Furthermore, the numerical difficulties associated with calculating concentrations from insignificant reactions occur only in the thermodynamic computations. The kinetic species are retained solely for the purpose of preventing discontinuities in (3.19). Moreover, when an insignificant kinetic species is retained, the concentration of that species is small, due to the cut-off criteria. Thus, the contribution of the retained kinetic species to changes in chemical speciation is small, and the rate of reaction at this point is quite slow because of (3.16).

There are two precipitated kinetic species associated with the reaction network used in this effort (see Table 2.1). Since the precipitated species are immobile, they do not need a transport equation. However, the precipitated species may be composed of components that are not present in all

compartments. In this study, the component Mn is only present in compartments two and three (for $MnO_2(s)$) and associated aqueous complexes) and the component Fe is only present in compartment three (for $Fe(OH)_3(s)$) and associated aqueous complexes). Again, there is the potential for discontinuities in transport equations that could be handled with moving boundaries. This time, however, it is (3.17) that could encounter a discontinuity at compartment boundaries, because the transported entities (i.e., dissolved Mn and Fe) are components, not kinetic species. A strategy similar to that used for aqueous kinetic species is employed. Since the incoming water is pristine (i.e., in compartment one), Mn and Fe are defined as having a dissolved concentration of zero at the upstream boundary but an initial condition throughout the spatial domain that consists solely of precipitated concentration. This allows T_{Mn} and T_{Fe} to be continuous across the spatial domain because of (3.18).

Linkage

Inspection of (3.2) and (3.3) reveals that there is yet another potential for discontinuities in T_j during the course of redox zone development. This second type of discontinuity cannot be handled in a manner similar to the kinetic species because it occurs with components that are present in all compartments. The cause of the discontinuity is that some components may experience a large change in value at compartmental boundaries. Clearly, such discontinuities would wreak havoc on most numerical methods for solute transport. An

alternative formulation for the compartmentalized approach that circumvents this problem is:

$$T_j^n = T_j^1 + \sum_{i=1}^{R_n} a_{ij}\, y_i^n \Big|_{y_i^n \neq y_i^1} - \sum_{i=1}^{n-1} s_{(n-1)j}^h x_{n-1}^h \qquad n = 1, k;\, j = 1, N_c \tag{3.20}$$

When simulating perturbed redox systems, it can usually be assumed that the dissolved redox species are either initially zero or initially the maximum value for that particular setting. For these conditions, it can be shown that (3.20) is equivalent to (3.2) through (3.4). As an example, consider the reaction network outlined in Chapter 2, which is also the reaction network used in this chapter. Expanding (3.2) and (3.3) for the total analytical concentration of H^+ in compartment two yields:

$$T_H^2 = -\mathrm{ALK} + 2[\mathrm{CO_2}]_\Gamma - [\mathrm{MnO_2}(s)]_\Gamma + 2[\mathrm{O_2(aq)}]^\circ - 2[\mathrm{O_2}(aq)] \tag{3.21}$$

Expanding (3.20) for the total analytical concentration for H^+ in compartment two yields:

$$T_H^2 = -\mathrm{ALK} + 2[\mathrm{CO_2}]_\Gamma + 2[\mathrm{O_2}]_\Gamma - [\mathrm{MnO_2}(s)]_\Gamma - 2[\mathrm{O_2}(aq)] \tag{3.22}$$

Since $[\mathrm{O_2}(aq)]^\circ = [\mathrm{O_2}]_\Gamma$, (3.21) and (3.22) are equivalent.

When (3.20) is used to account for compartmental switching, one simply transports only T_j^1 for components that are subject to large changes between compartments (in this effort H^+ and CO_3^{2-}). This alternative formulation for the compartmentalized approach eliminates the discontinuities associated with (3.2)-(3.4). T_j^n is calculated from (3.20) and then passed to the chemical module.

Flow chart of the model structure

The geochemical code KEMOD [*Yeh et al.*, 1993, 1998] and the coupled solute transport/geochemical code HYDROGEOCHEM 2.1 [*Yeh and Salvage*, 1995] were extensively modified for this study to incorporate the compartmentalized approach. HYDRAQL [*Papelis et al.*, 1988] was incorporated within the modified HYDROGEOCHEM 2.1 to calculate the equilibrium concentrations.

All of the solute transport simulations performed in this effort were conducted with the modified (compartmentalized) version of HYDROGEOCHEM 2.1. The flow chart in Figure 3.1 illustrates how the compartmentalized solute transport/geochemical model operates. Only the major subroutines are shown in Figure 3.1. It should be pointed out that each one of the subroutines shown in Figure 3.1 (except for truth.f) contains calls to other subroutines to perform various tasks related to the primary purpose of the calling routine. The new routines that were developed or modified for HYDROGEOCHEM 2.1 for this study are represented, respectively, by the dark

Figure 3.1. Two-part flow chart illustrating how the compartmentalized solute transport model operates. HYDROGEOCHEM 2.1 [*Yeh and Salvage*, 1995] was used as a framework in this study. Many of the routines from HYDROGEOCHEM 2.1 were not modified for this study (i.e., items with no shading). The new routines developed for this study are shown in dark gray. The existing routines that were modified, to varying degrees, are shown in light gray. Variables are as follows; t is time, t_f is the final time step, Tw is the iterate of T, n is the node number, nn is the total number of nodes. All other variables are either defined on the flow chart or are the same as already defined in this chapter or in Chapter 2. (a) gm2d is the major "controlling" subroutine of HYDROGEOCHEM 2.1. (b) ocspit is the HYDROGEOCHEM 2.1 subroutine that loops over all nodes to calculate the concentrations of all species.

(a)

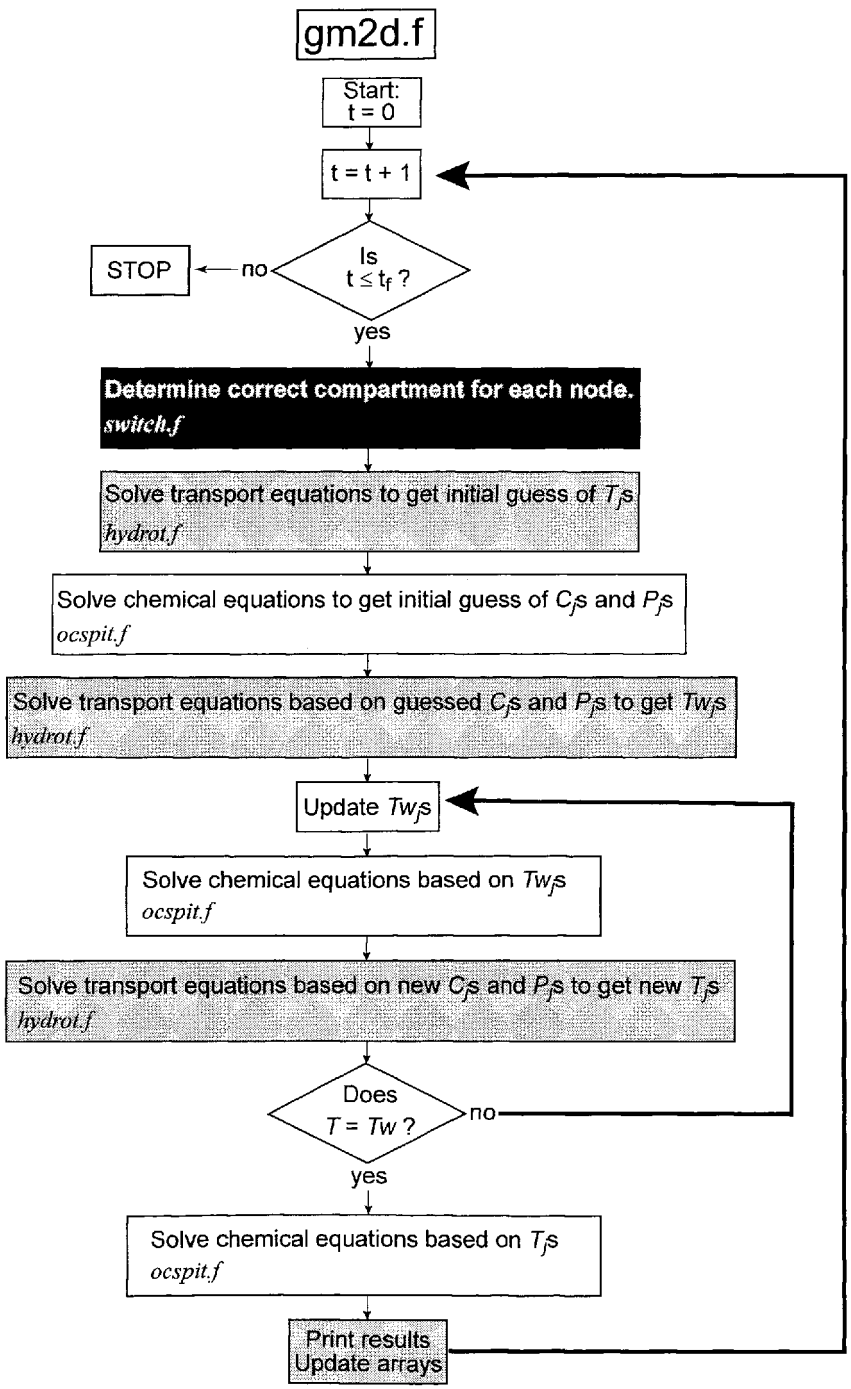
gm2d.f
Start:
t = 0
t = t + 1
Is
t ≤ tf ?
no
STOP
yes
Determine correct compartment for each node.
switch.f
Solve transport equations to get initial guess of Tjs
hydrot.f
Solve chemical equations to get initial guess of Cjs and Pjs
ocspit.f
Solve transport equations based on guessed Cjs and Pjs to get Twjs
hydrot.f
Update Twjs
Solve chemical equations based on Twjs
ocspit.f
Solve transport equations based on new Cjs and Pjs to get new Tjs
hydrot.f
Does
T = Tw ?
no
yes
Solve chemical equations based on Tjs
ocspit.f
Print results
Update arrays

(b)

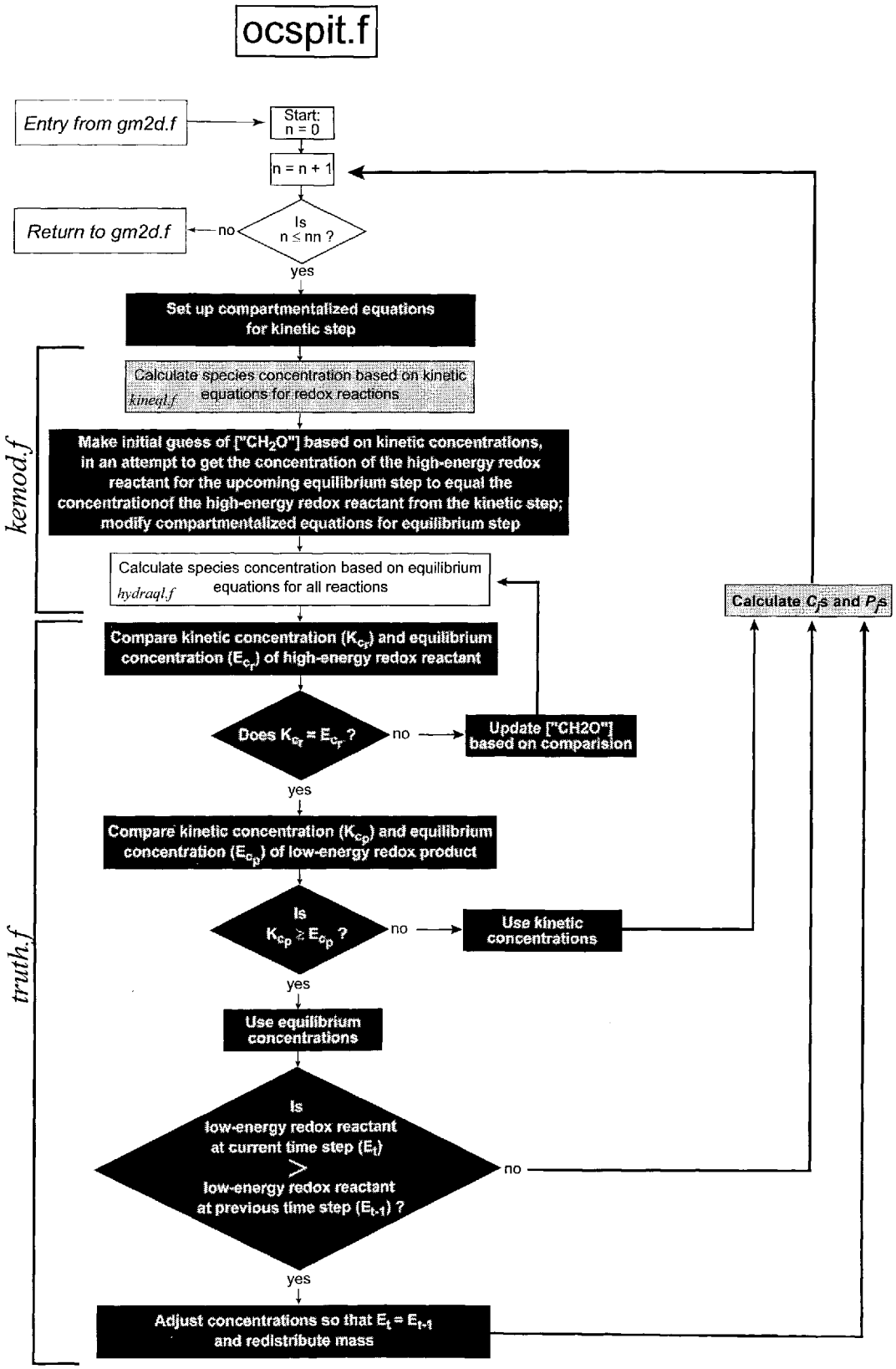
ocspit.f
Entry from gm2d.f
Start: n = 0
n = n + 1
Return to gm2d.f
no
Is n ≤ nn ?
yes
Set up compartmentalized equations for kinetic step
Calculate species concentration based on kinetic equations for redox reactions
kineql.f
Make initial guess of ["CH2O"] based on kinetic concentrations, in an attempt to get the concentration of the high-energy redox reactant for the upcoming equilibrium step to equal the concentrationof the high-energy redox reactant from the kinetic step; modify compartmentalized equations for equilibrium step
kemod.f
Calculate species concentration based on equilibrium equations for all reactions
hydraql.f
Calculate C_js and P_js
Compare kinetic concentration (K_{c_r}) and equilibrium concentration (E_{c_r}) of high-energy redox reactant
Does $K_{c_r} = E_{c_r}$?
no
Update ["CH2O"] based on comparision
yes
Compare kinetic concentration (K_{c_p}) and equilibrium concentration (E_{c_p}) of low-energy redox product
Is $K_{c_p} \geq E_{c_p}$?
no
Use kinetic concentrations
yes
Use equilibrium concentrations
Is low-energy redox reactant at current time step (E_t) > low-energy redox reactant at previous time step (E_{t-1}) ?
no
yes
Adjust concentrations so that $E_t = E_{t-1}$ and redistribute mass
truth.f

gray and light gray boxes in Figure 3.1. In addition to performing geochemical and solute transport calculations, the model essentially works by making two key decisions. The first decision to be made is to assign each node to the correct compartment. This decision is made by the subroutine switch.f (Figure 3.1a). The sequence of operations that is followed each time ocspit.f is called by gm2d.f is illustrated in the flow chart on Figure 3.1b.

The subroutine ocspit.f loops over the entire set of nodes in the boundary-value problem and calculates a "batch" geochemical solution at each node. The second major decision is made within the geochemical sequence of operations. A decision is made within the subroutine truth.f as to whether the lower-energy redox reaction within a given compartment is behaving in a rate-limited or thermodynamically-limited manner. This decision is made by determining whether the concentration of the lower-energy redox product is lower in the kinetic step or in the thermodynamic step. If it is lower in the kinetic step, then the reaction is rate-limited. If it is lower in the thermodynamic step, then the reaction is being limited by free energy constraints.

Elimination of Transport Equations

Depending on how the geochemical problem is formulated, it may not be necessary to write a transport equation (i.e., 3.17) for each component. Recall that the global mass of a component is reaction invariant and is also independent of other components. The compartmentalized approach allows the definition of

at least one reaction network in which the total analytical concentration (i.e., T_j) of some components does not change. These two ideas allow transport equations to be dropped from the system of equations under consideration.

Consider a pristine aquifer that is governed by oxic compartment conditions, in which the components are H^+, CO_3^{2-}, NO_3^-, and "CH_2O" and oxygen reduction and denitrification are the only redox reactions. By definition, these reactions cannot change T_H^1 or $T_{CO_3}^1$. The contaminants, $T_{NO_3}^1$ and $T_{"CH_2O"}^1$, are initially infinitesimal in the aquifer. The upgradient boundary is set to allow the influx of pristine groundwater (plus unreacted contaminants) that is also governed by oxic compartment conditions. Hence, the upstream boundary conditions for H^+ and CO_3^{2-} are equal to the initial conditions for H^+ and CO_3^{2-}, respectively. Thus, advection and dispersion cannot change T_H^1 or $T_{CO_3}^1$.

H^+ and CO_3^{2-} are components in each compartment. Solid phases that are present in later compartments can change the total analytical concentrations of H^+ and CO_3^{2-} due to advection and dispersion. Since only T_j^1 would be transported for H^+ or CO_3^{2-}, (3.17) is not needed for these components because T_H^1 and $T_{CO_3}^1$ do not change in time or space. One simply specifies that T_H^1 and $T_{CO_3}^1$ remain fixed in value. The chemistry is computed correctly because (3.20) is used to calculate T_H^n and $T_{CO_3}^n$ before passing them to the chemistry module. For the problem at hand, this reduces the total number of transport equations (i.e., (3.17) plus (3.19)) from eight to six.

Testing of the Compartmentalized Solute Transport Model

Implementation of the compartmentalized solute transport model consisted of coding equations 3.16 and 3.20 and necessary associated modifications into HYDROGEOCHEM 2.1 [*Yeh and Salvage*, 1995], debugging, and testing. To test the newly created model, a 1.0 m, one-dimensional solute transport problem and a two-dimensional, 0.1 m by 0.5 m solute transport problem were devised.

One-Dimensional Simulation

The one-dimensional simulation used for model testing can be conceptualized as a sand-filled laboratory column that is one meter in length. The flux of water into the column was set to 7×10^{-5} m d^{-1}. The porosity of the sand was assumed to be 0.3, which yields an average linear velocity of 2.3×10^{-4} m d^{-1}. The dispersivity was set to 0.025 m (i.e., the same as Δx).

The initial conditions, shown in Figure 3.2a, were designed to approximate pristine groundwater at the Cape Cod site; dissolved oxygen (DO) of 2.5×10^{-4} M, alkalinity of 0.06 meq l^{-1}, and total inorganic carbon of 5×10^{-4} M. These parameters yield an initial *p*H of 5.51. Two solid phases, $MnO_2(s)$ and $Fe(OH)_3(s)$, were initially present at 10^{-5} and 10^{-3} M, respectively. These two solids were conceptually considered to be weathering coatings on aquifer solids.

(a)

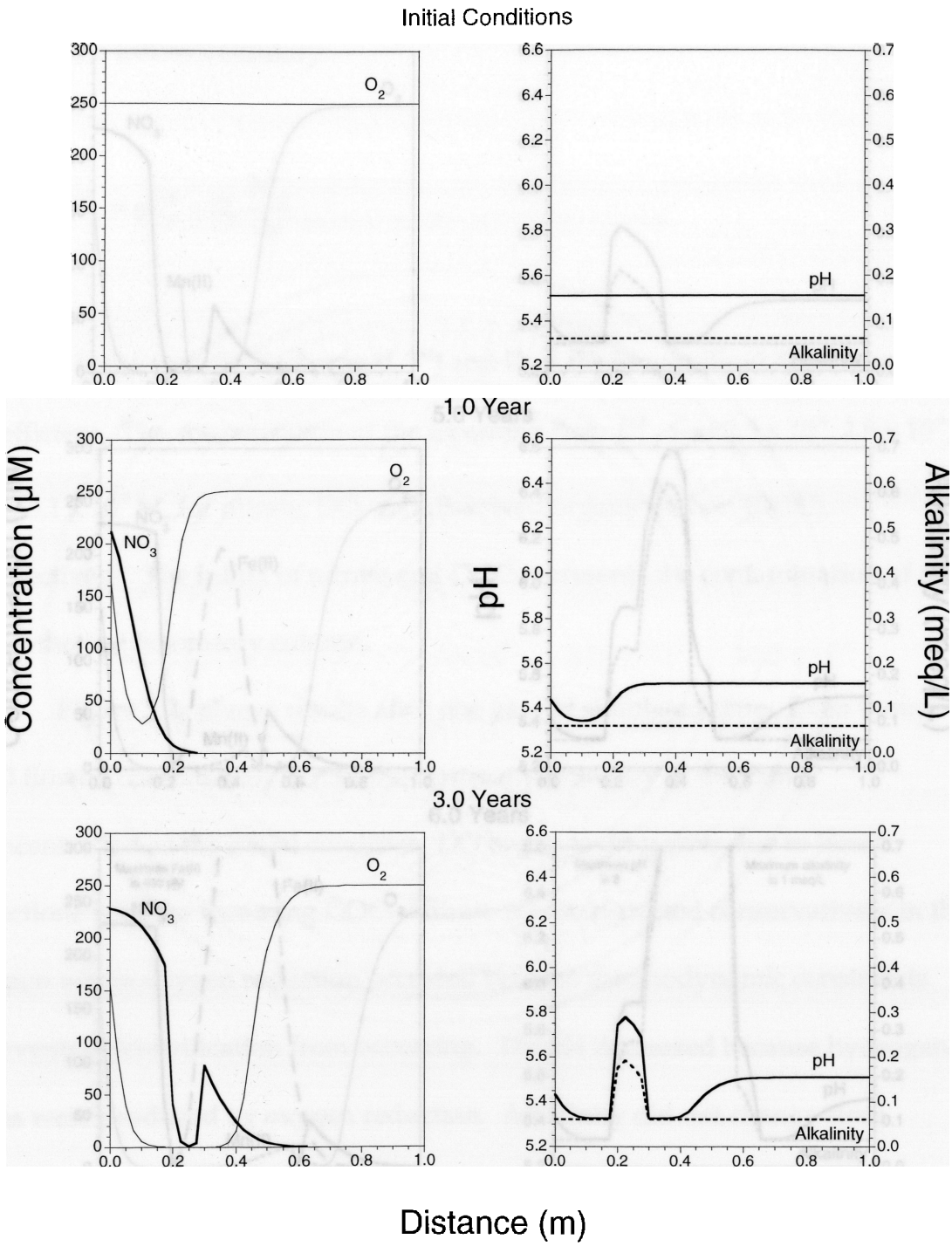

Figure 3.2. Concentration profiles for the one-dimensional test simulation showing (a) the initial conditions and results for 1.0, 3.0 years and (b) results for 3.5, 5.0, and 6.0 years.

(b)

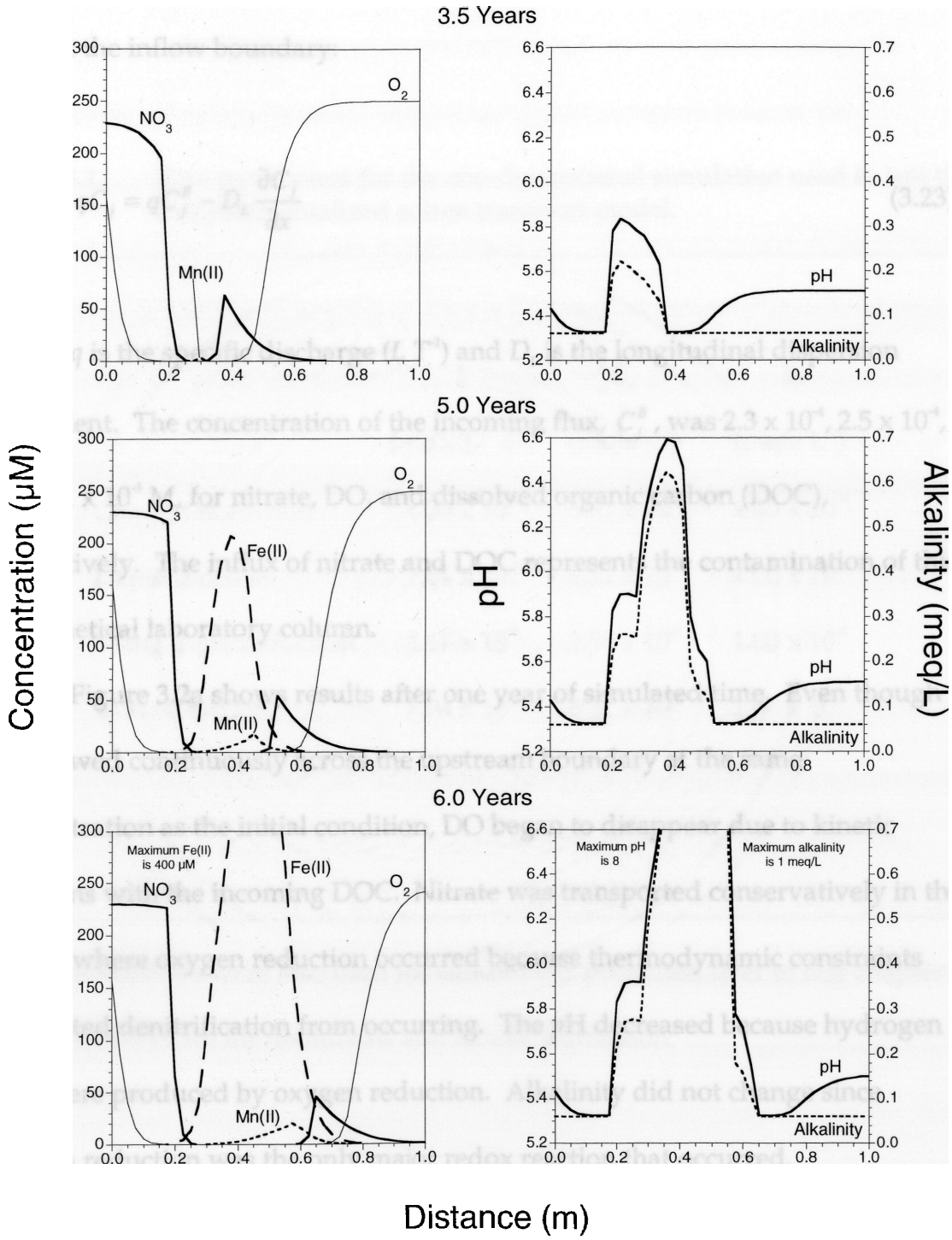
3.5 Years
5.0 Years
6.0 Years
NO3
O2
Mn(II)
Fe(II)
pH
Alkalinity
Maximum Fe(II) is 400 µM
Maximum pH is 8
Maximum alkalinity is 1 meq/L
Concentration (µM)
Alkalinity (meq/L)
Distance (m)

The rate parameters for the simulation are shown in Table 3.1.

To simulate contamination of the column, a flux boundary condition was used at the inflow boundary:

$$qC_j = qC_j^B - D_L \frac{\partial C_j}{\partial x} \tag{3.23}$$

where q is the specific discharge ($L\ T^{-1}$) and D_L is the longitudinal dispersion coefficient. The concentration of the incoming flux, C_j^B, was 2.3 x 10^{-4}, 2.5 x 10^{-4}, and 3.1 x 10^{-3} M, for nitrate, DO, and dissolved organic carbon (DOC), respectively. The influx of nitrate and DOC represents the contamination of this hypothetical laboratory column.

Figure 3.2a shows results after one year of simulated time. Even though DO flowed continuously across the upstream boundary at the same concentration as the initial condition, DO began to disappear due to kinetic reactions with the incoming DOC. Nitrate was transported conservatively in the region where oxygen reduction occurred because thermodynamic constraints prevented denitrification from occurring. The *p*H decreased because hydrogen ions were produced by oxygen reduction. Alkalinity did not change since oxygen reduction was the only major redox reaction that occurred.

As seen in Figure 3.2a, by three years of simulated time, consumption of DOC caused the DO concentration to decrease enough to allow denitrification to

Table 3.1. Rate parameters for the one-dimensional simulation used to test the compartmentalized solute transport model.

	k	k_c	k_s
	(mole L^{-1} d^{-1})	(mole L^{-1})	(mole L^{-1})
Oxygen reduction	1.26×10^{-6}	5.01×10^{-5}	1.00×10^{-5}
Denitrification	1.26×10^{-6}	2.51×10^{-5}	1.00×10^{-5}
Manganese reduction	4.47×10^{-7}	3.98×10^{-7}	1.00×10^{-5}
Iron reduction	7.94×10^{-7}	6.31×10^{-5}	1.00×10^{-5}

These parameters were also used for simulations presented later in this chapter.

See equation (3.16) for definitions and kinetic expression.

commence. Accordingly, the nitrate profile exhibits a region of "missing mass" where denitrification has occurred. Also, the *p*H increased due to the consumption of hydrogen ions via denitrification. A very small amount of manganese reduction occurred in the denitrification region because the thermodynamic calculation indicated that manganese reduction was not quite completely inhibited, although it was nearly so. The concentration of dissolved manganese is too low to be seen on Figure 3.2a at three years of simulated time.

After 3.5 years of simulated time (Figure 3.2b), the zone of denitrification had grown to cover approximately 0.15 m of the column. The concentration of dissolved manganese increased enough via kinetic reductive dissolution of $MnO_2(s)$ to just appear on the plot (approximately 3 μM). The *p*H had almost reached 5.9 and the alkalinity continued to increase.

By five years of simulated time (Figure 3.2b), an iron zone had formed due to the reduction of $Fe(OH)_3(s)$. This final redox reaction was thermodynamically feasible after the available $MnO_2(s)$ had been exhausted. The peak dissolved manganese concentration on Figure 3.2b is approximately 20 μM. The *p*H values reached about 6.6 in the zone of iron reduction. Denitrification was still thermodynamically-inhibited in the first 0.2 m due to the constant influx of DO.

The test simulation illustrated in Figure 3.2 was stopped at six years. As more and more $MnO_2(s)$ was depleted, the iron reducing zone continued to expand in length. The peak dissolved iron concentration after six years was approximately 400μM, and the *p*H had reached a value of approximately 8. The

last remaining high concentrations of oxygen left over from the initial condition had almost been swept from the problem domain.

Two-Dimensional Simulation

Motivation

The two-dimensional test simulation can be conceptualized as a longitudinal, vertical slice through a plot-scale reactive tracer test. The spatial domain for the simulation was 0.5 m long by 0.1 m high. The plot scale simulation demonstrates that the approach taken in this effort is functional in two dimensions. The ability to perform two-dimensional simulations is useful because not all of the transport phenomena known to occur can be simulated in one dimension.

The phenomenon focused upon in the two-dimensional simulation presented in this section is vertical transverse dispersion. This focus was motivated by the observation that at the Cape Cod site, sharp, vertical gradients in key chemical constituents persist over travel distances of at least 3000 m [*Smith et al.*, 1991b]. *Smith et al.* proposed that these gradients result from the accumulation of natural recharge water on top of the sewage plume. While this is certainly the dominant cause, it is worth pointing out that the sharp, vertical gradients also exist below the plume (see Figure 1.4). In actuality, the recharge water may make the chemical gradient less steep. The sharp concentration

gradients are present through a suboxic transition zone that exists between the anoxic core of the plume and the pristine, oxic groundwater.

It appears that the existence of the suboxic transition zone is the result of transverse mixing between contaminated and uncontaminated groundwater. It is reasonable to assume, if there were no vertical mixing at all, that the chemical gradients would be even steeper, in theory, tending toward infinity. Of course, there are no situations in nature where mixing is nonexistent. There is always some molecular-scale diffusion. *Garabedian et al.* [1991] determined the longitudinal dispersivity to be 0.96 m and vertical transverse dispersivity to be 1.5×10^{-3} m at the Cape Cod site. While the transverse dispersivity represents a very small amount of mixing, it is reasonable to assume that the largest fraction of the mixing is due to mechanical dispersion and not molecular diffusion. This being the case, the question asked, relative to the work described in Chapter 2 and this chapter is: Can the compartmentalized approach be expected to simulate the formation of the suboxic transition zone?

I hypothesize that there are two distinct reasons why there are persistent suboxic zones. The first reason is due purely to rate-limited chemical reactions. This can be seen by examining the results of the one-dimensional simulation presented in the previous section. In the one-dimensional simulation, there is a suboxic zone that is persistent between the upgradient boundary and the anoxic zone. The constant influx of DO maintains the concentrations of DO that are characteristic of the suboxic zone, which are between the DO concentrations in

the denitrifying and iron reducing zones and the DO concentrations in the oxic zone (e.g., the boundary condition for DO). Such a suboxic region would occur in the absence of mixing.

The mixing hypothesis, proposed here, states that dispersion is the primary cause of the suboxic transition zones that exist above, below, and immediately downgradient of the anoxic zone. Rate-limited chemical reactions are at most a secondary cause of these transition zones. The dispersion that causes these transition zones could be predominantly molecular or mechanical. For the purposes of testing the mixing hypothesis, no distinction is made between spreading, mixing, diffusion, or dispersion, nor the causes thereof. Such distinctions are well beyond the scope of this dissertation, as they are areas of intense, continuing research.

Problem setup

To test the mixing hypothesis proposed above, a two-dimensional compartmentalized solute transport simulation that included transverse dispersion was conducted. A two-dimensional simulation was needed because one-dimensional simulations can only simulate a mixing-derived suboxic transition zone immediately downgradient of the anoxic zone.

The boundary-value problem was constructed such that it included only a horizontal component of velocity (i.e., 2.6×10^{-5} m d^{-1}), but included transverse and longitudinal dispersivities, using values that were obtained during

experiments at the Cape Cod site [*Garabedian et al.*, 1991]. In this way, the purely chemically-based suboxic zone will still form as it did in the one-dimensional simulations presented above, i.e., between the contaminant source and the anoxic zone, along a flow path. The mixing hypothesis predicts that a suboxic zone will develop above and below the anoxic zone due to transverse dispersion and downgradient of the anoxic zone due to longitudinal dispersion. It should be pointed out that this test problem did not require a flow simulation because the desired velocity was determined *a priori*. The velocity in this test problem has no relation to actual velocities at the Cape Cod site.

The numerical technique used to solve the solute transport equations was an Eulerian finite-element method. Trial-and-error simulations indicated that a mesh Peclet number of 0.5 in the vertical direction was needed to avoid significant oscillations in the transverse direction. The vertical transverse dispersivity calculated by *Garabedian et al.* [1991] during their experiments at the Cape Cod site was 1.5×10^{-3} m, so the vertical discretization (i.e., Δz) was chosen to be 8×10^{-4} m. Oscillations in the longitudinal direction were not an issue because the longitudinal dispersivity determined by *Garabedian et al.* (i.e., 0.96 m) is about twice as large as the length of the spatial domain. Nonetheless, the horizontal discretization was also relatively fine ($\Delta x = 1.5 \times 10^{-2}$ m) so that the aspect ratio (i.e., $\Delta x/\Delta z$) of the model elements was not excessively large. Such a fine spatial discretization required a proportionately fine temporal discretization.

The use of spatial and temporal increments of such a small magnitude for the field-scale simulation presented later in this chapter would have resulted in a finite-element mesh containing 3.3×10^8 nodes. Fortunately, the impact of transverse dispersion can be explored effectively at the plot scale. Thus, the concept-development simulations presented in this section utilizing the small spatial and temporal increments were performed at the plot scale.

The initial conditions for the two-dimensional, plot-scale simulation were designed to approximate pristine groundwater at the Cape Cod site. The initial concentration of DO was 2.5×10^{-4} M, the initial alkalinity was 0.06 meq l^{-1}, and the initial total inorganic carbon was 5×10^{-4} M. These parameters yield an initial *p*H of 5.51. Two solid phases, $MnO_2(s)$ and $Fe(OH)_3(s)$, conceptually considered to be weathering coatings on aquifer solids, were initially present at 10^{-5} and 10^{-3} M, respectively. The rate parameters for the two-dimensional, plot scale simulation are those given in Table 3.2.

The boundary conditions for solute transport for the two-dimensional, plot-scale simulation are shown in Figure 3.3. The total analytical concentration of each component (i.e., the value of each tenad) was fixed at the upgradient boundary (i.e., a constant concentration boundary condition was imposed). Over most of the upgradient boundary, the incoming water was the same as the water that was initially present in the aquifer, i.e., it had characteristics of pristine groundwater. Over a small distance in the middle of the upgradient boundary (2.4×10^{-3} m) the incoming water also contained nitrate and DOC at 2.3×10^{-4} and

Table 3.2. Rate parameters used for the plot-scale, two-dimensional test simulation.

	k (mole L^{-1} d^{-1})	k_c (mole L^{-1})	k_s (mole L^{-1})
Oxygen reduction	1.99×10^{-6}	1.58×10^{-5}	1.00×10^{-5}
Denitrification	1.58×10^{-6}	1.58×10^{-5}	1.00×10^{-5}
Manganese reduction	3.16×10^{-6}	3.98×10^{-7}	1.00×10^{-5}
Iron reduction	3.16×10^{-6}	1.58×10^{-5}	1.00×10^{-5}

These parameters were also used for simulations presented later in this chapter.

See equation (3.16) for definitions and kinetic expression

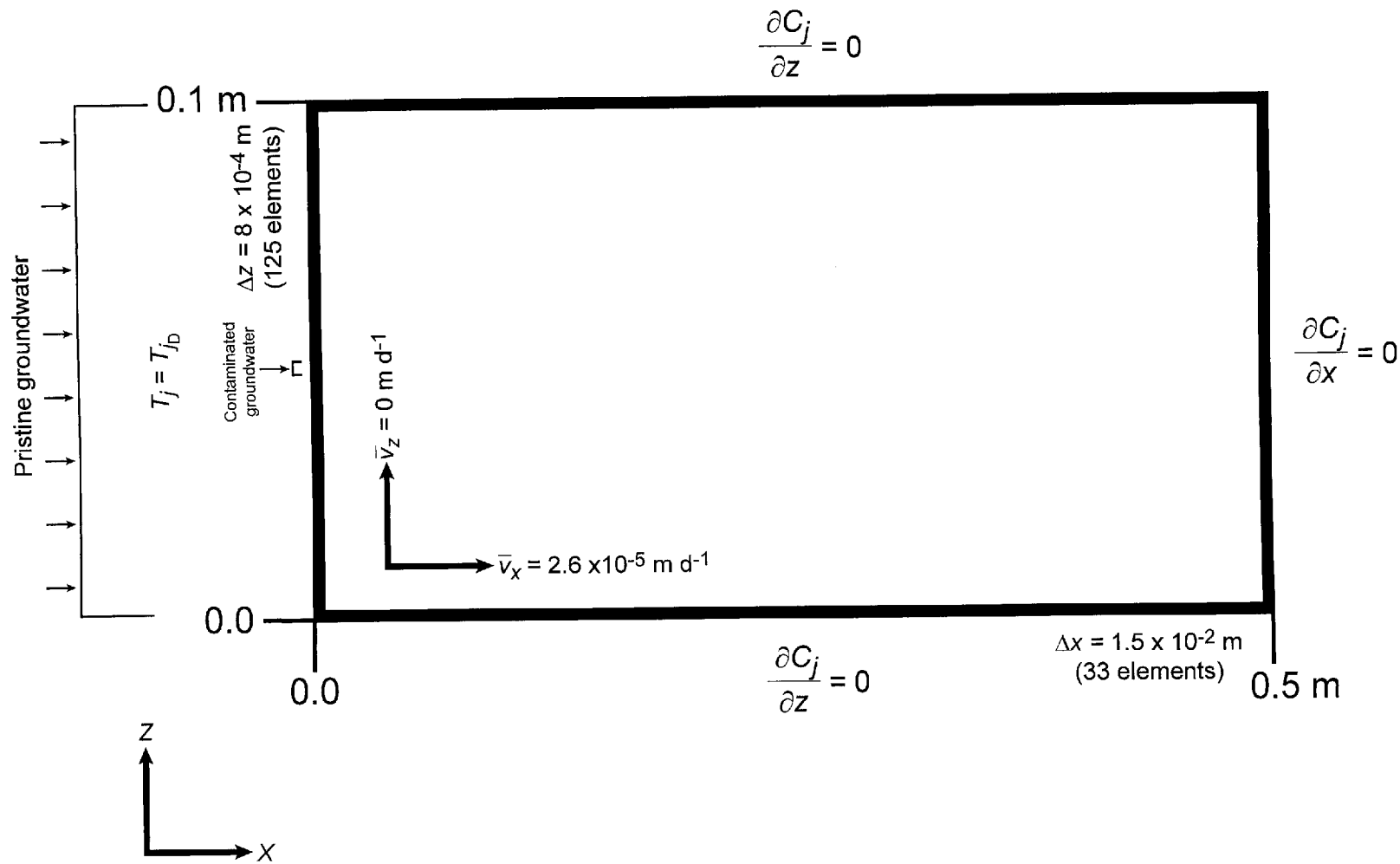

Figure 3.3. Boundary-value problem for the plot-scale, two-dimensional compartmentalized solute transport test simulation. T_{jD} is the total analytical concentration that is fixed at constant concentration boundary nodes.

5.9×10^{-2} M, respectively. The influx of nitrate and DOC represented the contamination of the aquifer. The small contaminant source serves to ensure that the contaminant plume does not interact with the lateral boundaries of the spatial domain. It also allows the mixing zones caused by transverse dispersion to be large relative to the width of the plume.

Simulation results

Results at 2.8 years are presented in Figure 3.4. Cross-sections showing concentrations of DO and nitrate are presented in Figure 3.4a. Note that when viewed on a linear scale, the DO plot shows a relatively large region of what appears to be zero concentrations. One must make a decision regarding what really represents "zero" concentrations. For example, Figure 1.2 shows a cross-section through the study area on which concentrations of DO are plotted. The zero contour is actually drawn for measurements that were fifty parts per billion (1.56 μM) or less [see *Walter et al.*, 1996]. However, oxygen concentrations that are significantly lower than 50 ppb have been measured at the Cape Cod site [*Savoie and LeBlanc*, 1998].

Zero concentrations are never calculated in a thermodynamically-based model, although extremely small concentrations are (e.g., 10^{-25} M). One might choose to consider one part per billion or one part per trillion to represent a concentration of zero. Whatever choice is made, the range of DO concentrations from the initial condition to "zero" is extremely large (i.e., spanning from four to

Figure 3.4. Plot-scale, two-dimensional simulation results at 2.8 years of simulation time. (a) DO and nitrate, (b) dissolved manganese and dissolved iron, and (c) *p*H and alkalinity. Both linear and logarithmic scales are shown.

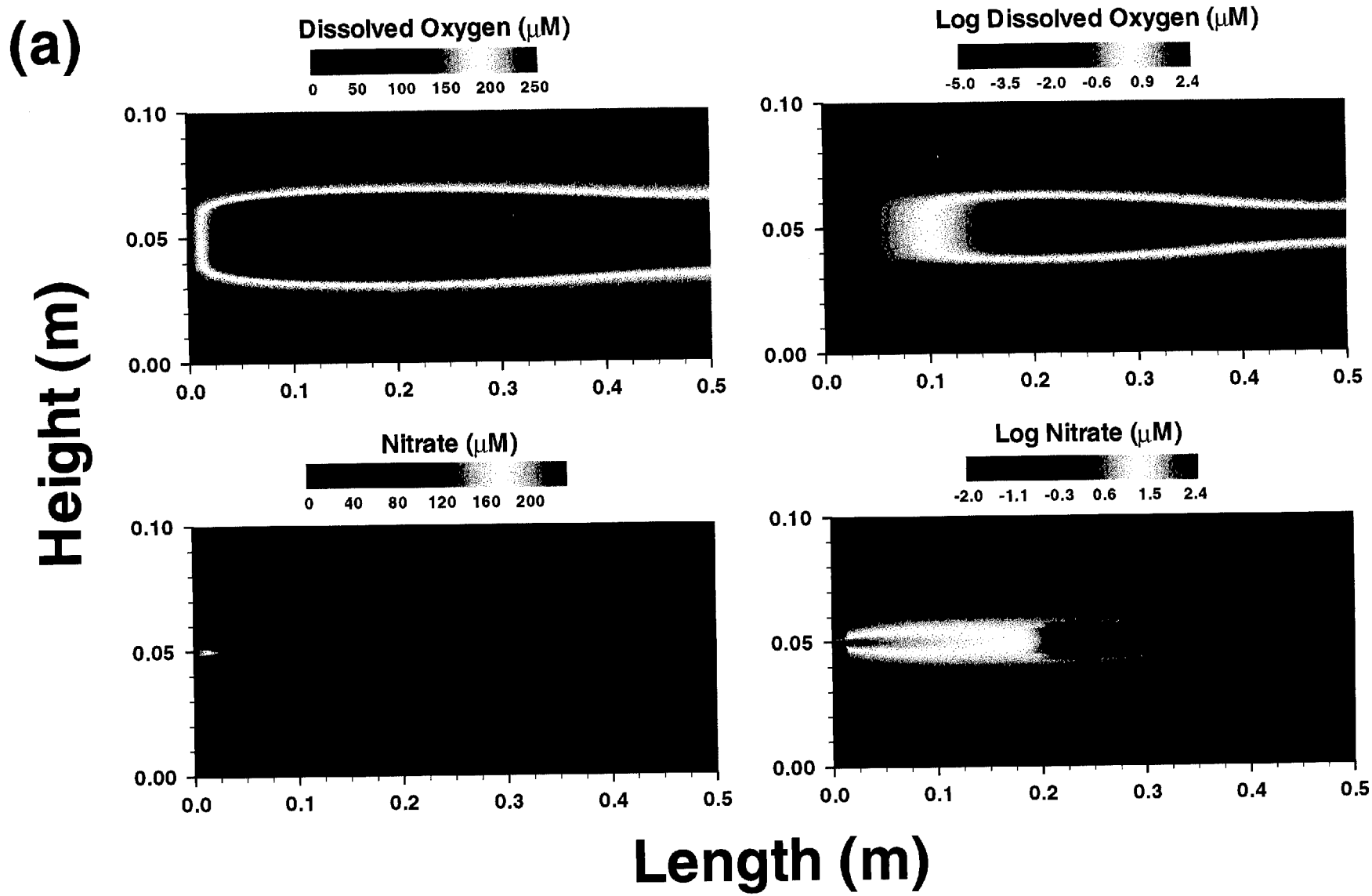
(a)
Dissolved Oxygen (μM)
0 50 100 150 200 250
Log Dissolved Oxygen (μM)
-5.0 -3.5 -2.0 -0.6 0.9 2.4
Nitrate (μM)
0 40 80 120 160 200
Log Nitrate (μM)
-2.0 -1.1 -0.3 0.6 1.5 2.4
Height (m)
0.10
0.05
0.00
0.0 0.1 0.2 0.3 0.4 0.5
Length (m)

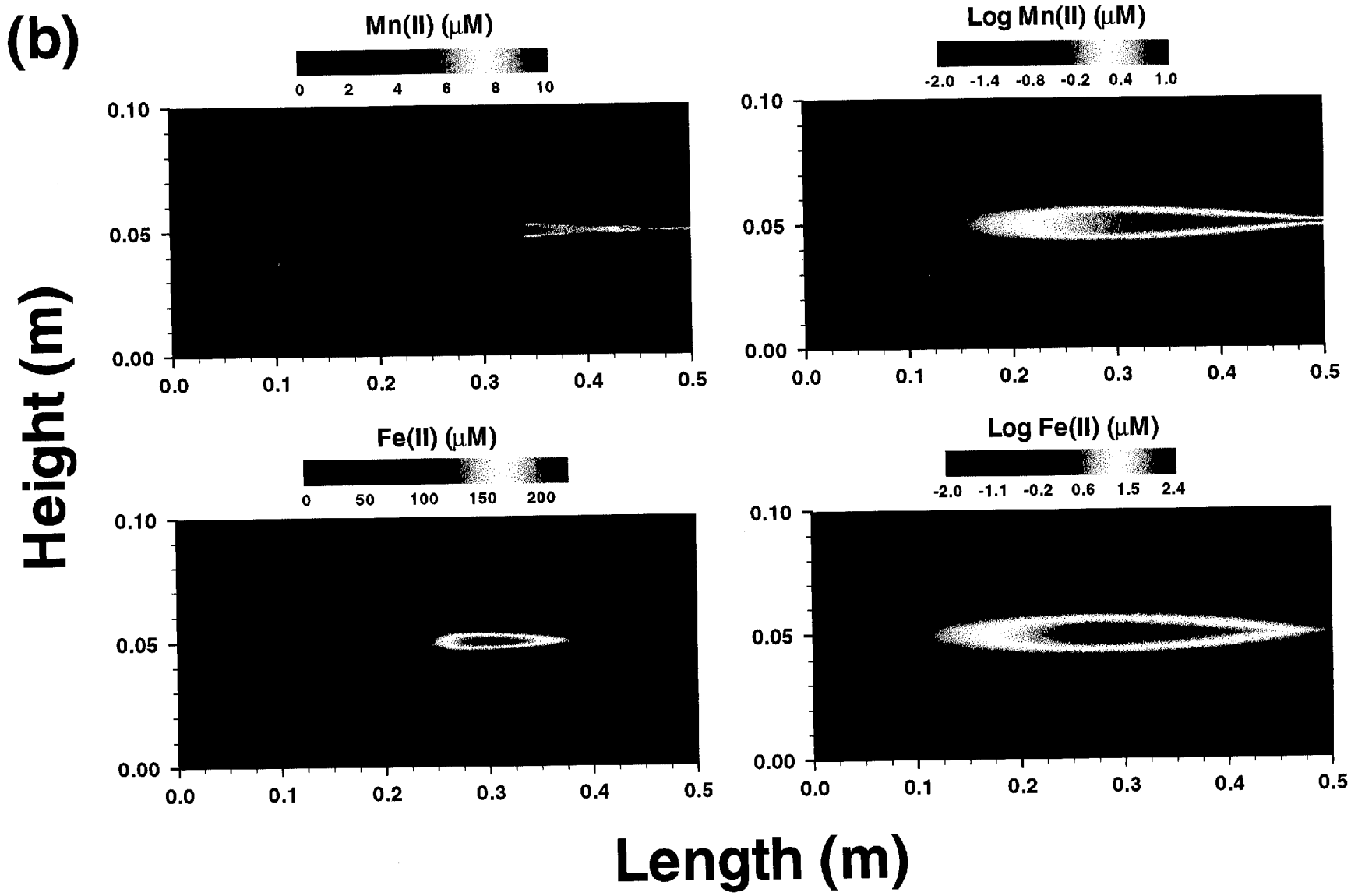
(b)
Mn(II) (μM)
0 2 4 6 8 10
Log Mn(II) (μM)
-2.0 -1.4 -0.8 -0.2 0.4 1.0
Fe(II) (μM)
0 50 100 150 200
Log Fe(II) (μM)
-2.0 -1.1 -0.2 0.6 1.5 2.4
0.10
0.05
0.00
0.0 0.1 0.2 0.3 0.4 0.5
Height (m)
Length (m)

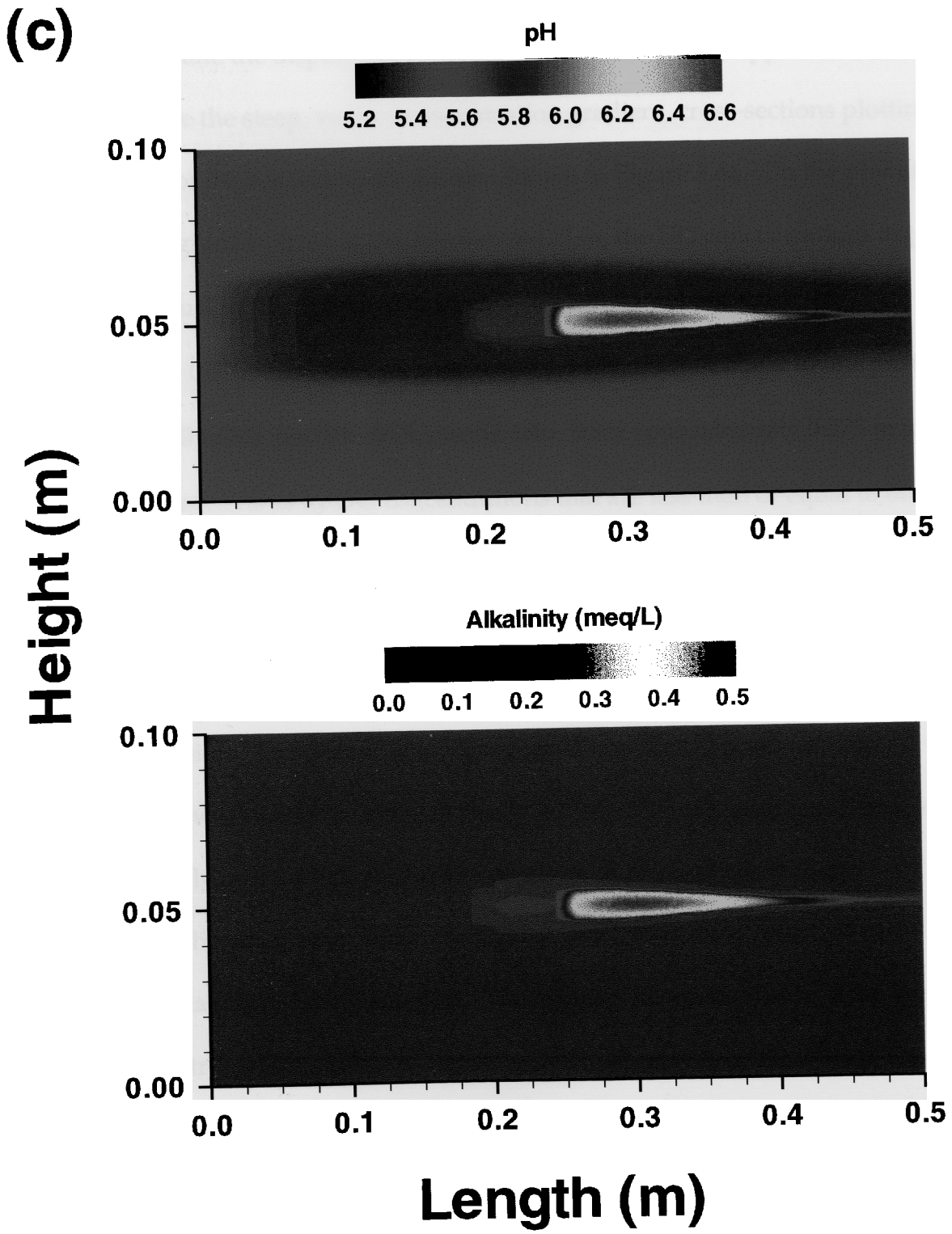
(c)
pH
5.2 5.4 5.6 5.8 6.0 6.2 6.4 6.6
0.10
0.05
0.00
0.0 0.1 0.2 0.3 0.4 0.5
Height (m)
Alkalinity (meq/L)
0.0 0.1 0.2 0.3 0.4 0.5
0.10
0.05
0.00
0.0 0.1 0.2 0.3 0.4 0.5
Length (m)

seven orders of magnitude, depending on the choice of "zero").

To facilitate the display of simulated concentrations that approach zero, and to illustrate the steep, vertical concentration gradient, cross-sections plotting the logarithm of the concentration are also shown in Figure 3.4a. On the plot of log DO, downgradient from approximately 0.125 m, the DO concentrations are less than or equal to fifty parts per billion (1.56 μM), downgradient from approximately 0.175 m the DO concentrations are less than or equal to one part per billion (0.031 μM), and the dark purple area, from approximately 0.275 m to 0.375 m, is characterized by DO concentrations that are less than or equal to one part per trillion (3.12×10^{-5} μM).

The utility of the log plots is again seen for the cross-sections of nitrate concentrations. The linear scale shows a profound absence of nitrate throughout most of the aquifer. The generally low concentrations occur because nitrate concentrations were initially "zero" (actually 10^{-9} M). The contaminant source is displayed clearly as the small region at a height of approximately 0.05 m. Denitrification began at approximately 0.175 m and accordingly nitrate is not seen in the remainder of the linear plot. The log plot, however, displays the zone of intense denitrification nicely. A "feather edge", representing nitrate that was transported conservatively (due to inhibition by DO), is seen to surround the region where nitrate concentrations are the lowest (downgradient from approximately 0.2 m). The irregular contour pattern seen around 0.2 m is an

artifact of the numerical grid spacing in the horizontal direction (i.e., $\Delta x = 19(\Delta z)$).

Figure 3.4b shows plots of dissolved manganese and dissolved iron. The linear-scale plot of dissolved manganese shows that some oscillations occur. The log plot of dissolved manganese suggests that the oscillations may not be significant with respect to the shape and extent of the concentration profile of dissolved manganese. Time series plots of dissolved manganese might shed some light on this minor issue, but such an analysis is outside of the scope of the purpose of these simulations. The linear plot of dissolved iron illustrates well that the zone of elevated iron concentrations occurs where DO concentrations are the lowest. The log plot of dissolved iron shows how the size of the iron zone was increased by longitudinal and transverse dispersion of DOC and dissolved iron. The maximum concentration of DOC is large (i.e., 5.9×10^{-2} M), which led to a large dispersive flux of DOC because DOC was initially zero. The large dispersive flux allowed a relatively large area of the aquifer to be affected by reductive iron dissolution as DOC encountered solid phase Fe(III) away from the longitudinal axis of the solute plume.

Figure 3.4c shows plots of alkalinity and *p*H. These two plots illustrate that both the highest alkalinities and *p*Hs occur in the iron zone, where DO concentrations are the lowest. The *p*H plot also shows how the two-dimensional distribution of *p*H was affected by the different redox reactions. The *p*H is seen to have decreased where oxygen reduction occurred, increased where

denitrification commenced, and increased even further where iron reduction occurred.

All of the concentration plots in Figure 3.4 show the development of suboxic transition zones (e.g., where nitrate is transported conservatively) above and below the longitudinal axis of the contaminant plume. The mixing-based suboxic transition zone that forms immediately downgradient of the anoxic zone is not displayed in Figure 3.4 because the plume has been transported beyond the downgradient boundary, but it can be seen in the one-dimensional simulation shown in Figure 3.2. The vertical component of velocity was zero for the two-dimensional simulation shown in Figure 3.4. If transverse dispersion did not occur, the vertical concentration gradients from the longitudinal axis of the plume to the edges would be infinite. Therefore, the mixing hypothesis, viewed in terms of the stated assumptions related to dispersion, cannot be rejected.

Application and Results

The laboratory- and plot-scale simulations described above demonstrate that the compartmental solute transport model described in this chapter functions properly. The simulation of the laboratory column showed that the redox zones developed as a function of space and time under the thermodynamic and kinetic constraints described in this chapter and in Chapter 2. The plot-scale simulation demonstrated that the compartmental solute

transport model is functional in two dimensions. The plot-scale simulation also supported the hypothesis that certain suboxic zones occur dominantly due to dispersion.

Two additional simulations are presented in this section demonstrating that the compartmental solute transport model is functional at the field scale.

One-Dimensional Simulation

A 400 m in length, one-dimensional solute transport simulation was performed as a first step toward demonstrating the new compartmental solute transport model's applicability to field-scale problems. The simulation was based upon average field conditions at the Cape Cod site. This simulation was not intended to represent a historical account of the development of redox zones at the site. Rather, the intention was to show in a conceptual, yet quantitative, manner that the redox zones developed as a result of the processes that were hypothesized, and that the compartmentalized approach to solving the thermodynamic/kinetic problem is a reliable and robust method for solving the numerical problem.

Reaction rates were abstracted from field experiments conducted at the Cape Cod site in 1996 [*Penarrieta*, 1998]. The results of these experiments showed an oxygen consumption rate of 2.85×10^{-6} mole L^{-1} d^{-1}. The rate constants and half-saturation constants used in the field-scale simulation are those given in Table 3.2. The hydraulic conductivity, porosity, and dispersivity values used for

the field-scale, one-dimensional simulation were taken from the Cape Cod site data and assumed to be spatially homogeneous. The hydraulic conductivity, porosity, and average hydraulic gradient yield an average linear velocity of 0.41 m d^{-1} [*LeBlanc et al.*, 1991]. It should be pointed out that this application of the compartmental solute transport model did not require a flow simulation because the desired velocity was already known.

The cut-off values used were 7×10^{-4}, for the switch between compartments one and two, and 1×10^{-2}, for the switch between compartments two and three. A statistical comparison in batch mode was performed pitting the compartmentalized approach model against the equilibrium test simulation described in Chapter 2 (see Figures 2.3 and 2.4 and Tables 2.3 and 2.4), using these cut-off values. The results of the comparison are shown in Table 3.3.

The boundary and initial conditions for the field-scale, one-dimensional simulation that are shown in Figure 3.5 were the same as those used for the one meter problem during model testing (i.e., Figure 3.2). The spatial increments for the field-scale simulation were 1.65 m. The major differences between the two one-dimensional simulations are that the spatial domain is now at the field scale, which required more than 5 times as many nodes, and that field-scale parameters were used in the simulation (e.g., solute velocity and dispersivity). The simulation results in Figure 3.5 demonstrate that the compartmentalized solute transport model is capable of simulating field-scale phenomena.

Table 3.3. Statistical comparison of a compartmentalized batch simulation to the equilibrium test problem described in Chapter 2. Cut-off vales of 7×10^{-4} and 1×10^{-2} for cut-offs one and two, respectively, were used.

Sample size (n) and model performance statistics	O_2	NO_3	Mn	Fe	*p*H	ALK	Perfect model
n	2500	5375	3332	457	5832	5832	
ME	0.0000	0.0000	0.0000	0.0000	0.0004	0.0000	0.0000
RMSE (%)	0.0001	0.0014	0.0996	0.0000	0.0009	0.0188	0.0000
CD	1.0000	1.0000	1.0000	1.0000	0.9999	1.0003	1.0000
EF	1.0000	1.0000	1.0000	1.0000	1.0000	1.0000	1.0000
CRM	0.0000	0.0000	0.0000	0.0000	0.0000	0.0001	0.0000

The model performance statistics used here are described by *Loague and Green* [1991] and are the same as those shown in Table 2.3 and used in Table 2.4. The lower limit for the ME (maximum error), RMSE (root mean square error), and CD (coefficient of determination) statistics is zero. The maximum value for EF (modeling efficiency) is one. Both EF and CRM (coefficient of residual mass) can become negative. If EF is less than zero, the compartmentalized approach values are worse than simply using the mean of the standard modeling approach results.

(a)

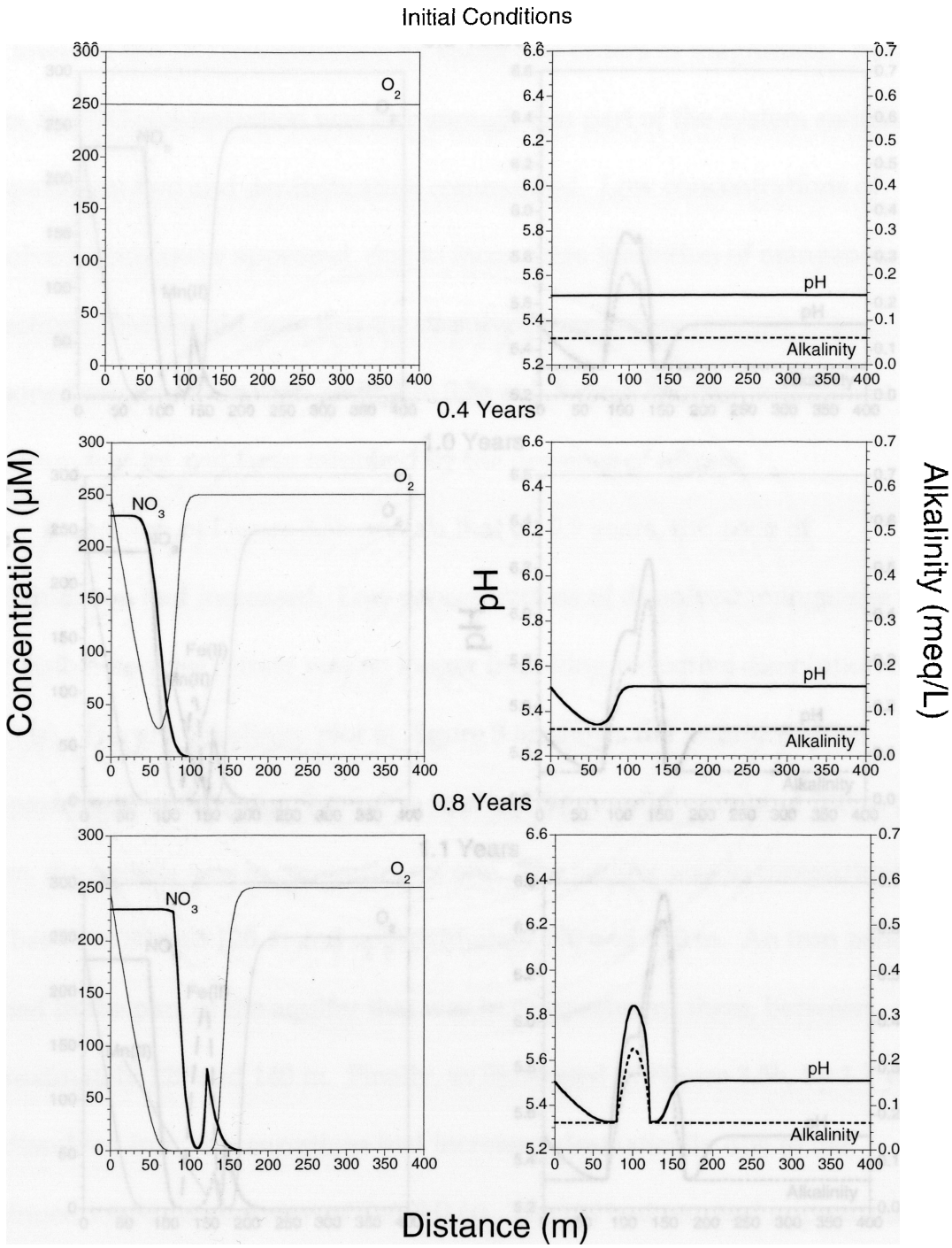

Figure 3.5. Concentration profiles for the one-dimensional, field-scale simulation showing (a) the initial conditions and results for 0.4, 0.8 years and (b) results for 0.9, 1.0, and 1.1 years.

(b)

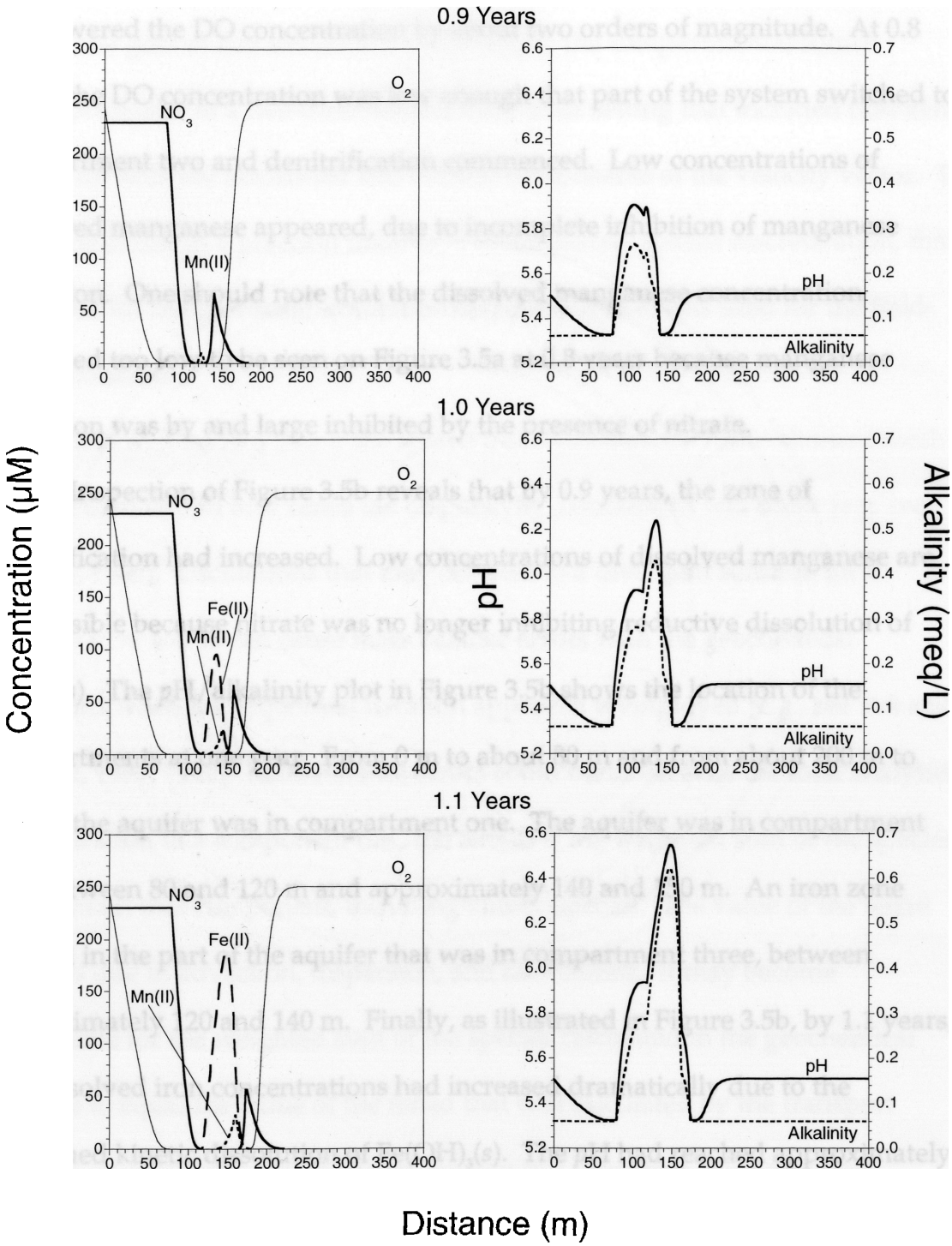
0.9 Years
1.0 Years
1.1 Years
NO3
O2
Mn(II)
Fe(II)
pH
Alkalinity
Concentration (μM)
Alkalinity (meq/L)
Distance (m)

As shown in Figure 3.5a, after 0.4 years, the leading edge of the nitrate profile had moved about 80 m, while over the same distance oxygen reduction had lowered the DO concentration by about two orders of magnitude. At 0.8 years, the DO concentration was low enough that part of the system switched to compartment two and denitrification commenced. Low concentrations of dissolved manganese appeared, due to incomplete inhibition of manganese reduction. One should note that the dissolved manganese concentration remained too low to be seen on Figure 3.5a at 0.8 years because manganese reduction was by and large inhibited by the presence of nitrate.

Inspection of Figure 3.5b reveals that by 0.9 years, the zone of denitrification had increased. Low concentrations of dissolved manganese are now visible because nitrate was no longer inhibiting reductive dissolution of $MnO_2(s)$. The *p*H/alkalinity plot in Figure 3.5b shows the location of the compartments at one year. From 0 m to about 80 m and from about 200 m to 400 m, the aquifer was in compartment one. The aquifer was in compartment two between 80 and 120 m and approximately 140 and 150 m. An iron zone formed in the part of the aquifer that was in compartment three, between approximately 120 and 140 m. Finally, as illustrated in Figure 3.5b, by 1.1 years, the dissolved iron concentrations had increased dramatically due to the continued kinetic dissolution of $Fe(OH)_3(s)$. The *p*H had reached approximately 6.5, which is nearly as high as has been observed at the Cape Cod site [*Kent et al.*, 1994]. The simulation was stopped at 1.1 years.

Two-Dimensional Simulation

Motivation

The goal of this simulation was to apply the compartmental solute transport model to a two-dimensional, field-scale setting that included non-zero values for both the horizontal and vertical components of the velocity vector. To accomplish this in a practical manner, a much coarser spatial discretization, than that used for the plot-scale simulation discussed above, was used for the field-scale simulation.

It is well known that if the spatial discretization of a finite-element mesh is greater than two to four times the dispersivity, oscillations will occur [e.g. see *Marsily*, 1986]. Oscillations that may not lead to a divergent solution for a conservative solute can cause mass balance errors with the geochemical equations when the sequential iteration approach is employed [e.g., see *Yeh and Tripathi*, 1989, 1991]. Mass balance errors could occur because the total analytical concentration of a component (i.e., the tenad) is the weighted sum of the species that contain that component, including kinetic species. The value of the tenad changes due to advection, dispersion, and oscillations. It may become impossible for the weighted sum of the species calculated in the geochemical module to equal the value of the tenad that was calculated by the transport module if oscillations are excessive, leading to a divergent solution. The threshold for "excessive oscillations" is probably problem-dependent, but its determination is outside of the scope of this dissertation.

To enable the coarser discretization, a Lagrangian-Eulerian finite-element framework that uses single-step reverse particle tracking for the advective term was used for the field-scale, two-dimensional simulation. This numerical scheme is an option in HYDROGEOCHEM 2.1 [*Yeh and Salvage*, 1995]. The single-step reverse particle tracking procedure is a generalized approximation of the upstream difference technique [*Yeh and Gwo*, 1990]. Some numerical dispersion can be expected using this procedure. The dispersive term is solved in the Eulerian framework, and oscillations can occur because of this treatment. To avoid oscillations, dispersivity values were set to zero, eliminating the dispersion terms in (3.17) and (3.19). Thus, the dispersion seen in the field-scale, two-dimensional simulation results was due solely to numerical dispersion.

Problem setup

The field-scale, two-dimensional simulation was designed to be the closest approximation to the Cape Cod site of any of the simulations presented in this dissertation. The 400 m length of the spatial domain is the same as the field-scale, one-dimensional simulation presented above. Since this field-scale simulation was conducted in two dimensions, vertical flow due to recharge from precipitation could be simulated.

A steady-state groundwater flow simulation was performed to obtain the two-dimensional hydraulic head field. The primary goal of the two-dimensional, field-scale transport simulation was to apply the compartmental solute transport

model to a realistic velocity field that had nonzero values for both components of the velocity vector. The effects of a free-surface boundary or the influence of the unsaturated zone are beyond the scope of this dissertation. As such, a reasonable distribution of hydraulic head can be obtained by considering that the domain behaves like a confined aquifer, even though the aquifer at the Cape Cod site is unconfined. The steady-state groundwater flow equation, with no sources or sinks, used to calculate the hydraulic head distribution is:

$$K_x \frac{\partial^2 h}{\partial x^2} + K_z \frac{\partial^2 h}{\partial z^2} = 0 \tag{3.24}$$

where K_i is the hydraulic conductivity in the ith direction ($L\ T^{-1}$) and h is the hydraulic head (L). The hydraulic conductivity of the aquifer was assumed to be homogeneous and anisotropic with the principal axes of anisotropy aligned with the coordinates. The horizontal hydraulic conductivity was taken to be 1.27×10^{-3} m s^{-1}. The ratio of the horizontal to vertical conductivity was assumed to be 3.5:1, yielding a vertical hydraulic conductivity of 3.64×10^{-4} m s^{-1} [*LeBlanc et al.*, 1991; *Hess et al.*, 1992].

The boundary conditions for the groundwater flow problem are shown in Figure 3.6. The spatial discretization for the finite-element grid was $\Delta x = 1.65$ m and $\Delta z = 0.53$ m. Recharge from precipitation was simulated as a constant flux across the upper boundary. The value for the specific flux was taken from

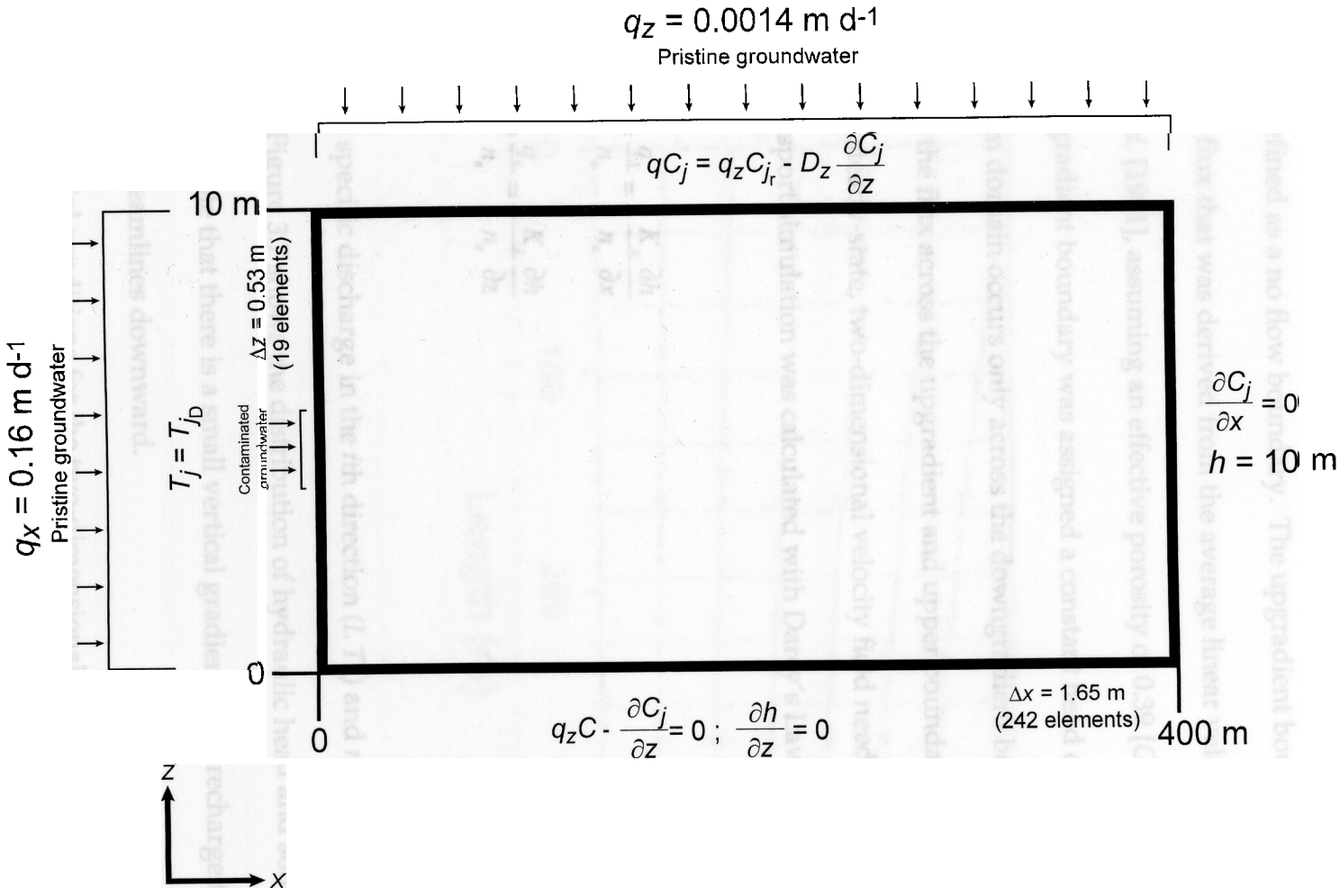

Figure 3.6 Boundary-value problem for the field-scale, two-dimensional compartmentalized solute transport simulation. T_{jD} is the total analytical concentration that is fixed at constant concentration boundary nodes.

LeBlanc et al. [1991]. Since groundwater flow at the Cape Cod site is dominantly horizontal [*LeBlanc et al.*, 1991], the lower boundary was taken to be a flow line and was defined as a no flow boundary. The upgradient boundary was assigned a specified flux that was derived from the average linear velocity reported in *LeBlanc et al.* [1991], assuming an effective porosity of 0.39 [*Garabedian et al.*, 1991]. The downgradient boundary was assigned a constant head of 10 m. Flow out of the problem domain occurs only across the downgradient boundary and equals the sum of the flux across the upgradient and upper boundaries.

The steady-state, two-dimensional velocity field needed for the transient solute transport simulation was calculated with Darcy's Law:

$$\overline{v_x} = \frac{q_x}{n_e} = -\frac{K_x}{n_e}\frac{\partial h}{\partial x} \tag{3.25}$$

$$\overline{v_z} = \frac{q_z}{n_e} = -\frac{K_z}{n_e}\frac{\partial h}{\partial z} \tag{3.26}$$

where q_i is specific discharge in the ith direction ($L\ T^{-1}$) and n_e is the effective porosity. Figure 3.7 shows the distribution of hydraulic head and some streamlines; note that there is a small vertical gradient from recharge that gently deflects the streamlines downward.

The initial conditions for the two-dimensional, field-scale solute transport simulation are the same as for the plot-scale simulation described in the previous section. The boundary conditions are shown in Figure 3.6. Pristine groundwater

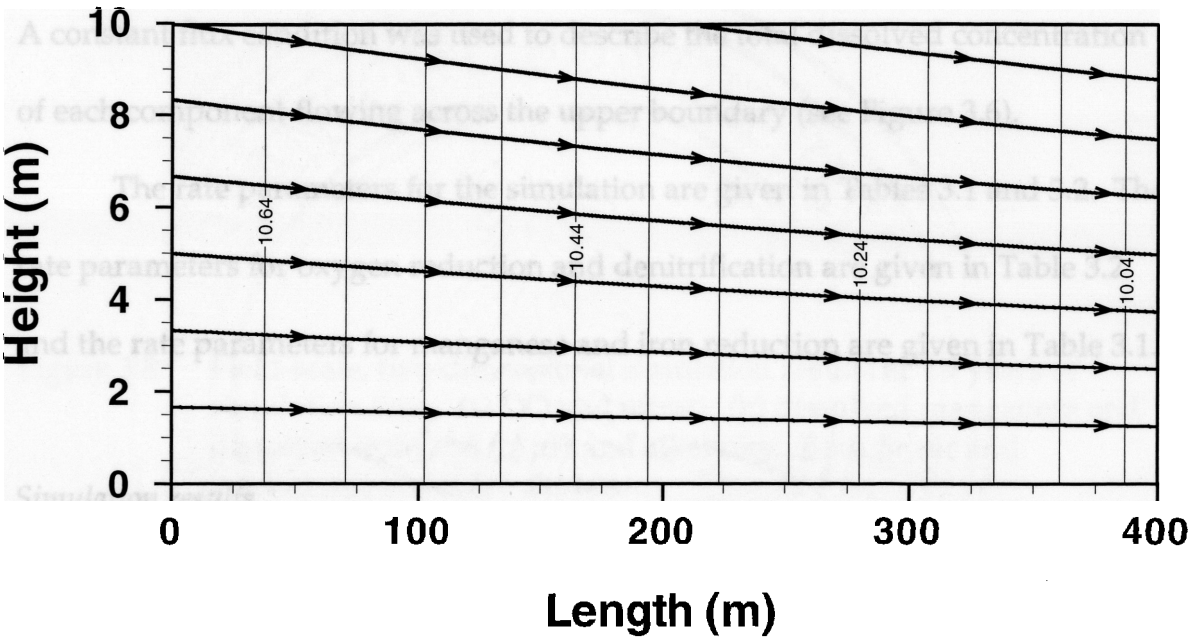

Figure 3.7. Cross-section showing hydraulic head (m) and flow lines. The head contours are labeled with their values and the flow lines have arrows on them indicating the flow direction

was allowed to enter the spatial domain at both flux boundaries. Over a 1.1 m distance in the middle of the upgradient boundary the incoming water also contains contaminants in the form of nitrate and DOC at 2.3×10^{-4} and 4.0×10^{-2} M, respectively. At the upgradient boundary, a constant concentration boundary condition was used so that the total analytical concentration of each component would be the same at each node where contaminated groundwater was specified. A constant flux condition was used to describe the total dissolved concentration of each component flowing across the upper boundary (see Figure 3.6).

The rate parameters for the simulation are given in Tables 3.1 and 3.2. The rate parameters for oxygen reduction and denitrification are given in Table 3.2 and the rate parameters for manganese and iron reduction are given in Table 3.1.

Simulation results

Results at 1.9 years are presented in Figure 3.8. Inspection of the DO plots shows that the vertical flow from recharge has influenced the shape of the suboxic and anoxic zones. The lower edge of the oxygen reduction region has been moved downward. Flux of DOC due to numerical dispersion, because of the steep, vertical DOC concentration gradient, has caused the upper edge of the oxygen reduction region to appear uninfluenced by the vertical component of groundwater flow. The dispersive flux led to DOC being transported toward the upper boundary, where it reacted with DO. The magnitude of the residual between the dispersive and advective fluxes in this area, in conjunction with the

Figure 3.8. Field-scale, two-dimensional simulation results at 1.9 years of simulation time. (a) DO and nitrate, (b) dissolved manganese and dissolved iron, and (c) *p*H and alkalinity. Both linear and logarithmic scales are shown.

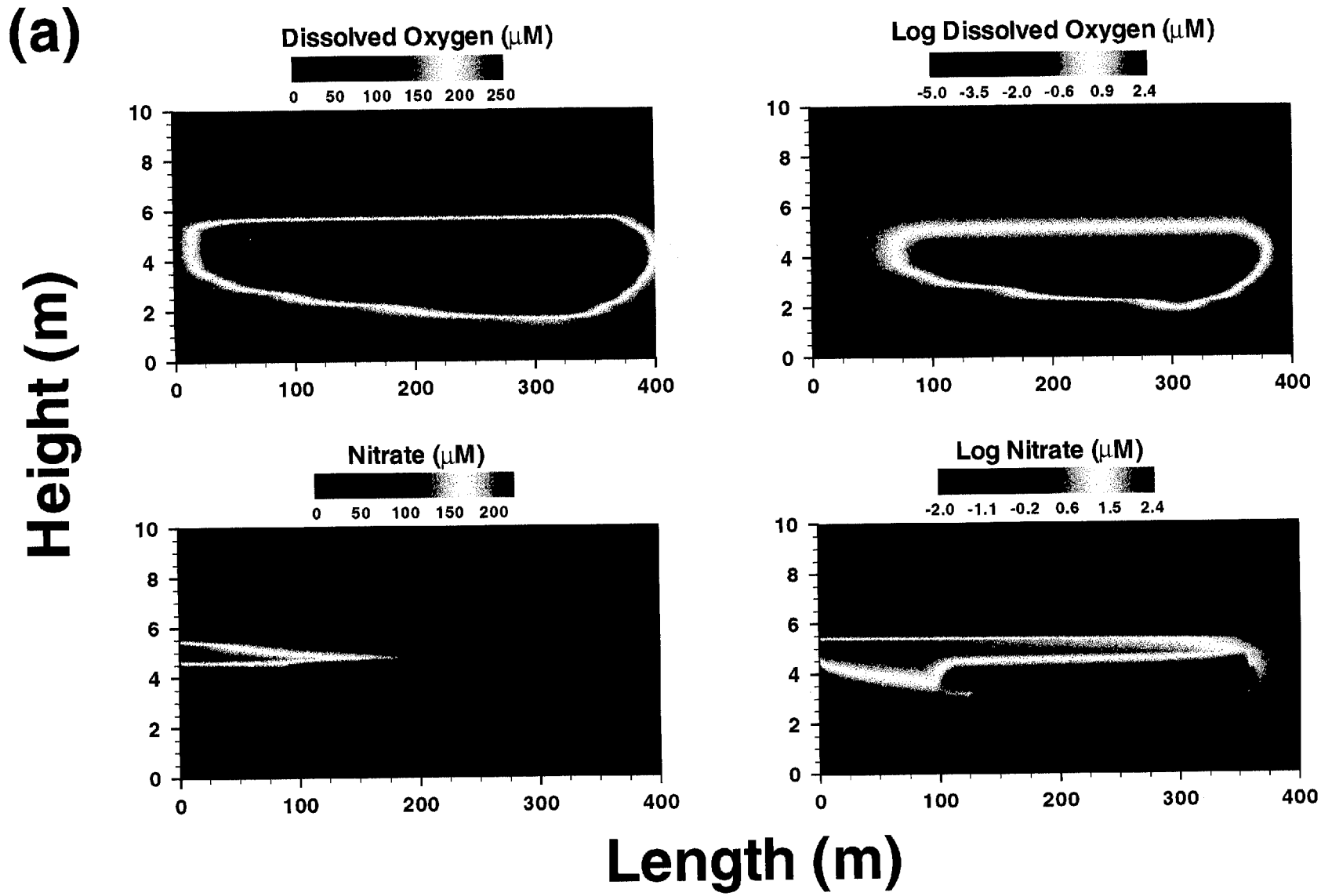
(a)
Dissolved Oxygen (μM)
0 50 100 150 200 250
Log Dissolved Oxygen (μM)
-5.0 -3.5 -2.0 -0.6 0.9 2.4
Nitrate (μM)
0 50 100 150 200
Log Nitrate (μM)
-2.0 -1.1 -0.2 0.6 1.5 2.4
Height (m)
Length (m)
0 2 4 6 8 10
0 100 200 300 400

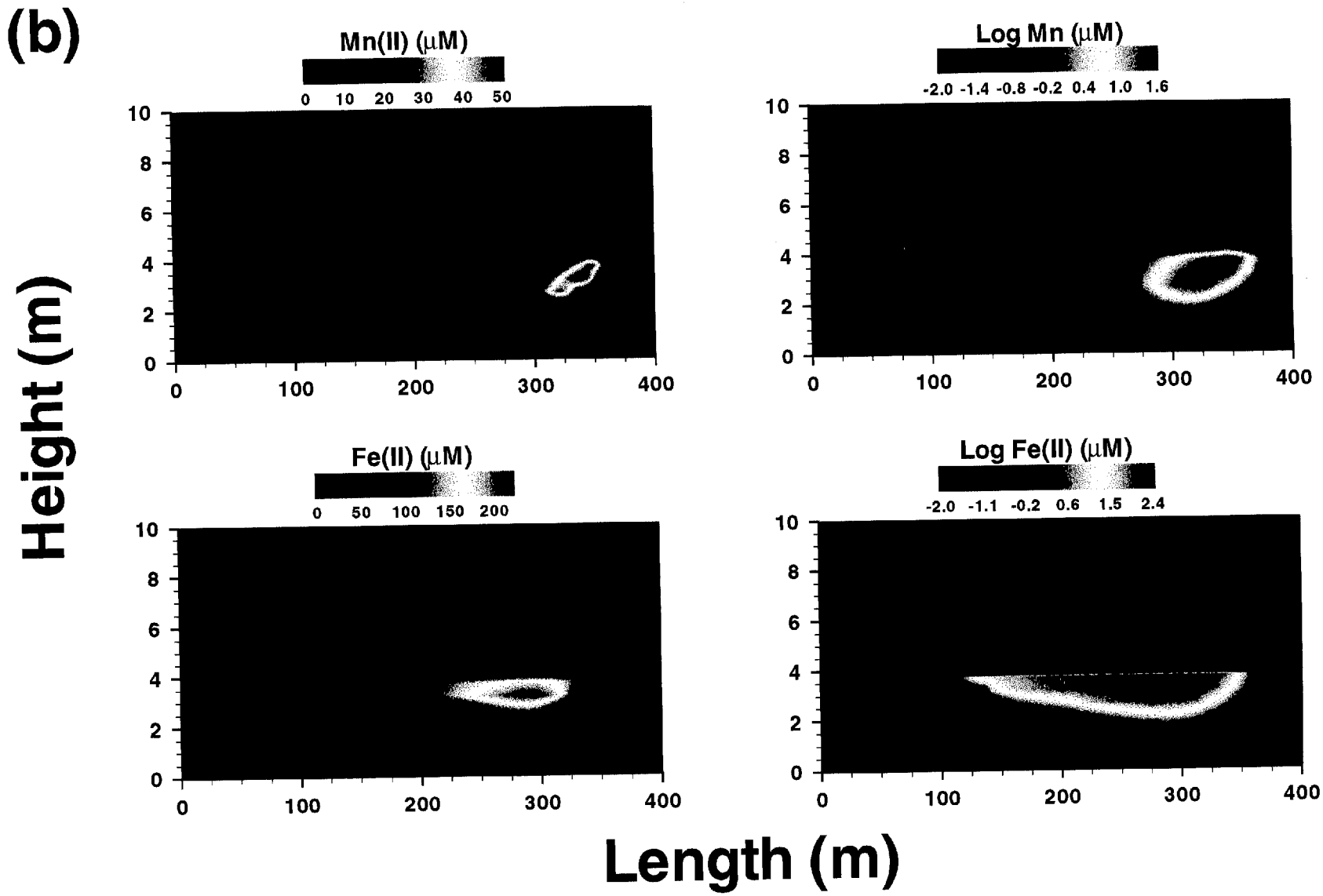
(b)
Mn(II) (μM)
0 10 20 30 40 50
Log Mn (μM)
-2.0 -1.4 -0.8 -0.2 0.4 1.0 1.6
Fe(II) (μM)
0 50 100 150 200
Log Fe(II) (μM)
-2.0 -1.1 -0.2 0.6 1.5 2.4
Height (m)
Length (m)
0 2 4 6 8 10
0 100 200 300 400

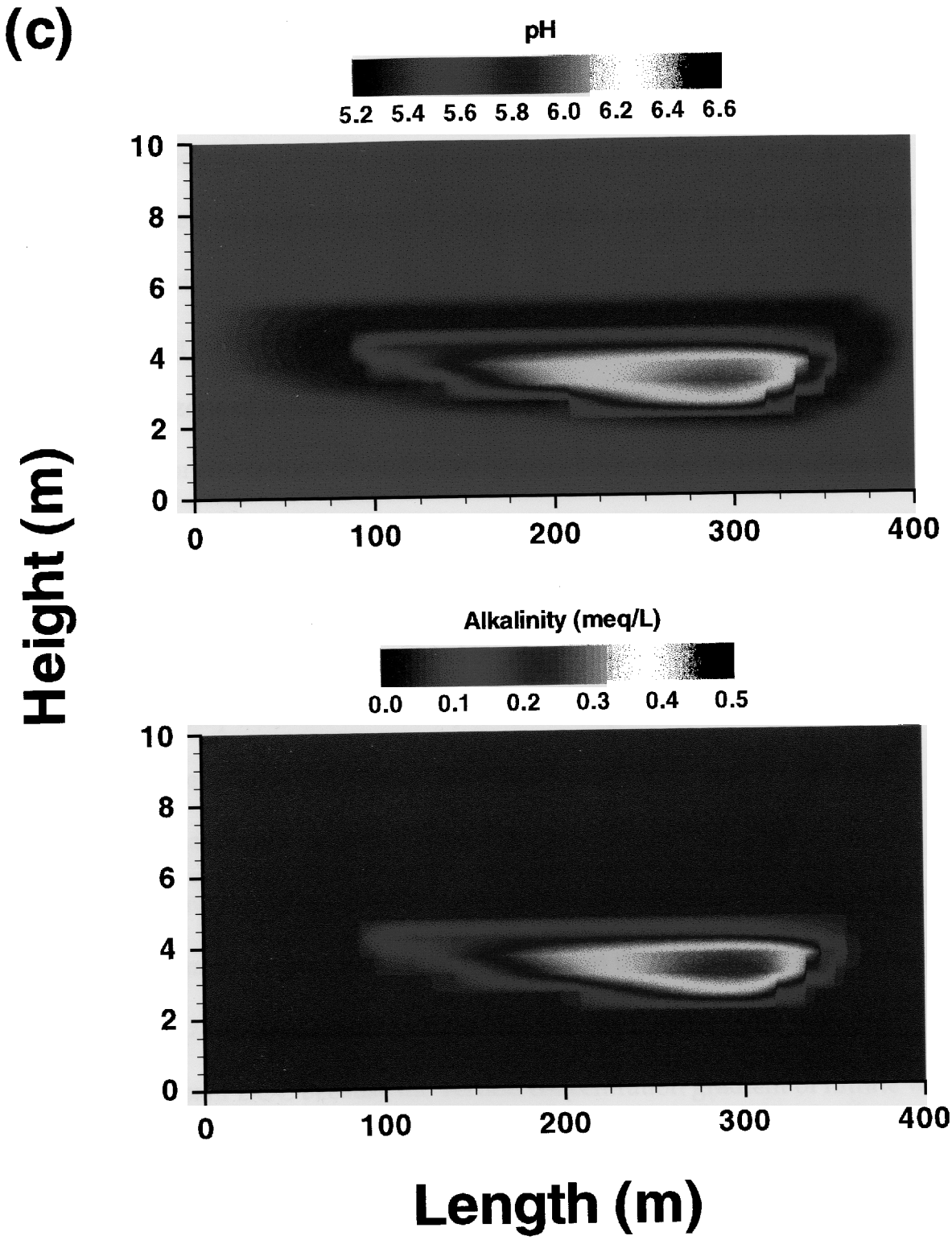
(c)
pH
5.2 5.4 5.6 5.8 6.0 6.2 6.4 6.6
10
8
6
4
2
0
0 100 200 300 400
Alkalinity (meq/L)
0.0 0.1 0.2 0.3 0.4 0.5
10
8
6
4
2
0
0 100 200 300 400
Height (m)
Length (m)

coarse discretization, resulted in a horizontal upper edge to the zone of oxygen reduction. The log plot of DO concentrations in Figure 3.8a illustrates the steep, vertical DO gradient very well. The range of concentrations is illustrated much better on the log plot. The log plot also shows how the zone of "zero" DO, as defined by the dark purple region, is actually much smaller than the linear plot would suggest.

The log plot of nitrate concentrations in Figure 3.8a clearly shows the extent of the zone of intense denitrification, which coincides with the anoxic zone. Low concentrations of nitrate can be seen below, and downgradient of, the anoxic zone. These areas represent places where denitrification was inhibited thermodynamically by the presence of sufficient concentrations of DO. Areas where nitrate concentrations are about 50 μM or greater represent areas where nitrate was transported conservatively. The linear plot of nitrate concentrations shows well the influence of vertical flow, particularly if the red, yellow, and green shaded areas are examined. The dispersive flux of DOC did not affect nitrate the same as it affected DO because nitrate concentrations are restricted to a relatively narrow region, compared to DO. Even though nitrate concentrations were initially zero, the dispersive flux of nitrate was much smaller than the dispersive flux of DOC because the vertical concentration gradient of nitrate was much smaller (compare the boundary conditions of nitrate and DOC).

The linear plot of dissolved manganese (Figure 3.8b) highlights the leading edge of the dissolved manganese plume. Since the trailing edge

represents areas of the aquifer where $MnO_2(s)$ was depleted, the concentrations seen in Figure 3.8b are quite low. These low concentrations in the trailing portion of the plume show up well on the log plot of dissolved manganese.

The linear plot of dissolved iron shows the extent of the iron zone. The log plot exaggerates the interplay between reaction rate and flow rate. If there were no vertical flow in the domain (i.e., flow lines were completely horizontal), then there would be no transverse spreading at all because the dispersivities were set to zero. The plume of dissolved iron would have infinite concentration gradients in the vertical direction at the edges of the plume. Since there was a component of vertical flow, the dissolved iron plume was forced downward and the leading and bottom edges were subject to numerical dispersion. The upper edge, however, was not affected significantly by numerical dispersion because the reaction rates were fast compared to the flow rate. The relatively fast reaction rate prevented the concentration of dissolved iron from becoming low at the upper edge of the iron zone, which maintained the steep concentration gradient. The phenomenon appeared in the iron plot and not the manganese log plot because the reaction rate is relatively faster for iron reduction at this snapshot in time, due to the much higher concentrations of $Fe(OH)_3(s)$ as compared to $MnO_2(s)$. The difference in the appearance of the upper edge of the dissolved iron plume (Figure 3.8b) and the upper edge of the oxygen reduction zone (Figure 3.8a) is related to the fact that the DO plot shows the disappearance of a mobile, dissolved solute. In contrast, the dissolved iron plot shows the

appearance of a dissolved solute that resulted from the dissolution of an immobile solid phase.

Figure 3.8c clearly shows the changes in *p*H associated with the different redox reactions. Oxygen reduction resulted in decreased *p*H, while the other three redox reactions resulted in a *p*H increase. Iron reduction caused the *p*H values to exceed 6.0 and tend toward 6.6. Alkalinity increased in areas where oxygen reduction had ceased. Both the *p*H and alkalinity plots illustrate the overall downward movement of the contaminant plume.

The two dimensional, field-scale simulation results do not allow the rejection of the mixing hypothesis that was proposed in the section on model testing. The simulation suggests that the overlying and underlying suboxic zones are indeed transitional mixing zones. The anoxic zone is surrounded by "suboxic" water. That is, water with higher oxygen concentrations than the core of the plume but certainly lower than pristine water.

The general features of the redox zones are captured well. The anoxic zone is tucked neatly within the suboxic zone, which is surrounded by oxic groundwater. The field-scale, two-dimensional simulation reported here, designed to approximate the Cape Cod site, misses certain features of the observed plume. The simplified reaction network and approximated reaction rates may prevent correct simulation of the actual timing of the development of the zones. It should be pointed out that it is not known when the zones developed, as the earliest data available are from 1978, a full 42 years after

sewage disposal began. Possible extensions related to history matching and prediction for the Cape Cod site with the compartmental solute transport model are discussed in Chapter 4.

One question that is difficult to answer with the simulation approach used in this study is why, at the Cape Cod site, the leading edge of the overall sewage plume is so far downgradient relative to the leading edge of the anoxic zone. In the field, the extent of the iron zone correlates with the extent of the anoxic zone. This may be due to the fact that by far the most thermodynamically stable form of iron in the presence of oxygen is Fe(III), which is highly insoluble. Therefore, if any oxygen is present, Fe(II) is not. A possible cause for the downgradient limit of the anoxic zone is horizontal transverse dispersion of dissolved oxygen from the suboxic zone. A three dimensional model would be needed to correctly simulate this process.

Discussion

Implications of the Thermodynamic Inhibition Mechanism

A chief advantage of the compartmentalized approach is that kinetic constraints are embedded within a thermodynamic framework. This allows a redox reaction that yields sufficiently lower-energy to be automatically inhibited in the presence of a higher-energy reaction. The compartmentalized approach therefore does not need empirical or ad-hoc approaches to reaction inhibition.

A disadvantage of the compartmentalized approach is that redox reactions are considered to be equilibrium reactions for part of each time step. This is done to check thermodynamic feasibility of the lower-energy redox reaction in a given compartment and to compute the amount of reaction inhibition, but not necessarily to control reaction progress (see Chapter 2 and Figure 3.1). The implication is that it is possible to misinterpret a reaction as reversible. For example, consider the manganese reduction reaction:

$$MnO_2(s) + \frac{1}{2}\text{"}CH_2O\text{"} + H^+ = Mn^{2+} + \frac{1}{2}CO_3^{2-} + H_2O \tag{3.27}$$

If it is allowed to be reversible, $MnO_2(s)$ could precipitate from a combination of Mn^{2+}, CO_3^{2-}, and H_2O. This could occur if some dissolved manganese is transported downgradient to a location where no, or very little, manganese reduction has occurred. In this case, the total analytical concentration of manganese would be greater than the initial condition because the precipitated phase would still be at the initial concentration. Under geochemical conditions in which manganese reduction is not favored, the thermodynamic calculation would force the total precipitated concentration of manganese to equal the total analytical concentration of manganese via (3.27) and (3.18). Reaction (3.27) would also produce DOC. Clearly, this would be incorrect, since organic carbon is not intended to be produced by any reaction under consideration. Thus it is necessary to ensure that the code does not allow the amount of redox-sensitive

reactants to increase due to chemical reactions. This is accomplished by preventing the concentration of the redox reactant from increasing from one time step to the next due to chemical reactions (see flow chart in Figure 3.1). Conceptually, this is particularly important for precipitated species because chemical reactions are the only way that it is possible for the amount of a solid to increase in the system under consideration (i.e., solids are immobile).

Implications of the Simplified Reaction Network

The reactions used in this study represent overall processes. For example, *Smith et al.* [1996] suggested that denitrification does not proceed directly from NO_3^- to N_2. Rather, there is at least one intermediate step and N_2O is a product of this reaction step. While the end result would be the same, intermediate reaction products are not captured in these simulations. The use of overall reactions has a larger impact on the kinetic calculations than the equilibrium calculations. This is because in a thermodynamic framework, only the starting and final states are important. In a kinetic framework, however, the actual reaction paths are important because reactions may not go to completion.

Since only primary redox reactions are used (i.e., reactions hypothesized to represent the dominant microbiological process), additional sinks for, say, oxygen may be missed. For example, abiotic redox reactions may contribute, to some degree, to the consumption of the proposed electron acceptors. Of particular concern is dissolved Mn^{2+}, which can react with oxygen to form

$MnO_2(s)$. In the simulations presented in this chapter, there is the potential for Mn^{2+} to come in contact with oxygen. Low concentrations of oxygen are present in the early stages of compartment two. In addition, there is the potential for these two constituents to come into contact at the spatial boundary between parts of the aquifer that are in compartment one and parts that are in compartment two. Even so, reactions between oxygen and Mn^{2+} should be thermodynamically inhibited by the presence of DOC. The oxygen-DOC reaction is much more energetically-favorable.

A source of uncertainty in all the simulations presented in this dissertation is the relationship between nitrate and dissolved manganese. The field data (Figure 1.4) show dissolved manganese in the presence of abundant nitrate. However, the model developed for this effort calculates, based upon thermodynamics, that manganese reduction should occur only after nitrate concentrations are quite small. There are several possible explanations for this apparent contradiction, each of which suggests a possible experiment, either field-based, laboratory, numerical, or some combination thereof. First, the dissolved manganese may have diffused or dispersed into the nitrate-bearing areas. Second, the range of reducible manganese solids is probably not represented accurately by a single solid with one equilibrium constant. This could be tested with a numerical model and then followed up with laboratory and/or field experiments.

Perhaps the use of "CH_2O" is too much of a simplification. The actual DOC soup is most likely a combination of several different organic compounds that have a range of reactivities. Again, numerical experiments in conjunction with laboratory and/or field experiments might shed some light on this. Different microbial populations are likely to be involved in denitrification and manganese reduction. It is possible that different metabolic mechanisms are involved. If so, the different reaction mechanisms (or organisms) might be oxidizing different compounds for denitrification than for manganese reduction. The simplified treatment presented in this study cannot account for this directly. It is important to stress, however, that if more is known about the various reactants and reaction pathways, the information can be incorporated into the compartmentalized approach, additional reactions can be written, and another simulation can be conducted using the same methodology (e.g., see Chapter 4).

Alternative Organic Carbon Sources

Although the modeling exercises in this dissertation used dissolved organic carbon to drive the development of the redox zones, there are other possible carbon sources. For instance, the majority of the organic matter may actually be sorbed to the aquifer sediments. It is known that the magnitude of the sewage source at the Cape Cod site was much larger during World War II than at any other time [*LeBlanc*, 1984a]. It is conceivable that there was a huge influx of organic matter early in the history of the base, and that most of this

organic matter has been slowly decaying since then. Recent work at the Cape Cod site points to a considerable pool of sorbed organic carbon. This scenario suggests that the recent source history could be relatively devoid of organic carbon, and the real source could be from the aquifer sediments.

Carbon Limited System?

The reaction network used in this study was patterned after field conditions at the Cape Cod site. As previously noted, sulfide is not present at Cape Cod, even though sulfate is. This suggests, due to thermodynamic constraints, that either the iron reduction reaction is extremely slow or the plume is organic carbon limited. Work by *Thurman et al.* [1986] suggested that the latter is the case. The relationship between *p*H and iron in the simulations performed for this study does not reject their hypothesis, but more work would be needed in which the source concentrations were varied and additional *p*H buffers were included if the simulated concentrations of reaction products in this effort were to be used to further constrain their conclusion.

The initial concentrations of $MnO_2(s)$ and $Fe(OH)_3(s)$ used throughout this dissertation were estimated. Examination of Figures 2.3, 3.2, and 3.5 shows that the reductive dissolution of $MnO_2(s)$ contributed little to changes in *p*H, while the reductive dissolution of $Fe(OH)_3(s)$ produced significant increases in *p*H. This can also be seen by inspecting the respective chemical reactions in Table 2.1. For every mole of "CH_2O" consumed, two moles of hydrogen ions are consumed for

manganese reduction, while six moles of hydrogen ions are consumed for iron reduction. When iron reduction was allowed to continue until about half the $Fe(OH)_3(s)$ was depleted, simulated *p*H values above those observed at the field site were obtained (approximately *p*H 8; see Figure 3.2). Such high *p*H values have never been observed in the sewage plume at the Cape Cod site.

The only *p*H buffering reactions included in the effort reported in this dissertation were those of the aqueous carbonate system (see Table 2.1). As noted in Chapter 2, surface complexation reactions between surface sites on the aquifer sediments and hydrogen ions would provide additional *p*H buffering [*Stollenwerk*, 1995]. The simulations conducted for this dissertation suggest that in the absence of additional *p*H buffers, the *p*H values observed in the field would be higher than those that have been observed if the field setting were not carbon limited. In addition, sulfate reduction would become thermodynamically feasible after any excess DOC finally exhausted the available $Fe(OH)_3(s)$. Sulfate reduction would have resulted in the appearance of sulfide.

Experiments designed to determine the iron reduction rate at the Cape Cod site would aid in answering the question of a carbon limited system. In addition, numerical experiments could be performed to test the impact of additional *p*H buffers and other chemical reactions (see Chapter 4).

Conclusions

Redox zones have developed at many contaminated sites throughout the world. The concept-development simulations performed in this chapter with the new compartmental solute transport model suggest that the redox zones at the U.S. Geological Survey's Cape Cod site have developed as a result of the sequential reduction of oxygen, nitrate, manganese oxide(s), and iron oxyhydroxide(s). The electron source, organic carbon, was introduced to the Cape Cod aquifer over approximately sixty years due to the purposeful infiltration of treated sewage. It has been shown here with the compartmentalized solute transport simulations that the qualitative description of the field-scale development of redox zones, which is usually described in terms of thermodynamics, can be quantified. The sequential, rate-limited use of various electron acceptors leads to the formation of the zones.

Incorporating the compartmentalized approach into a solute transport framework has allowed the simulation of the development of redox zones at the field scale under thermodynamic and kinetic constraints. Lower-energy redox reactions can be either thermodynamically- or kinetically-inhibited, depending on local geochemical conditions. The number of solute transport equations that are needed to simulate a particular system can be reduced due to the fact that the reaction networks are decoupled. The solute transport portions of the model are

treated in a process-based manner by explicitly considering advection and dispersion.

Simplifications related to abstracting the conceptual model from reality have minimal impact on the stated goals of the simulations presented in this chapter. For instance, the source of the contamination at the Cape Cod site varied in intensity and concentration over the contamination period. Simplification of the contaminants into two components, nitrate and DOC, and the use of a constant source concentration, facilitated the testing of the hypothesis that the redox zones developed as a result of the chemical reactions and transport processes proposed in this dissertation. The treatment of microbiological processes as overall chemical reactions and the neglect of secondary redox reactions has little effect on the conclusions drawn from the transport simulations reported in this chapter. These simplifications do not reduce the utility of the model. They do, however, provide possible avenues for further research.

Chapter 4

Future Directions

Introduction

The major goal of this dissertation was to develop simulation protocols for the development of redox zones. To do this, simulations based upon the Cape Cod field site were constructed and used to develop and test the coupled compartmentalized approach.

The work reported in Chapters 2 and 3 represents two major new contributions. The first contribution is the ability to simulate sequential, competing redox reactions under thermodynamic and kinetic constraints. The second contribution is the ability for the model to treat lower-energy redox reactions as either thermodynamically-limited or kinetically-limited in the presence of higher-energy redox reactions. The batch simulations and the four solute transport simulations that were performed for this effort demonstrate the effectiveness of the compartmentalized approach. Each simulation builds upon the simulations that preceded it. Some simplifying assumptions were made so that the dominant processes that drive redox zone development could be focused upon and used as a tool for model and concept development.

This chapter outlines some of the extensions that could be applied to the compartmentalized approach now that the methodology is fully developed and tested. While some of the following extensions are applicable in a general sense, others are useful on a site-specific basis to enable history matching and predictions of solute fate and transport.

Additional Reactions

One of the simplifying assumptions made for this effort was not to consider chemical reactions that lead to retardation of the redox-sensitive solutes discussed here. These include sorption reactions, redox reactions (including precipitation), and precipitation reactions that do not involve the transfer of electrons. This decision was made because retardation does not play a major role in redox zone development. The general topology of the redox zones is not affected by retardation. Retardation is a secondary effect that could not be considered or analyzed until the simulation protocol for the development of redox zones had been designed and tested.

The extent of the zone of dissolved iron and the extent of the region of dissolved manganese could be limited by sorption reactions. Such sorption reactions could slow the rate at which dissolved iron and manganese move. Sorption could also cause decreases in the maximum dissolved concentrations. If the concentrations of these dissolved metals were high enough, a decrease in *p*H

could accompany their sorption because hydrogen ions would most likely be released by the solid surface sites.

A potential redox reaction that could cause limitations to the size of the iron zone is:

$$2\ Fe^{2+} + MnO_2(s) + 4\ H_2O \rightarrow 2\ Fe(OH)_3(s) + Mn^{2+} + 2\ H^+ \qquad (4.1)$$

The precipitation/dissolution reaction in (4.1) is a redox reaction where manganese is reduced and iron is oxidized. It is questionable if the reaction in (4.1) would have a discernable impact on the simulation results. First of all, "CH_2O", and by inference most reactive DOC, is a much more favorable reductant than Fe^{2+}. Thus, if Fe^{2+} and DOC were both available in the presence of $MnO_2(s)$, thermodynamics predicts that DOC would be the dominant reactant. Fe^{2+} would most likely not become an important reactant until there was virtually no more DOC available.

It should be pointed out that reaction (4.1) would not be an important player for the simulations performed in the effort reported here. Due to the rate limitations placed on the redox reactions that were simulated, the DOC front was always ahead of the dissolved iron front. Therefore, $MnO_2(s)$ was depleted by DOC before any dissolved iron could reach it. If the iron sorption reaction described above were to play any role in the simulated reaction network, the spatial lag between the DOC front and the dissolved iron front would be even

greater. Potentially, there could be some sorption of DOC, which may cancel out the iron sorption effect.

The interplay of reaction rates is very important when considering the impact of not including reaction (4.1) in the reaction network shown in Table 2.1. In the following discussion, all the reactions described are those shown in Table 2.1 unless otherwise noted. Consider a situation where the manganese reduction reaction is slow compared to the iron reduction reaction and reaction (4.1) is included in the reaction network. Assuming that the distribution of $MnO_2(s)$ is uniform (as it was in the simulations in this study), the fast iron reduction rate could allow relatively high concentrations of dissolved iron to be in contact with appreciable $MnO_2(s)$. If at a later time, downgradient from the general location of iron reduction, DOC were to become exhausted, reaction (4.1) would become feasible, resulting in the sequestering of Fe^{2+} and the production of Mn^{2+}. This argument of course assumes that reaction (4.1) is not unduly kinetically-limited.

If manganese reduction is fast compared to iron reduction or the rates are similar, reaction (4.1) would probably not be a factor. Consider the following two scenarios. If the location in question is downgradient from the general location of iron reduction, it is likely that $MnO_2(s)$ would be sufficiently depleted by the time Fe^{2+} arrived so that (4.1) would not be significant. On the other hand, if the location in question were the same location as iron reduction, (4.1) would not be significant unless DOC were exhausted; if DOC were gone, then iron reduction would not be occurring.

At the Cape Cod site itself, the situation is a bit murkier than has been considered in the preceding examples. As suggested by *Thurman et al.* [1986], the site is carbon-limited. As discussed in Chapter 3, the carbon limitation may be manifested in the observation that sulfate reduction does not appear to occur in the aquifer. This being the case, it is possible that the only observed manganese reduction that is driven by DOC occurs upgradient of the anoxic zone. If this is true, then the remaining dissolved manganese may be a result of a reaction like (4.1). In this scenario, DOC becomes exhausted after producing high concentrations of dissolved iron. The dissolved iron moves downgradient, reacts with $MnO_2(s)$, precipitates $Fe(OH)_3(s)$, releases Mn^{2+}, and "limits" the extent of the iron zone. It should be pointed out that reaction (4.1) also has the potential to lower *p*H.

Additional Compartments

Reacting Complex Organic Compounds

One might consider a sort of "precursor" compartment, where complex organic matter is broken down into simpler compounds that can then be readily utilized. This step is actually necessary for iron reduction to be of much consequence. Most of the Fe(II) produced by microorganisms is coupled to the oxidation of acetate, but aromatics, other fatty acids, and H_2 can also be oxidized by iron reducers [*Lovley*, 1991]. In this study, all the various reactive organic

compounds have been lumped together as "CH_2O" for the sake of simplicity. If data were available, the breakdown of complex organic matter and the inclusion of one or more specific organic reactants could be included in the compartmentalized approach.

As an example of the breakdown of complex organic matter, consider a sequence of reactions, catalyzed by various microorganisms, that leads to the production of organic compounds that can be used by iron reducing bacteria to reduce significant quantities of poorly crystalline Fe(III) oxyhydroxides [*Lovley*, 1993]. In this study, $Fe(OH)_3(s)$ was used to represent such iron oxyhydroxides. Figure 4.1 shows a conceptualized illustration of the multi-step process by which complex organic matter is broken down to simpler metabolites. In the first step, hydrolytic enzymes break down complex organic matter into smaller constituents such as sugars, amino acids, fatty acids, and aromatic compounds. The sugars and amino acids are then metabolized by fermentative microorganisms. The most important fermentation acid that can then be utilized by the iron reducers is acetate [*Lovley*, 1991].

The reactions that represent the processes shown in Figure 4.1 would need to be determined on a case-by-case basis. Generically, the reactions can be represented by:

$$\text{complex organic matter} \rightarrow \text{glucose } (C_6H_{12}O_6) \tag{4.2}$$

$$C_6H_{12}O_6 \rightarrow 3 \text{ acetate } (CH_3COO^-) + 3\ H^+ \tag{4.3}$$

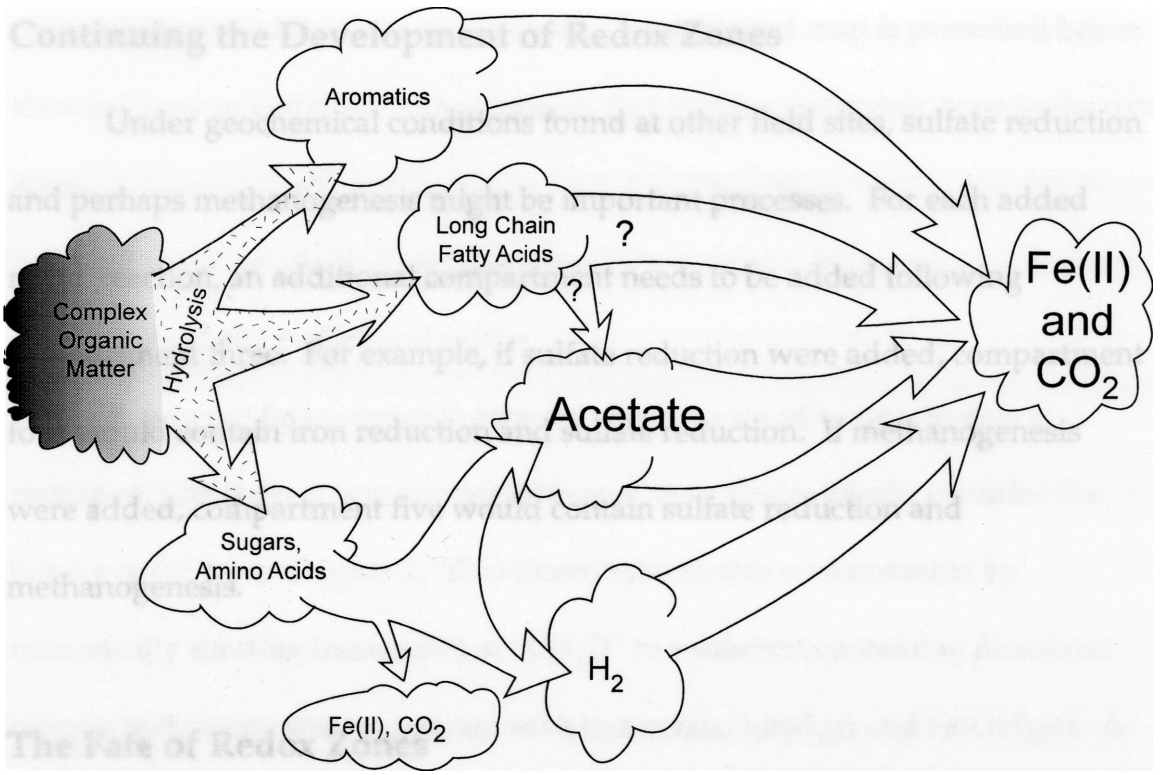

Figure 4.1. Conceptual model of the breakdown of complex organic matter into smaller organic compounds and CO_2. Arrows show the pathways by which microbes catalyze reactions. Unknown or questionable pathways are indicated by a question mark. This example uses Fe(III) as an electron acceptor (at any reaction step). A similar conceptual framework would also apply to other oxidants. Modified from *Lovley* [1993].

The reactions in this potential compartment can be changed, or if more reactions are needed they can be added to an existing compartment, or another compartment could be added.

Continuing the Development of Redox Zones

Under geochemical conditions found at other field sites, sulfate reduction and perhaps methanogenesis might be important processes. For each added redox reaction, an additional compartment needs to be added following compartment three. For example, if sulfate reduction were added, compartment four would contain iron reduction and sulfate reduction. If methanogenesis were added, compartment five would contain sulfate reduction and methanogenesis.

The Fate of Redox Zones

The effort reported in this study focused on the development of redox zones starting from pristine groundwater and subsequently introducing contaminants. Reaction (4.1) could also be included in a separate network of reactions that controls the *fate* of redox zones. The second reaction network would address the question, what happens to the redox zones when there is no more DOC? In theory, it would not be difficult to include a separate sequence of reactions describing the fate of redox zones. These reactions, in a sense, would be a sequence of oxidation reactions because the overall geochemistry of the

groundwater would become more oxidizing (i.e., the redox potential would be increasing). Another cut-off value would be needed if one were to include such a sequence. The second cut-off would represent a decision regarding whether the aquifer is being contaminated or whether it is being restored to a pre-contaminated condition. As an example, a general road map is presented below showing how to add three compartments that go from the anoxic zone to the oxic zone.

Example 1: A batch geochemical system

It may not be as straightforward to design a set of compartments to restore an aquifer as it is to contaminate one. As a first example, consider the batch system from Chapter 2. That closed system was contaminated by numerically titrating increments of "CH_2O" to a solution containing dissolved oxygen and nitrate that was mixed with two solids, $MnO_2(s)$ and $Fe(OH)_3(s)$. A reverse numerical titration could be performed by adding increments of dissolved oxygen to the final solution. To do this, only two compartments would be required, using the following reactions:

$$Fe^{2+} + \frac{1}{4}\,O_2(aq) + \frac{5}{2}\,H_2O \rightarrow Fe(OH)_3(s) + 2\,H^+ \tag{4.4}$$

$$Mn^{2+} + \frac{1}{2}\,O_2(aq) + H_2O \rightarrow MnO_2(s) + 2\,H^+ \tag{4.5}$$

$$N_2(aq) + \frac{5}{2}\,O_2(aq) + H_2O \rightarrow 2\,NO_3^- + 2\,H^+ \tag{4.6}$$

The first compartment (i.e., compartment four, if a continuous simulation were performed from the initial conditions described in Chapter 2) would contain (4.4) and (4.5). Compartment five would contain (4.5) and (4.6).

The implicit assumption was made in Chapter 2 that the batch system, although conceptually located in an unconfined aquifer, was essentially isolated from the atmosphere. This assumption is satisfied, in a conceptual manner, by assuming a large enough distance between the water table and the simulation location. The time scales of diffusion are then assumed to be much greater than the time scale of the chemical reactions. The batch system could, however, also be modeled as an open system. Atmospheric partial pressures of oxygen and carbon dioxide could be used to equilibrate the solution. Reactions between the aqueous and gaseous phases would then be needed:

$$O_2(aq) = O_2(g) \tag{4.7}$$

$$CO_2(aq) = CO_2(g) \tag{4.8}$$

If the system is considered to be open, then a decision must be made regarding what form of nitrogen is used in (4.6). If experimental evidence suggests that the gaseous form of nitrogen is actually the more reactive species, then $N_2(g)$ should be substituted for $N_2(aq)$ in (4.6) and the denitrification reaction shown in Table 2.1 should be similarly modified. If the aqueous species is more reactive, (4.6)

can be left as written, but to account for the fact that the system is open to the atmosphere, another reaction would be needed:

$$N_2(aq) = N_2(g) \tag{4.9}$$

Example 2: A solute transport system

A second example of an aquifer that is being geochemically restored to an uncontaminated state is the consideration of a solute transport system. Consider a moving parcel of water. Assume that this parcel of water has reached a *p*H of 6.5, all of the $MnO_2(s)$ at its current location and immediately downgradient of it has been reacted away, and dissolved iron has reached a concentration of about 200 μM (i.e., the approximate end point of the simulated field conditions in the iron zone). As the parcel of water advects along, dissolved oxygen can enter it via dispersion, initiating a reaction sequence described by (4.4) – (4.6). This reaction sequence could be compartmentalized in the same manner as discussed for the closed batch system.

Now consider that not all of the $MnO_2(s)$ was exhausted at the parcel's location (or downgradient from it) when the DOC ran out. In this case, the reaction network would likely need some modifications. Although dissolved oxygen is thermodynamically favored over $MnO_2(s)$ as an oxidant for dissolved iron, DO is at a disadvantage, as long as reaction (4.1) is not unduly limited kinetically, due to the fact that it can only reach the dissolved iron by dispersion

(except at the edges of the iron zone). The revised reaction network might include (4.1), (4.4), (4.5), and (4.6). This network yields a three compartment system (following the original three compartment system that was used to simulate the contamination of the aquifer in Chapters 2 and 3) where compartment four contains (4.1) and (4.4), compartment five contains (4.4) and (4.5), and compartment six contains (4.5) and (4.6).

For all of the compartmentalized reaction networks discussed thus far, there has only been one driving component (i.e., "CH_2O"). For this example, there would be two, but they do not operate together. Fe^{2+} would be the driving component for compartment four, allowing for the thermodynamic competition between (4.1) and (4.4). Compartments five and six would then use dissolved oxygen as the driving component.

Groundwater Flow and Solute Transport Modeling

A statistical model performance evaluation, similar to that done in Chapter 2, could be performed pitting simulation data against field data. If the model evaluation yields unsatisfactory results, the many parameters in the geochemical and groundwater flow models would need to be adjusted within the range of reasonable values. The important parameters are the reaction rates and the hydraulic conductivity distribution. Source term variations are also important. Clearly, there are many degrees of freedom here and, potentially,

there are an infinite number of combinations of these variables and parameters that could provide a reasonable fit to the field data.

At the Cape Cod site, source term variations are likely to be the most difficult to quantify because of the long, variable history of the sewage treatment facility. Complete records of effluent output and quality do not exist [*LeBlanc*, 1984a; *D. R. LeBlanc*, personal communication, 1996]. Not only did the quantity and quality of the effluent at Cape Cod vary temporally, it also varied spatially (see Figure 1.1). Perhaps the best tack to take in calibrating the source term is to quantify the other unknown parameters, leaving the source term as the residual for the final adjustment.

Macroscopic, field-scale oxygen consumption rates are known reasonably well [*Penarrieta*, 1998]. Denitrification rates have been quantified at the laboratory scale [*Smith and Duff*, 1988; *Smith et al.*, 1991a; 1996]. To determine the rates of manganese and iron reduction at the site, field and laboratory experiments would be needed. As a first cut, it can be assumed that the rates are of similar magnitude to oxygen consumption and denitrification, as was done for this effort.

The spatial variability of hydraulic conductivity (K) for a portion of the Cape Cod site has been well-studied. Measured values of hydraulic conductivity range over approximately one order of magnitude [*Hess et al.*, 1992]. The geometric mean was determined to be 1.1×10^{-3} m s^{-1} and the correlation lengths were calculated to be 3.5 m in the horizontal direction and 0.19 m in the vertical

direction [*Hess et al.*, 1992]. It should be pointed out that the conductivity measurements for the *Hess et al.* study were made in only one small area (tens of meters) of the Cape Cod aquifer. As such, they really do not lend themselves to the generation of a kriged map of hydraulic conductivity for the entire site. However, stochastic simulation offers a method to generate equally probable realizations of the hydraulic conductivity field, while still honoring the data in the area of the *Hess et al.* study. Compartmentalized solute transport simulations could be conducted utilizing different realizations of hydraulic conductivity to investigate the impact of spatial variability on the model performance.

An interesting, but as yet unanswered, question is the relationship between hydraulic conductivity and the concentration of reactive weathering coatings that exist on sand grains. One might hypothesize that finer grained material, typically associated with lower hydraulic conductivity values, might contain higher concentrations of iron and manganese weathering coatings. This hypothesis is reasonable based on surface area-to-volume ratios. *Davis et al.* [1993] found that the vertical correlation scales for lead adsorption, zinc adsorption, and hydraulic conductivity were 0.1, 0.15, and 0.26 m, respectively. The similarity in these correlation lengths suggests that there may be a spatial correlation between adsorption of these metals and hydraulic conductivity. In addition, lead adsorption exhibited a weak negative correlation to hydraulic conductivity [*Davis et al.*, 1993]. *Davis et al.* also found that there is a strong positive correlation between lead and zinc adsorption and the amount of iron

that exists on aquifer material as coatings. This suggests that finer grain material (i.e., lower hydraulic conductivity material) may contain higher concentrations of iron oxyhydroxides than coarser grained material.

All of the possible future directions reviewed in this chapter represent extensions to the simulation methodology developed for this dissertation. They represent ways in which the coupled compartmentalized approach can be applied to other field sites and for history matching and predictive purposes. Since the primary objective of this dissertation was to develop simulation protocols, the extensions discussed in this chapter are well beyond the scope of this dissertation.

Chapter 5

Conclusions

This dissertation was motivated by field-scale observations of redox zones, which have been well documented in both contaminated and uncontaminated aquifers throughout the world. At the U.S. Geological Survey's Cape Cod research site near Falmouth, Massachusetts, an anoxic zone that contains high concentrations of dissolved iron has been characterized through careful and exhaustive sampling from thousands of observation points.

To simulate quantitatively the development of the anoxic/iron zone, the development of the redox zones that preceded it, the oxic and suboxic zones, were simulated first. The overall objective of this effort was to test the hypothesis that the redox zones at the Cape Cod site developed due to the interaction and interdependence of hydrogeological and geochemical processes. To address this hypothesis, new simulation concepts were developed that facilitate the use of a suite of currently available computer codes.

The major research questions asked were:

- What chemical reactions are responsible for the existence of the redox zones at the Cape Cod site? This question was addressed in Chapter 2.
- How does one solve the thermodynamic/kinetic reaction network? This question was addressed in Chapter 2.
- How can the compartmentalized approach, developed for batch geochemical systems, be integrated into a solute transport framework? This question was addressed in Chapter 3.
- Can the compartmentalized solute transport model simulate the development of redox zones in two dimensions at the field scale? This question was addressed in Chapter 3
- What are some ways in which the compartmentalized approach can be extended? This question was addressed in Chapter 4.

Redox zones often develop in contaminated aquifers as microbes oxidize organic carbon via reactions that are governed by thermodynamics. The oxidation reactions are typically coupled to the sequential reduction of various electron acceptors. The large differences in energy yields between the various redox reactions lead to sharp boundaries between redox zones, and also gives rise to systems of equations that are ill-conditioned. The numerical difficulties of

solving the ill-conditioned systems of equations were overcome in this effort by developing a rational method that allows the modeler to ignore insignificant reactions. The method operates by compartmentalizing the reaction network in a manner that is conceptually based on the redox zones themselves. The reactions that give rise to a particular zone are focused upon, while those that are not important due to reactant availability and energetic efficiency are ignored.

Solving redox problems can be challenging for many geochemical simulation codes. The large differences in energy yields of the major redox reactions that dominate the geochemistry under different conditions during a solute transport simulation translate to large differences in the concentrations of key redox constituents (see Figure 2.3). Note, this is a problem only if thermodynamic constraints (as opposed to empirical reaction inhibition) are used for the reactions.

The compartmentalized approach facilitates the use of a fixed component set by using reaction networks that do not contain insignificant reactions (i.e., basis switching techniques are not needed to improve numerical stability). A fixed component set makes it possible to greatly reduce the number of solute transport equations by making the total analytical concentration of the components (i.e., tenads) the dependent variables, rather than the individual chemical species. The concentrations of the equilibrium species can then be calculated outside of the solute transport simulator, since they are simply functions of the component set.

When a kinetic framework is imposed on the compartmentalized approach, the development of redox zones can be simulated as a function of time while still being constrained by thermodynamics. Empirical reaction inhibition is not required for redox reactions that compete for available organic carbon. Any kinetic formulation to constrain reaction progress can be used, while still using thermodynamics to prevent reactions from occurring under infeasible conditions.

Incorporating the compartmentalized approach into a solute transport framework has allowed the process-based simulation of the development of redox zones at the field scale. The geochemical portion of the model is constrained by thermodynamics and kinetics. The solute transport parts of the model are treated by explicitly considering advection and dispersion.

When the sequential iteration approach is used to simulate solute transport, with the total analytical concentration as the primary dependent variable, the number of transport equations needed can be greatly reduced. Furthermore, a wide variety of currently available geochemical codes can be used because most of these codes use the total analytical concentration of components as the primary variable to be solved. When the compartmentalized approach is implemented, it is possible to reduce the number of transport equations required to simulate solute transport coupled with geochemical reactions even further. This can be done because reaction networks for widely different geochemical conditions can be effectively decoupled.

The ability of the compartmentalized solute transport model to apply either a rate-limited or thermodynamically-limited solution is a distinct advantage over other currently available reactive transport codes. No currently available model that I am aware of is capable of simulating multiple competitive, kinetic reactions that are subject to thermodynamic constraints. Other models that use thermodynamics calculate the competition between redox reactions based on equilibrium relationships only. The question that is not asked with these codes is if the lower-energy reaction (i.e., the loser in the thermodynamic competition) is rate-limited. The compartmentalized solute transport model developed for this dissertation allows for this flexibility. The procedure used in the compartmentalized approach can easily check that the progress of kinetic reactions does not violate thermodynamic constraints.

The compartmentalized solute transport model is capable of solving field-scale problems of greater than one dimension. Possible extensions could incorporate other reactions or more complicated fluid flow. Now that the basic framework is in place, many possibilities lay ahead.

REFERENCES

Abrams, R. H., K. Loague, and D. B. Kent, Development and testing of a compartmentalized reaction network model for redox zones in contaminated aquifers, *Water Resour. Res.*, *34* (6), 1531-1541, 1998. Copyright by the American Geophysical Union.

Arnold, R. G., T. M. Olson, and M. R. Hoffman, Kinetics and mechanism of dissimilative Fe(III) reduction by *Pseudomonas* sp. 200, *Biotech. and Bioeng.*, 28, 1657-1671, 1986.

Arnold, R. G., T. J. DiChristina, and M. R. Hoffman, Reductive dissolution of Fe(III) oxides by *Pseudomonas* sp. 200, *Biotech. and Bioeng.*, 32, 1081-1096, 1988.

Back, W., and I. Barnes, Relation of electrochemical potentials and iron content to ground-water flow patterns, *U.S. Geol. Surv. Prof. Pap.*, *498-C*, 16 pp., 1965.

Baedecker, M. J., and W. Back, Hydrogeological processes and chemical reactions at a landfill, *Ground Water*, *15*(5), 429-437, 1979a.

Baedecker, M. J., and W. Back, Modern marine sediments as a natural analog to the chemically stressed environment of a landfill, *J. Hydrol.*, *43*, 393-414, 1979b.

Baedecker, M. J., D. I. Siegel, P. Bennett, and I. M. Cozzarelli, The fate and effects of crude oil in a shallow aquifer I. The distribution of chemical species and geochemical facies, in *U. S. Geological Survey Toxic Substances Hydrology Program-Proceedings of the Technical Meeting*, edited by G. E. Mallard and S. E. Magone, pp. 13-20, U.S. Geol. Surv., Water Res. Invest. Rep 88-4220, Phoenix, AZ, 1989.

Baedecker, M. J., I. M. Cozzarelli, R. P. Eganhouse, D. I. Siegel, and P. Bennett, Crude oil in a shallow sand and gravel aquifer-III. Biogeochemical reactions and mass balance modeling in anoxic groundwater, *Appl. Geochem.*, *8*, 569-586, 1993.

Bailey, J. E., and D. F. Ollis, *Biochemical Engineering Fundamentals*, 753 pp., McGraw-Hill, New York, 1977.

Barber, L. B., II, Influence of geochemical heterogeneity in a sand and gravel aquifer on the transport of nonionic organic solutes: Methods of sediment characterization, in *U.S. Geological Survey Program on Ground-Water Contamination: Proceedings of the Third Technical Meeting*, pp. B45-B51, U.S. Geol. Surv., 1987.

Barcelona, M. J., T. R. Holm, M. R. Schock, and G. K. George, Spatial and temporal gradients in aquifer oxidation-reduction conditions, *Water Resour. Res.*, *25*(5), 991-1003, 1989.

Barlow, P. M., The use of temperature as a ground-water tracer in glacial outwash, Master's thesis, Univ. of Ariz., Tucson, 1987.

Bekins, B. A., E. Warren, and E. M. Godsy, A comparison of zero-order, first order, and Monod biotransformation models, *Ground Water, 36* (2), 261-268, 1998.

Beller, H. R., D. Gribic´-Galic´, and M. Reinhard, Microbial degradation of toluene under sulfate-reducing conditions and the influence of iron on the process, *Appl. Environ. Microbiol.*, 58(3), 786-793, 1992.

Bennett, P. C., D. I. Siegel, M. J. Baedecker, and M. F. Hult, Crude oil in a shallow sand and gravel aquifer-I. Hydrogeology and inorganic geochemistry, *Appl. Geochem., 8*, 529-549, 1993.

Bethke, C. M., *Geochemical Reaction Modeling*, Oxford Univ. Press, New York, N.Y., 1996.

Bjerg, P. L., K. Rügge, J. K. Pedersen, and T. H. Christensen, Distribution of redox sensitive groundwater quality parameters downgradient of a landfill (Grindsted, Denmark), *Environ. Sci. Tech.*, 29(5), 1387-1394, 1995.

Borden, R. C., C. A. Gomez, and M. T. Becker, Geochemical indicators of intrinsic bioremediation, *Ground Water*, 33(2), 180-189, 1995.

Champ, D. R., J. Gullens, and R. E. Jackson, Oxidation-reduction sequences in ground water flow systems, *Can. J. Earth Sci., 16*, 12-23, 1979.

Chapelle, F. H., and D. R. Lovley, Competitive exclusion of sulfate reduction by Fe(III)-reducing bacteria: A mechanism for producing discrete zones of high-iron ground water, *Ground Water, 30*(1), 29-36, 1992.

Coston, J. A., C. C. Fuller, and J. A. Davis, Pb^{2+} and Zn^{2+} adsorption by a natural Al- and Fe-bearing surface coating on an aquifer sand, *Geochim. Cosmochim. Acta, 59*(17), 3535-3547, 1995.

Cozzarelli, I. M., M. J. Baedecker, R. P. Eganhouse, and D. F. Goerlitz, The geochemical evolution of low-molecular-weight organic acids derived from the degradation of petroleum contaminants in groundwater, *Geochim. Cosmochim. Acta, 58*(2), 863-877, 1994.

Cozzarelli, I. M., J. S. Herman, and M. J. Baedecker, Fate of microbial metabolites in a coastal plain aquifer: The role of electron acceptors, *Environ. Sci. Tech.*, 29(2), 458-469, 1995.

Davis, J. A., C. C. Fuller, J. A. Coston, K. M. Hess, and E. Dixon, Spatial heterogeneity of geochemical and hydrologic parameters affecting metal transport in ground water, *U. S. E. P. A., Environ. Res. Brief*, EPA/600/S-93/006, 22 pp., 1993.

Edmunds, W. M., A. H. Bath, and D. L. Miles, Hydrochemical evolution of the East Midlands Triassic sandstone aquifer, England, *Geochim. Cosmochim. Acta, 46*, 2069-2081, 1982.

Edmunds, W. M., D. L. Miles, and J. M. Cook, A comparative study of sequential redox processes in three British aquifers, in *Hydrochemical Balances of Freshwater Systems*, E. Eriksson ed., pp. 55-72, IAHS—AISH, Uppsala, SWE, 1984.

Edmunds, W. M., J. M. Cook, W. G. Darling, D. G. Kinniburgh, D. L. Miles, A. H. Bath, M. Morgan-Jones, and J. N. Andrews, Baseline geochemical conditions in the Chalk aquifer, Berkshire, U.K.: A basis for groundwater quality management, *Applied Geochemistry, 2*, 251-274, 1987.

Eganhouse, R. P., M. J. Baedecker, I. M. Cozzarelli, G. R. Aiken, K. A. Thorn, and T. F. Dorsey, Crude oil in a shallow sand and gravel aquifer-II. Organic geochemistry, *Appl. Geochem., 8*, 551-567, 1993.

Engesgaard, P., and K. L. Kipp, A geochemical transport model for redox-controlled movement of mineral fronts in groundwater flow systems: A case of nitrate removal by oxidation of pyrite, *Water Resour. Res., 28*(10), 2829-2843, 1992.

Essaid, H. I., B. A. Bekins, E. M. Godsy, E. Warren, M. J. Baedecker, and I. M. Cozzarelli, Simulation of aerobic and anaerobic biodegradation processes at a crude oil spill site, *Water Resour. Res., 31*(12), 1995.

Freeze, R. A., and J. A. Cherry, *Groundwater*, 604 pp., Prentice-Hall, Englewood Cliffs, NJ, 1979.

Froelich, P. N., G. P. Klinkhammer, M. L. Bender, N. A. Luedtke, G. R. Heath, D. Cullen, P. Dauphin, D. Hammond, B. Hartman, and V. Maynard, Early oxidation of organic matter in pelagic sediments of the eastern equatorial Atlantic: suboxic diagenesis, *Geochim. Cosmochim. Acta, 43*, 1075-1090, 1979.

Furrer, G., P. Sollins, and J. Westall, The study of soil chemistry through quasi-steady-state models: II. Acidity of soil solution, *Geochim. Cosmochim. Acta,* 54, 2363-2374, 1990.

Furrer, G., U. v. Gunten, and J. Zobrist, Steady-state modelling of biogeochemical processes in columns with aquifer material, 1. Speciation and mass balances, *Chem. Geol., 133,* 15-28, 1996.

Garabedian, S. P., L. W. Gelhar, and M. A. Celia, Large-scale dispersive transport in aquifers: Field experiments and reactive transport theory, Ralph M. Parsons Lab., Dept. of Civ. Eng., Mass. Inst. of Tech., Cambridge, *Rep. 315,* 1988.

Garabedian, S. P., D. R. LeBlanc, L. W. Gelhar, and M. A. Celia, Large-scale natural gradient tracer test in sand and gravel, Cape Cod, Massachusetts, 3, Analysis of spatial moments for a nonreactive tracer, *Water Resour. Res., 27* (5), 911-924, 1991.

Guswa, J. H., and D. R. LeBlanc, Digital models of ground-water flow in the Cape Cod aquifer system, Massachusetts, *U.S. Geol. Surv. Water Supply Pap., 2209,* 112 pp., 1985.

Hess, K. M., Use of a borehole flowmeter to determine spatial heterogeneity of hydraulic conductivity and macrodispersion in a sand and gravel aquifer, Cape Cod, Massachusetts, in *Proceedings of the Conference on New Field Techniques for Quantifying the Physical and Chemical Properties of Heterogeneous Aquifers*, edited by F. J. Molz, J. G. Melville, and O. Güven, pp. 497-508, National Water Well Association, Dublin, Ohio, 1989.

Hess, K. M., S. H. Wolf, and M. A. Celia, Large-scale natural gradient tracer test in sand and gravel, Cape Cod, Massachusetts, 2, Hydraulic conductivity variability and calculated macrodispersivities, *Water Resour. Res.*, *28* (8), 2011-2027, 1992.

Hess, K. M., J. A. Davis, J. A. Coston, and D. B. Kent, Multispecies reactive transport under spatially variable chemical conditions: Dispersion of bromide and nickel tracers, in *U. S. Geological Survey Toxic Substances Hydrology Program-Proceedings of the Technical Meeting — Vol. 3 — Subsurface Contamination from Point Sources*, edited by D. W. Morganwalp and H. T. Buxton, U.S. Geol. Surv., Water Res. Invest. Rep 99-4018C, Charleston, S. C., 1999.

Jackson, R. E., and R. J. Patterson, Interpretation of pH and Eh trends in a fluvial-sand aquifer system, *Water Resour. Res.*, *18*(4), 1255-1268, 1982.

Keating, E. H., Reactive transport modeling: An application to redox geochemistry of groundwater discharging to a stream in northern Wisconsin, Ph.D. Thesis, Univ. of Wisc., Madison, 1995.

Keating, E. H., and J. M. Bahr, Reactive transport modeling of redox geochemistry: Approaches to chemical disequilibrium and reaction rate estimation at a site in northern Wisconsin, *Water Resour. Res.*, *34*(12), 3573-3584, 1998.

Kent, D. B., J. A. Davis, L. C. D. Anderson, B. A. Rea, and T. D. Waite, Transport of chromium and selenium in the suboxic zone of a shallow aquifer: Influence of redox and adsorption reactions, *Water Resour. Res.*, *30*(4), 1099-1114, 1994.

Kindred, J. S., and M. A. Celia, Contaminant transport and biodegradation, 2, Conceptual model and test simulations, *Water Resour. Res.*, *25*(6), 1149-1159, 1989.

Kinzelbach, W., W. Schäfer, and J. Herzer, Numerical modeling of natural and enhanced denitrification processes in aquifers, *Water Resour. Res.*, *27*(6), 1123-1135, 1991.

Kirkner, D. J., A. A. Jennings, and T. L. Theis, Multicomponent solute transport with sorption and soluble complexation, *Adv. Water Resour.*, *7*, 120-125, 1984.

Kirkner, D. J., A. A. Jennings, and T. L. Theis, Multicomponent mass transport with chemical interaction kinetics, *J. Hydrol.*, *76*, 107-117, 1985.

László, F., and F. Székely, Simulation of groundwater flow and redox processes around bank-filtration wells, in *Groundwater Contamination*, L. Abriola ed., pp. 51-55, IAHS—AISH, Baltimore, MD, 1989.

LeBlanc, D. R., Sewage plume in a sand and gravel aquifer, Cape Cod, Massachusetts, *U.S. Geol. Surv. Water Supply Pap., 2218,* 28 pp., 1984a.

LeBlanc, D. R., Digital Modeling of solute transport in a plume of sewage-contaminated ground water, Cape Cod, Massachusetts: U.S. Geological Survey Toxic Waste Ground-Water Contamination Program, *U.S. Geol. Surv. Open File Rep., 84-475,* 11-45, 1984b.

LeBlanc, D. R., J. H. Guswa, M. H. Frimpter, and C. J. Londquist, Ground-Water resources of Cape Cod, Massachusetts, *Hydrol. Invest. Atlas, HA-692,* 4 sheets, U.S. Geol. Surv., Reston, Va., 1986.

LeBlanc, D. R., S. P. Garabedian, K. M. Hess, L. W. Gelhar, R. D. Quadri, K. G. Stollenwerk, and W. W. Wood, Large-scale natural gradient tracer test in sand and gravel, Cape Cod, Massachusetts, 1, Experimental design and observed tracer movement, *Water Resour. Res., 27*(5), 895-910, 1991.

Lee, R. W., Geochemistry of sewage-contaminated water in the shallow sand and gravel, glacial outwash aquifer, Cape Cod, Massachusetts, Ph.D. thesis, Univ. of Texas, Austin, 1996.

Lee, R. W., Effects of carbon dioxide variations in the unsaturated zone on water chemistry in a glacial-outwash aquifer. *Appl. Geochem.; 12*(4), 347-366, 1997.

Lensing, H. J., M. Vogt, and B. Herring, Modeling of biologically mediated redox processes in the subsurface, *J. Hydrol., 159,* 125-143, 1994.

Lichtner, P. C., Time-space continuum description of fluid/rock interaction in permeable media, *Water Resour. Res., 28*, 3135-3155, 1992.

Lindberg, R. D. and D. D. Runnells, Ground water redox reactions: An analysis of equilibrium state applied to Eh measurements and geochemical modeling, *Science, 225*, 925-927, 1984.

Liu, C. W., and T. N. Narasimhan, Redox-controlled multiple-species reactive chemical transport, 1. Model development, *Water Resour. Res., 25*(5), 869-882, 1989a.

Liu, C. W., and T. N. Narasimhan, Redox-controlled multiple-species reactive chemical transport, 2. Verification and application, *Water Resour. Res., 25*(5), 883-910, 1989b.

Loague, K., and R. E. Green, Statistical and graphical methods for evaluating solute transport models: Overview and application, *J. Contam. Hydrol., 7*, 261-283, 1991.

Lovley, D. R., Dissimilatory Fe(III) and Mn(IV) reduction, *Microbiol. Rev.*, 55(2), 259-287, 1991.

Lovley, D. R., Anaerobes into heavy metal: Dissimilatory metal reduction in anoxic environments, *Trends in Ecology and Evolution*, 8(6), 213-217, 1993.

Lovley, D. R., and D. J. Lonergan, Anaerobic oxidation of toluene, phenol, and *p*-cresol by the dissimilatory iron-reducing organism, GS-15, *Appl. Environ. Microbiol.*, 56(6), 1858-1864, 1990.

Lovley, D. R., M. J. Baedecker, D. J. Lonergan, I. M. Cozzarelli, E. J. P. Phillips, and D. I. Siegel, Oxidation of aromatic contaminants coupled to microbial iron reduction, *Nature*, 339, 297-300, 1989.

Lovley, D. R., F. H. Chappelle, and J. C. Woodward, Use of dissolved H_2 concentrations to determine distribution of microbially catalyzed redox reactions in anoxic groundwater, *Environ. Sci. Technol.* ,*28*(7), 1205-1210, 1994.

Lyngkilde, J. L. and T. H. Christensen, Redox zones in a landfill leachate pollution plume (Vejen, Denmark), *J. Contam. Hydrol. 10*(4), 273-289, 1992.

Marsily, G. de, *Quantitative Hydrogeology*, Academic Press, San Diego, CA, 1986.

McCarty, P. L., Energetics and bacterial growth, in *Organic Compounds in Aquatic Environments*, S. D. Faust and J. V. Hunter ed., pp. 495-531, Marcel Dekker, New York, 1971.

McCarty, P. L., Stoichiometry of biological reactions, *Progress in Water Tech.*, 7, 157-172, 1975.

McFarland, M. J., and R. C. Sims, Thermodynamic framework for evaluating PAH degradation in the subsurface, *Ground Water*, 29(6), 885-896, 1991.

McNab, W. W., and T. N. Narasimhan, A multiple species transport model with sequential decay chain interactions in heterogeneous subsurface environments, *Water Resour. Res.*, *29* (8), 2737-2746, 1993.

McNab, W. W., and T. N. Narasimhan, Modeling reactive transport of organic compounds in groundwater using a partial redox disequilibrium approach, *Water Resour. Res., 30*(9), 2619-2635, 1994.

McNab, W. W., and T. N. Narasimhan, Reactive transport of petroleum hydrocarbon constituents in a shallow aquifer: Modeling geochemical interactions between organic and inorganic species, *Water Resour. Res.*, 31(8), 2027-2033, 1995.

Mihelcic, J. R., and R. G. Luthy, Degradation of polycyclic aromatic hydrocarbon compounds under various redox conditions in soil-water systems, *Appl. Environ. Microbiol.*, 54(5), 1182-1187, 1988a.

Mihelcic, J. R., and R. G. Luthy, Microbial degradation of acenaphthalene and naphthalene under denitrification conditions in soil-water systems, *Appl. Environ. Microbiol.*, 54(5), 1188-1198, 1988b.

Molz, F. J., M. A. Widdowson, and L. D. Benefield, Simulation of microbial growth dynamics coupled to nutrient and oxygen transport in porous media, *Water Resour. Res., 22* (8), 1207-1216, 1986.

Morel, F. M. M., and J. G. Hering, *Principles and Applications of Aquatic Chemistry*, John Wiley & Sons, New York, N.Y., 1993.

Morganwalp, D. W., and D. A. Aronson, U.S. Geological Survey Toxic Substances Hydrology Program—Proceedings of the Technical Meeting, Colorado Springs, CO, September 20-24, 1993, *U.S. Geol. Surv. Water-Resour. Investig. Rep.* 94-4015, 1996.

National Research Council (NRC), *Alternatives for Groundwater Cleanup*, National Academy Press, Washington, DC, 1994.

Papelis, C., K. F. Hayes, and J. O. Leckie, HYDRAQL: A program for the computation of chemical equilibrium composition of aqueous batch systems including surface-complexation modeling of ion adsorption at the oxide/solution interface, *Stanford Univ. Dept. of Civ. Eng. Tech. Rep., 306*, 130 pp., 1988.

Parkhurst, D. L., User's guide to PHREEQC: A computer program for speciation, reaction-path, advective-transport, and inverse geochemical calculations, *Water Resources Investigations Report 95-4227*, 143 pp., U.S. Geological Survey, 1995.

Parkhurst, D. L., and C. A. J. Appelo, Enhancements to the geochemical model PHREEQC: 1D advection and dispersion, diffusion to stagnant zones, and reaction kinetics, *Supplement to EOS Transactions, 78* (17), 167, 1997.

Penarrieta, C. T., Assessment of microbial oxygen consumption in a Cape Cod aquifer using a natural gradient tracer test and core incubations, Master's. thesis, University of Colorado, Boulder, CO, 1998.

Postma, D., C. Boesen, H. Kristiansen, and F. Larsen, Nitrate reduction in an unconfined sandy aquifer: Water chemistry, reduction processes, and geochemical modeling, *Water Resour. Res.*, 27(8), 2027-2045, 1991.

Rehfeldt, K. R., P. Hufschmeid, L. W. Gelhar, and M. E. Schaefer, Measuring hydraulic conductivity with the borehole flowmeter, *Top. Rep. EN-6511, Elec. Power Res. Inst.*, Palo Alto, Calif., 1989.

Rubin, J., Transport of reacting solutes in porous media: Relation between mathematical nature of problem formulation and chemical nature of reactions, *Water Resour. Res., 19* (5), 1231-1252, 1983.

Savoie, J. and D. R. LeBlanc, Water-quality data and methods of analysis for samples collected near a plume of sewage-contaminated ground water, Ashumet Valley, Cape Cod, Massachusetts, 1993-1994, *U.S. Geol. Surv. Water-Resour. Investig. Rep., 97-4269*, 208 pp., 1998.

Schäfer, W., and R. Therrien, Simulating transport and removal of xylene during remediation of a sandy aquifer, *J. Contam. Hydrol., 19*, 205-236, 1995.

Smith, R. L. and J. H. Duff, Denitrification in a sand and gravel aquifer, *Applied Environ. Microbiology, 54*(5), 1071-1078, 1988.

Smith, R. L., B. L. Howes, and J. H. Duff, Denitrification in nitrate-contaminated groundwater: Occurrence in steep vertical geochemical gradients, *Geochim. Cosmochim. Acta, 55*, 1815-1825, 1991a.

Smith, R.L., R. W. Harvey, and D. R. LeBlanc, Importance of closely spaced vertical sampling in delineating chemical and microbiological gradients in groundwater studies, *J. Contam. Hydrol., 7*, 285-300, 1991b.

Smith, R. L., Garabedian, S. P., and Brooks, M. H., Comparison of denitrification activity measurements in groundwater using cores and natural-gradient tracer tests, *Environ. Sci. Tech.*, *30*(12), 3448-3456, 1996.

Smith, S. L., and P. R. Jaffé, Modeling the transport and reaction of trace metals in water-saturated soils and sediments, *Water Resour. Res..*, *34* (11), 3135-3147, 1998.

Steefel, C. I., and A. C. Lasaga, A coupled model for transport of multiple chemical species and kinetic precipitation/dissolution reactions with application to reactive flow in single phase hydrothermal systems, *Amer. J. Sci*, *294*, 529-592, 1994.

Steefel, C. I., and S. B. Yabusaki, OS3D/GIMRT: Software for multicomponent-multidimensional reactive transport: User manual and programmer's guide, PNL-11166, Pacific Northwest Laboratory, 1996.

Stollenwerk, K. G., Modeling the effects of variable groundwater chemistry on adsorption of molybdate, *Water Resour. Res. 31*(2), 347-357, 1995.

Stumm, W., and J. J. Morgan, *Aquatic Chemistry*, John Wiley & Sons, New York, N.Y., 1981.

Theis, T. L., D. J. Kirkner, and A. A. Jennings, Multi-solute subsurface transport modeling for energy solid wastes, *Tech. Progr. Rep., C00-10253-3*, dept. of Civ. Eng., Univ. of Notre Dame, Notre Dame, Ind., 1982.

Thurman, E. M., L. B. Barber, and D. R. LeBlanc, Movement and fate of detergents in groundwater: A field study, *J. Contam. Hydrol.*, *1*, 143-161, 1986.

Valentine, R. L., Nonbiological transformation, in *Vadose Zone Modeling of Organic Pollutants*, S. C. Hern and S. M. Melancon ed., pp. 223-243, Lewis Publishers, Chelsea, MI, 1986a.

Valentine, R. L., and J. L. Schnoor, Biotransformation, in *Vadose Zone Modeling of Organic Pollutants*, S. C. Hern and S. M. Melancon ed., pp. 191-222, Lewis Publishers, Chelsea, MI, 1986b.

Van Cappellan, P. and J-F Gaillard, Biogeochemical dynamics in aquatic sediments, in *Reactive Transport in Porous Media*, P. C. Lichtner, C. I. Steefel, and E. H. Oelkers ,eds., pp.335-375, Rev. in Mineralogy, *34*, Mineralogical Society of America, Wash., D.C., 1996.

Vogel, T. M., C. S. Criddle, and P. L. McCarty, Transformations of halogenated aliphatic compounds, *Environ. Sci. Tech.*, 21(8), 722-736, 1987.

Vroblesky, D. A., and F. H. Chapelle, Temporal and spatial changes of terminal electron-accepting processes in a petroleum hydrocarbon-contaminated aquifer and the significance for contaminant biodegradation, *Water Resour. Res.*, 30(5), 1561-1570, 1994.

Walter, A. L., E. O. Frind, D.W. Blowes, C. J. Ptacek, and J. W. Molson, Modeling multicomponent reactive transport in groundwater, 1. Model development and evaluation, *Water Resour. Res.*, *30*(11), 3137-3148, 1994a.

Walter, A. L., E. O. Frind, D.W. Blowes, C. J. Ptacek, and J. W. Molson, Modeling multicomponent reactive transport in groundwater, 2. Metal mobility in aquifers impacted by acidic mine tailings discharge, *Water Resour. Res.*, *30*(11), 3149-3158, 1994b.

Walter, D. A., B. A. Rea, K. G. Stollenwerk, and J. Savoie, Geochemical and hydrologic controls on phosphorus transport in a sewage contaminated sand and gravel aquifer near Ashumet Pond, Cape Cod, Massachusetts, *U.S. Geol. Surv. Water Supply Pap.*, *2463*, 89 pp., 1996.

Westall, J. C., J. L. Zachary, and F. M. M. Morel, MINEQL: A computer program for the calculation of the chemical equilibrium composition of aqueous systems, Ralph M. Parsons Lab Technical Note No. 18, Mass. Inst. of Tech. Cambridge, MA, 1976.

Wolf, S. H., Spatial variability of hydraulic conductivity in a sand and gravel aquifer, Engineer's thesis, Mass. Inst. of Technol., Cambridge, 1988.

Wolf, S. H., M. A. Celia, and K. M. Hess, Evaluation of hydraulic conductivities calculated from multiport-permeameter measurements, *Ground Water*, *29* (4), 516-525, 1991.

Wunderly, M. D., D. W. Blowes, E. O. Frind, and C. J. Ptacek, Sulfide mineral oxidation and subsequent reactive transport of oxidation products in mine tailings impoundments: A numerical model, *Water Resour. Res.*, *32*(10), 3173-3187, 1996.

Yeh, G. T., and V. S. Tripathi, A critical evaluation of recent developments in hydrogeochemical transport models of reactive multichemical components, *Water Resour. Res.*, *25* (1), 93-108, 1989

Yeh, G. T., and V. S. Tripathi, HYDROGEOCHEM: A coupled model of hydrological and geochemical equilibrium of multicomponent systems, Oak Ridge Natl. Lab., Oak Ridge, Tenn., Rep. ORNL-6371, 1990.

Yeh, G. T. and J. P. Gwo, A Lagrangian-Eulerian approach to modeling multicomponent reactive transport, in *Computational Methods in Subsurface Hydrology*, edited by G. Gambolati, A. Rinaldo, A.; C. A. Brebbia, W. G. Gray; G. F. Pinder, pp. 419-427, Comput. Mech. Publ., Southampton, GBR., 1990.

Yeh, G. T., and V. S. Tripathi, A model for simulating transport of reactive multispecies components: Model development and demonstration, *Water Resour. Res.*, *27*(12), 3075-3094, 1991.

Yeh, G. T., G. Iskra, J. M. Zachara, and J. E. Szecsody, KEMOD: A Mixed Chemical Kinetic and Equilibrium Model of Complexation, Adsorption, Ion-exchange, Precipitation/Dissolution, Redox, and Acid-base Reactions, *Penn State Univ. Dept. of Civ and Environ. Eng. Tech. Rep.*, 1993.

Yeh, G. T., G. Iskra, J. M. Zachara, and J. E. Szecsody, Development and Verifications of a Mixed Chemical Kinetic and Equilibrium Model, *Adv. Environ. Res.*, *2* (1), 24-56, 1998.

Yeh, G. T. and K. Salvage, HYDROGEOCHEM 2.1: A coupled model of hydrologic transport and geochemistry with both equilibrium and kinetic reactions, *Penn State Univ. Dept. of Civ and Environ. Eng. Tech. Rep.*, 1995.